IMPROVEMENT OF HOLDASE ACTIVITY OF A SMALL HEAT SHOCK PROTEIN FROM EXTREMELY ACIDOPHILIC ARCHAEA

A THESIS SUBMITTED TO
THE GRADUATE SCHOOL OF NATURAL AND APPLIED SCIENCES
OF
MIDDLE EAST TECHNICAL UNIVERSITY

BY

YAĞMUR KAÇER

IN PARTIAL FULFILLMENT OF THE REQUIREMENTS
FOR
THE DEGREE OF MASTER OF SCIENCE
IN
BIOCHEMISTRY

APRIL 2019

Approval of the thesis:

IMPROVEMENT OF HOLDASE ACTIVITY OF A SMALL HEAT SHOCK PROTEIN FROM EXTREMELY ACIDOPHILIC ARCHAEA

submitted by **YAĞMUR KAÇER** in partial fulfillment of the requirements for the degree of **Master of Science** in **Biochemistry Department, Middle East Technical University** by,

Prof. Dr. Halil Kalıpçılar
Dean, Graduate School of **Natural and Applied Sciences** _____

Assoc. Prof. Dr. Yeşim Soyer
Head of Department, **Biochemistry** _____

Prof. Dr. Semra Kocabıyık
Supervisor, **Biological Sciences Dept., METU** _____

Prof. Dr. Candan Gürakan
Co-Supervisor, **Food Engineering Dept., METU** _____

Examining Committee Members:

Prof. Dr. Fatih İzgü
Biological Sciences Dept., METU _____

Prof. Dr. Semra Kocabıyık
Biological Sciences Dept., METU _____

Prof. Dr. Özlem Darcansoy İşeri
Molecular Bio. and Genetic Dept., Baskent Uni. _____

Assoc. Prof. Dr. Tülin Yanık
Biological Sciences Dept., METU _____

Prof. Dr. Ayşen Tezcaner
Engineering Sciences Dept., METU _____

Date: 26.04.2019

I hereby declare that all information in this document has been obtained and presented in accordance with academic rules and ethical conduct. I also declare that, as required by these rules and conduct, I have fully cited and referenced all material and results that are not original to this work.

Name, Surname: Yağmur Kaçer

Signature:

ABSTRACT

IMPROVEMENT OF HOLDASE ACTIVITY OF A SMALL HEAT SHOCK PROTEIN FROM EXTREMELY ACIDOPHILIC ARCHAEA

Kaçer, Yağmur
Master of Science, Biochemistry
Supervisor: Prof. Dr. Semra Kocabıyık
Co-Supervisor: Prof. Dr. Candan Gürakan

April 2019, 108 pages

In this study, a small heat shock protein gene (po-sHSP20) of archaeon *Picrophilus oshimae* which is the most thermoacidophilic organism known, was cloned and overexpressed in *E.coli* for the first time. The recombinant po-sHSP20 protein that was resistant to high temperature was purified to homogeneity by affinity chromatography. Oligomeric structure analysis of the po-sHSP20 by Size Exclusion Chromatography showed that it exists mostly as 12- and 18-mer oligomers with some dimeric/monomeric units under physiological conditions. Highly conserved K99 residue of the po-sHSP20 was substituted by glutamic acid and glycine. Mutant proteins were successfully expressed in *E.coli*. Chaperone activities of the po-sHSP20 variants were studied by using pig heart citrate synthase as the client protein. The K99E and K99G variants better protected citrate synthase (2.3- and 2-fold, respectively) from heat inactivation at 47ºC, as compared to wild-type. All chaperone variants could prevent thermal aggregation of citrate synthase at a molar ratio of 1:7 and 1:35. The analysis of the 3D model structure of the po-sHSP20 showed that its monomer consists of an alpha crystallin domain flanked by an N-terminal α-helix and C-terminal coiled structure. Dimerization occurs *via* interactions of β6-strand of one monomer with β2-strand of other monomer.

According to model structure analyses of K99G and K99E mutations resulted in loss of the intermolecular hydrogen bond, together with the some intramolecular hydrogen and hydrophobic bonds that K99 residue participates.

Keywords: Archaea, Chaperone activity, *Picrophilus oshimae*, Small heat shock protein, Substrate binding activity

ÖZ

AŞIRI DERECEDE ASİDOFİLİK ARKEADAN ELDE EDİLEN KÜÇÜK ISI ŞOKU PROTEİNİNİN HOLDAZ AKTİVİTESİNİN GELİŞTİRİLMESİ

Kaçer, Yağmur
Yüksek Lisans, Biyokimya
Tez Danışmanı: Prof. Dr. Semra Kocabıyık
Ortak Tez Danışmanı: Prof. Dr. Candan Gürakan

Nisan 2019, 108 sayfa

Bu çalışmada, bilinen en asidofilik organizma olan arkeabakteri *Picrophilus oshimae'*nin moleküler bir küçük ısı şoku protein geni (po-sHSP20) ilk kez *E.coli*'de klonlanmış ve genin yüksek düzeyde anlatımı yapılmıştır. Yüksek ısıya dayanıklı olan rekombinant *po*-sHSP20 proteini, afinite kromotagrafisi ile homojen bir şekilde saflaştırılmıştır. *po*-sHSP20'nin Boyut Dışlama Kromatografisi ile yapılan oligomerik yapı analizi proteinin çoğunlukla 12-mer, 18-mer ve bazı dimerik/monomerik birimler halinde bulunduğunu göstermiştir. *po*-sHSP20'nin yüksek oranda korunmuş K99 grubu glutamik asit ve glisinle değiştirilmiştir. Mutant proteinlerin *E.coli*'de anlatımı başarıyla gerçekleşmiştir. *po*-sHSP20 varyantlarının şaperon aktiviteleri, domuz kalbi sitrat sentaz enzimi substrat olarak kullanılarak çalışılmıştır. K99E and K99G varyantları sitrat sentazın 47ºC'de ısı kaynaklı inaktivasyonunu yabanıl tipe göre daha iyi önlemişlerdir (sırasıyla, 2.3 ve 2 kat). Tüm şaperon varyantları sitrat sentazın ısı kaynaklı kümelenmesini, 1:7 ve 1:35 molar oranlarında önleyebilmiştir. po-sHSP20'nin 3 boyutlu model yapısının analizi, monomerin alfa kristalin bölgesi ile α-heliks N-terminal ve sarmal C-terminal bölgeleri bulunduğunu göstermiştir. Dimerleşme bir monomerin β6 ipliği ile diğer monomerin β2 ipliği arasındaki etkileşimle olmaktadır. Model yapı analizlerine göre,

K99G and K99E mutasyonları sonucu K99 grubunun yer aldığı moleküller arası hidrojen bağı ile birlikte bazı molekül içi hidrojen ve hidrofobik bağlar kaybolmuştur.

Anahtar Kelimeler: Arkeabakteri, Şaperon activitesi, *Picrophilus oshimae*, Küçük ısı şoku proteini, Substrat bağlanma aktivitesi

Dedicated to my family,

ACKNOWLEDGMENTS

I would like to express my sincere gratitude to my advisor Prof.Dr. Semra Kocabıyık for her endless support, enthusiasm, profound knowledge and patience during my study. Her guidance helped me in all the time of research and writing of this thesis.

I would like to thank my laboratory mates Sema Zabcı and Azra Rafiq for their friendship and help whenever I needed.

Finally, I want to thank my father Muzaffer Kaçer who is my first teacher giving me the meaning of life with his valuable ideas. Also, I want to thank my brother, Anıl Kaçer who always support me, and to my mother Gönül Kaçer for supporting me spiritually throughout my life and everything in my life.

TABLE OF CONTENTS

LIST OF TABLES

TABLES

LIST OF FIGURES

FIGURES

LIST OF ABBREVATIONS

ABBREVATIONS

ACD	Alpha Crystallin Domain
3D	Three Dimensional Structure
CS	Citrate Synthase
E.coli	*Escherichia coli*
HPLC	High Performance Liquid Chromatography
Ni-NTA	Nickel-Nitrilotriacetic Acid
po-sHSP20	*Picrophilus oshimae* Small Heat Shock Protein
SEC	Size Exclusion Chromatography
sHSP	Small Heat Shock Protein
WT	Wild-type

CHAPTER 1

INTRODUCTION

1.1. Small Heat Shock Proteins

Cells have a complex organization of protein quality control machinery that prolongs proteostasis and the functions of proteins. Heat shock proteins (HSP) which are major group of stress proteins are essential constituents of proteostatis network since they protect the proteins from aggregation. The failure of proteostasis network is a basic threaten for the cells because of the deposition of insoluble proteins that can damage cells.

Heat shock proteins also known as chaperones are classified based on their molecular weight, structure and function. They are divided into several families such as Hsp70, Hsp90, Hsp60, Hsp100, Hsp40 and small heat shock proteins, (sHSPs). They all function in an ATP-dependent manner, except sHSPs. The sHSPs are conventionally named as holdase chaperones due to their remarkable ability of binding misfolded proteins, and keep them as soluble complexes until they are targeted by ATP-dependent chaperones (Richter *et al*., 2010). They are found in all living organisms (Archaea, Bacteria, and Euakarya) and cyanobacterial phages (Bourrelle-Langlois *et al*; 2016; Maaroufi and Tanguay 2013). Besides their significant roles in cell physiology under normal conditions (Morrow and Tanguay 2012), they also support protein refolding under stress conditions such as high temperature. Their target proteins might be amyloid fibrils, cytoskeleton, growth factors and steroid receptors (Basha *et al.* 2011).

1.1.1. Structure of Small Heat Shock Proteins

A small heat shock protein consists of a non-conserved N-terminal region, a highly conserved α-crystallin domain (ACD) and a non-conserved C-terminal region, as illustrated in Figure 1.1. The α-crystallin domain is approximately 80 amino acid in length (Basha *et al*., 2012; Haslbeck *et al*., 2015). The N-terminal and C-terminal regions are varying in both sequence and length (Treweek *et al*.,2015). C-terminal domain contains a conserved IXI motif localized at the middle of a nine amino acid palindromic sequence and contributes to organization into oligomeric assembly. Most sHSPs exist as polydisperse, large and dynamic oligomers that are subject to subunit exchange involved in chaperone mechanism (Aquilina *et al*., 2013).

The monomeric molecular mass of sHSPs ranges from 12 to 43 kDa. It has been determined by light scattering that the oligomer mass of αB-crystallins of humans ranges from 420 to 980 kDa and is roughly 650 kDa in average (Bakthisaran *et al*., 2015; Treweek *et al*., 2015).

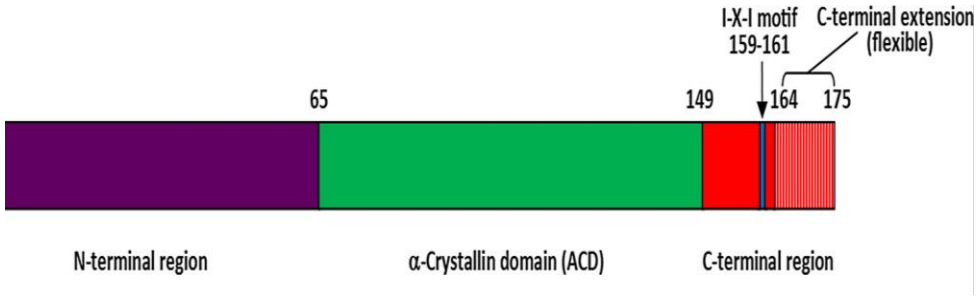

Figure 1.1. The linear structure of a sHSP (data from Treweek *et al*., 2015)

Up to the present, crystal structures of 19 sHSPs have been published. Some family members of sHSPs whose structures have been characterized are as follows.

The first structured archaeal sHSP is the HSP16.5 from *Methanococcus jannaschii* (Kim *et. al*., 1998). Its crystal structure revealed a hollow spherical complex of 24

subunits arranged in octahedral symmetry. The ACD of each monomer is arranged into an immunoglobulin fold.

Hsp14.0 from *Sulfolobus tokodaii* strain 7 is similar to Hsp16.5. It is composed of 24 subunits (Usui *et al*. 2001). Hsp14.1 from *Sulfolobus solfatataricus* consists of a homotetramer arranged into asymmetric structure (Liu *et al*., 2015).

Hsp16.3 from *Mycobacterium tuberculosis* forms a spherical complex with 12 subunits arranged in tetrahedral symmetry (Kennaway *et al*., 2005). Hsp16.9 from *Triticum aestivum* (wheat) builts a barrel-shaped structure consisting of two hexameric double disks with 12 subunits (Montfort *et al*., 2001). Moreover, Hsp16 from *S. pombe* is found as ellipsoidal 16-mer and Hsp26 from *S.cerevisiae* is cubic 24-mer that forms hollow, ball-like structure (Haslbeck *et al*., 1999 and White *et al*., 2006). Hsp21 from *Arabidopsis thaliana* is also found as a dodecamer consisting of two hexameric disks (Lambert *et al*., 2011).

Mammalian sHSPs such as Hsp27, α-crystallins and Hsp20 exist as polydispersed oligomeric complexes. In contrast to these, HspB6 does not form large oligomeric assemblies. It forms a homotetramer arranged in dihedral symmetry (Weeks *et al*., 2014). The α-crystallins may have up to 50 subunits per complex in their polydispered oligomeric structures (Aquilina *et al*., 2005). The αB-crystallin oligomer is a hollow spherical complex of roughly 13.5 nm diameter consisting of 24 subunits arranged in tetrahedral symmetry (Bakthisaran *et al*., 2015).

1.1.2. Dimer Formation of Small Heat Shock Proteins

sHSPs are not found in monomeric form in their functional state. They have various higher level organizations. The ACD has a compact β-sandwich which is similar to the immunoglobulin fold and plays a crucial role in dimerization. The dimeric building block then assembles into large oligomers through the interactions in the N-terminal domain and a C-terminal tail. The β-sandwich is composed of two anti-parallel sheets of three and four β-strands, connected by a short inter-domain loop. The compact β-sandwich is conserved among the sHSP family during evolution

(Haslbeck *et al*., 2008). It has been reported that dimerization via the alpha-crystallin domain arises in two separate ways called as ‘’β6-swapped dimer’’ and ‘’β7-interface dimer’’(Haslbeck *et al*., 2015; Baldwin *et al*., 2011). ‘’β6-swapped dimer’’ has been observed in yeast, plant, bacterial and archaeal sHSPs. It is also known as ‘’bacterial type of dimerization’’ (Haslbeck and Vierling, 2015). β6-swapped dimer arises through the reciprocal switching of β6-strands onto the β-sandwich of the neighboring monomer (Figure 1.2). ‘’β7-interface dimer’’ is found in metazoans**.** In this type of dimerization, β6- and β7-strands are fused into an elongated strand that forms the dimer interface with its counterpart from the adjacent monomer in an anti-parallel position. β7-interface dimer is illustrated in Figure 1.2 (right).

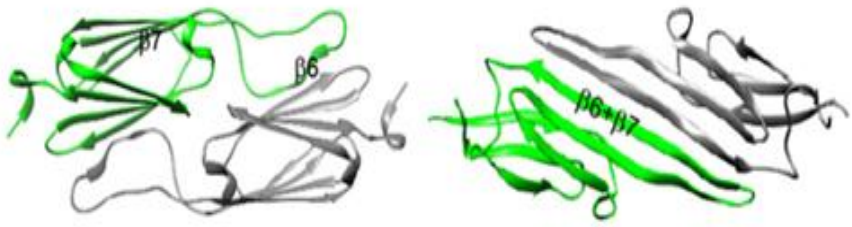

Figure 1.2. β6 dimer of the ACD of MjHsp16.5 on X-ray crystallograpghy (left) and β7 dimer structure of the ACD of αB-crystallin (right) (Haslbeck et al., 2015)

1.1.3. Oligomerization of Small Heat Shock Proteins

Most of the sHSPs exist as oligomeric structures in their native state. One of the typical properties of sHSPs is their organization into large, sphere-like structures mostly comprising 12 or 24 subunits (Haslbeck *et al*., 2008). Oligomerization is intervened by C-terminal domain of a dimer and ACD of adjacent dimer. The stabilization of oligomers is provided by N-terminal domain interactions (Jovcevski *et al*., 2018). Therefore, all three domains are required for oligomerization.

The dimeric structure of αB-crystallin from human is illustrated in Figure 1.3. The interactions in the dimer interface occur between β6-strand and β7-strand of each subunit, arranged in an anti-parallel fashion (Delbecq et al., 2012). In assembly of the oligomeric structures, IXI motif binds in a hydrophobic groove formed between the β4- and β8-strands on the alpha-crystallin domain of a adjacent dimer This binding leads to the higher level of organizations of subunits and further assemble into oligomers through the interactions with N-terminal domain (Haslbeck and Vierling, 2015 and Treweek *et al*., 2015).

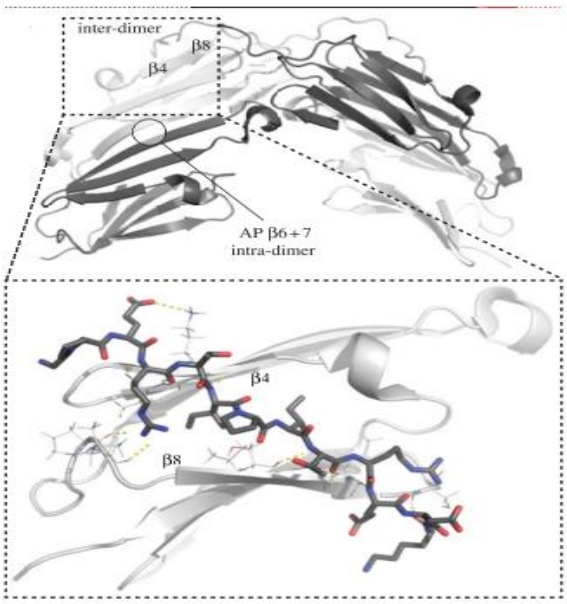

Figure 1.3. Crystal structure of the truncated αB-crystallin (Hilton et al., 2013)

1.1.3.1. The Role of Alpha-Crystallin Domain

The highly conserved α-crystallin domain from different organisms consists of roughly 80 amino acids (Basha *et al*., 2012; Haslbeck *et al*., 2015). The observations of three-dimensional structures of isolated α-crystallin domains have pointed out that the ACD is involved in formation of the dimeric structure (Bagneris *et al*., 2009). Besides, the role of ACD in oligomerization and chaperone activity has been demonstrated in several mutagenesis studies (Moutaoufik *et al*., 2017). Recently,

highly conserved three arginine residues (at positions 122, 131 and 135) in the ACD of the Hsp27 from *Drosophila melanogaster* were replaced with glycine. These mutations resulted in the increase of the size of oligomeric complex. The chaperone activities of such mutants of Hsp27 were measured by using insulin and luciferase as client proteins. The ability of mutant and wild-type proteins to prevent thermal aggregation of luciferase was almost the same. However, insulin protection from aggregation because of the reduction of disulfide bonds was increased in R122G and R131G mutants under reducing conditions, while R135G mutant showed similar chaperone activity with the wild-type (Moutaoufik *et al*., 2017).

In another study, the effects of arginine mutations in ACD of Hsp22 from *Drosophila melanogaster* on its structure and function were investigated. Arginine residues at position 105, 109 and 110 were changed with glycine. Mutant proteins formed same or smaller oligomers than the wild-type protein. With different substrates (luciferase, insulin, malate dehydrogenase and citrate syntase), chaperone activities of wild-type and arginine mutants were found to be nearly same (Dabbaghizadeh *et al*., 2017).

1.1.3.2. The Roles of N-terminal Domain and C-terminal Domain

The importance of both N-terminal and C-terminal domain has been studied by their deletions or mutations in this region and then performing chaperone activity assays.

Dynamic changes or a lack of stability of N-terminal domain might cause obtaining poor information about high resolution structure of this domain (Basha *et al*., 2012; McDonald *et al*., 2012).

It has been proposed that the N-terminal region regulates oligomerization, subunit dynamics and substrate recognition, binding and interaction (Ghosh *et al*., 2006; Basha *et al*., 2006 and Jaya *et al.,* 2009). Site-directed mutagenesis performed on specific N-terminal domain phenylalanine residues in αB-crystallin from human showed that Phe 27 is involved in binding of unfolded substrate since the replacement of phenylalanine with arginine demolished chaperone activity of αB-

crystallin (Plater *et al*., 1996). In a different study with Hsp16.3 from *Mycobacterium tuberculosis*, it has been demonstrated that N-terminal domain has dual role in oligomerization and binding unfolded substrate directly (Fu *et al*., 2005). Although the exact role of N-terminal domain in oligomer assembly is still unclear, there are evidences that this domain has a key role in the stability and distribution of oligomers and displays thermodynamic function in oligomerization (Delbecq *et al*., 2015). Recently, Jovcevski *et al*. (2018) have studied on N-terminal domain of αB-crystallin by introducing mutations. Their results have showed that the residues 54-60 in the N-terminal domain is not essential for assembly of oligomer but is required for the stabilization of oligomers. In a different study, it has been shown that phosphorylation of N-terminal domain residues in Hsp27 and αB-crystallin increases the dissociation of oligomers into smaller molecules and decreases the chaperone activity (Ito *et al*., 2001).

It has been shown that N-terminal domain of a sHsp from pea makes multiple contacts with both malate dehydrogenase and luciferase during heat denaturation (Jaya *et al*., 2009). Several studies suggested that there are both low and high affinity binding sites on sHsps (Sathish *et al*., 2003). The combination of multiple binding sites of N-terminal domain may form the highest affinity interaction with substrate compared to the other regions of sHSPs.

Moreover, the deletion of the N-terminal or C-terminal of IbpA which is a sHSP from *E.coli* caused failure of the chaperone function (Strózecka *et al*., 2011). Similarly, the truncations of N-terminal domain of HspB6 and αB-crystallin resulted in decrease or loss of chaperone activity (Weeks *et al*., 2014; Mainz *et al*. 2015). Also, chaperone activity studies on the truncated versions of Hsp18.5 from *Arabidopsis thaliana* suggest that the N-terminal domain is required for substrate protection under heat-induced conditions (Basha *et al.*, 2013).

On the other hand, C-terminal region of the sHSPs assists in chaperone function and oligomer formation. C-terminal extension in some mammalian sHSPs has

solubilising function for both under stress conditions and unstressed conditions (Carver *et al*., 2017). Under stress, the role of C-terminal extension is to make more soluble the complex that sHps form with aggregated substrates. In another study, it has been shown that removal of C-terminal extension decreases chaperone activity and causes destabilization of protein (Lindner *et al*., 2000). The importance of C-terminal domain of Hsp14 from a thermoacidophilic archaeon, *Sulfolobus tokodaii* has been examined by mutagenesis studies. Their results indicated that the hydrophobicity and size of aminoacids in the IXI motif play an important role in both oligomerization and the maintenance of secondary structure and hydrophobicity (Saji *et al*., 2008).

Furthermore, the point mutations on the C-terminal domain of αB-crystallin cause changes in oligomeric distribution and dynamics of subunit exchange. It was suggested that such mutations in C-terminal domain influenced the strength of quaternary dimer interfaces within the oligomers and their associated dynamics (Hilton *et al*., 2013).

In summary, molecular modelling, mass spectrometry, cryo-electron microscopy and small angle X-ray scattering have provided important structural informations about sHSPs, mainly their ACDs (Baldwin *et al*. 2011; Jehle *et al*. 2009). However, the functional and structural roles of N-terminal domain and C-terminal domain and their relationship with ACD to define the overall quaternary arrangement still remain unclear.

1.1.4. The Importance and Roles of sHSPs in Diseases

The sHSPs are involved in many cellular events such as the cell cycle, cell differentiation, cell death, signal transduction and the transformation of the cell into malignant state (Carra *et al*., 2017). They have anti-apoptotic activitiy and anti-inflammatory features (Bakthisaran *et al.,* 2015). As a result, misfunction of sHSPs or mutations in their genes results in the several diseases including various types of

cancer, eye lens cataract, myopathies and neurodegenerative disorders (Carra *et al*., 2017).

There are ten sHSPs in human named HspB1 to HspB10. They are classified into two groups. Class I includes Hsp27 (HspB1), αB-crystallin (HspB5), Hsp20 (HspB6) and Hsp22 (HspB8). Class II comprises HspB2, HspB3, αA-crystallin (HspB4), HspB7, HspB9 and HspB10. Class I sHSPs are widespread and located in numerous tissues. They are mostly induced by heat and involved in the survival of cell. On the other side, Class II sHSPs are associated with the cell differentiation and specilization for tissue-specific roles (Bakthisaran *et al.,* 2015). These roles of sHSPs provide several important implications in health and disease circumstances.

Mutations occured naturally can change their structure and/or chaperone activity and cause many diseases. For instance, the members of the sHSP family, α-crystallins (αA-crystallin and αB-crystallin) are primary lens structure proteins in the vertebrate eyes. Among sHSPs, the α-crystallins of eye lens are the most studied structurally and functionally (Horwitz, 2009). The α-crystallins provide lens transparency by preventing crystallin aggregation. Mutations in their genes cause lens crystalline and cytoskeleton aggregation (Clark *et al.* 2012). For example, congenital cataract is a result of mutation in αA-crystallin. The replacement of arginine at position 120 with glycine (R120G) is not only associated with cataract but also myopathies in human (Clark *et al.,* 2011; Andley *et al.,* 2011). On the other hand, the mutation of arginine to glycine of αB-crystallin cause cardiac arrhytmias in mice (Jiao *et al*., 2014). For example, it has been reported that R157H and G154S mutations in C-terminal region of αB-crystallin cause dilated cardiomyopathies (Inagaki *et al*., 2006). Also, αB-crystallin is especially expressed at high levels in the neurons and glial cells in various neurodegenerative dieases including Alzheimer's disease, Parkinson's disease and Huntington's disease (Carra *et al*., 2013; Treweek *et al*., 2015).

Also, sHSPs such as Hsp27 and αB-crystallin have been reported to be associated with the pathogenesis of cancer and multiple sclerosis. Patients with multiple sclerosis have many demyelinated plaques in their brain and spinal cord. αB-crystallin is found abundantly in these plaques (Han *et al.*, 2008). Hsp27 has been reported to be found at high amounts in metastatic tissues (Arrigo *et al*., 2007 and Moyano *et al*., 2006). For this reason, it has been suggested that Hsp27 and αB-crystallin might be the therapeutic targets (Arrigo *et al*., 2007).

Arginine residues have important roles in the organizations and chaperone activities of the sHSPs (Panda *et al*., 2016). It has been documented that mutations at highly conserved arginine residues of ACD in sHsps of mammalian are related to various diseases in different parts of the human body.

1.1.5. Chaperone-Like Functions of Small Heat Shock Proteins

The sHSPs from diverse organisms function as molecular chaperones by binding misfolded proteins and protecting them from aggregation in ATP-independent manner. They interact with partially unfolded substrates and refold them to functional state. They have high capacity of substrate binding. Different models have been suggested to explain the mechanism of action for sHSPs (Haslbeck *et al*., 2005).

The chaperone activity was first studied for α-crystallin preventing aggregation of β-crystallin, γ-crystallin and alcohol dehydrogenase under heat shock (Horwitz, 1992).

Figure 1.4 demonstrates the most favored model for the chaperone action of a small heat shock protein under heat shock. During stress, when substrates are destabilized and start to unfold, sHSPs bind to hydrophobic sites of these misfolded substrates in an ATP-independent way and keep them in folding state. sHSPs exist as ensembles of oligomers. These sHSP oligomers are activated by dissociation of oligomeric form into smaller species such as dimers. This alteration in the conformation of the sHSP enhances the exposure of its hydrophobic surfaces. Misfolded proteins are stabilized by these activated sHSP and captured in soluble sHSP/substrate

complexes. Then, sHSP-bound substrates are refolded by ATP-dependent chaperones or degraded by the cellular degradation pathway (Roman *et al*., 2015).

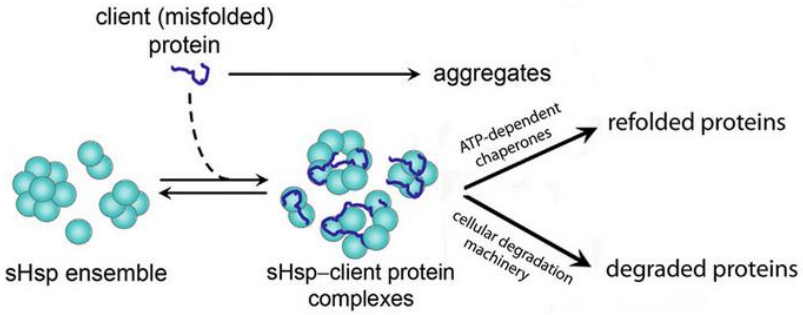

Figure 1.4. Model mechanism for chaperone activiy of sHSP (Roman *et al*., 2015).

sHSP/substrate complexes have been analyzed by mass spectrometry and electron microscopy (Stengel *et al*.,2010; Cheng *et a*l., 2008). It has been revealed that the sHSP/substrate complexes are distinct assemblies which are larger than the sHSP oligomers without the substrate.

Zhang *et al*. 2015 have suggested a different mechanism to explain how Hsp17 from *Caenorhabditis elegans* is activated for binding substrate proteins. The main properties of this mechanism are as follows: The Hsp17 exists as 24-mer spherical oligomers at low temperatures. It does not display chaperone-like activity. It has been thought that the unavailability of the buried N-terminal region that is involved in the substrate-binding might cause this. When the temperature increases, the spherical oligomers are converted into sheet-like super-molecular assemblies which exhibit chaperone-like activity. Thereby, the buried N-terminal region becomes accessible in the super-molecular assemblies and allows binding of substrate proteins (Zhang *et al*., 2015).

In this thesis project, *Picrophilus oshimae* which is the most acidophilic organism currently known has been used as the model organism.

1.2. Hyperacidophiles

Acidic environmets are formed by geothermal processes such as volcanic activity. Ferrous iron and reduced form of sulfur are found abundantly in such environments. Volcanic sulfur is oxidized to sulfuric acid and sulfuric acid is more concentrated by the evaporation of water (Nancucheo and Johnson, 2010).

Archaea represents the third kingdom of life which is evolutionarily separate from the Bacteria and Eucarya (Woese *et al*., 1990). Most Archaea which can survive under extreme conditions such as low pH, high temperature or high concentration of salt are named as extremophiles. Archaea which live at low pH is referred as ‘‘acidophiles’’.

Acidophiles live at low pH less than pH 3. These organisms must maintain pH homeostasis between the extracellular environment and cytoplasm to survive at low pH. For the maintenance of pH homeostasis, the cytoplasmic pH of acidophiles must be close to neutral (Baker-Austin and Dopson, 2007; Matin, 1990). Acidophiles have positive inside membrane potential formed by the entry of potassium ions, which blocks the entry of proton into the cell. A large pH gradient results in a proton motive force which is reduced by a positive inside reversed membrane potential. An acidophile with a near neutral cytoplasm separated from acidic environment undergoes a proton motive force across the membrane that can drive energy dependent processes.

Several members of acidophiles are classified in the orders Sulfolobales (Crenarchaeota) and Thermoplasmatales (Euryarchaeota), the phylum Acidobacterium (Bacteria), *Acontium cylatium* (fungi), *Cyanidium caldarium*, and *Dunaliella acidophila* (https://serc.carleton.edu/microbelife/extreme/acidic). The first thermoacidophilic archaea isolated in 1970s are *Thermoplasma acidophilum* and *Sulfolobus acidocaldarius* (Darland *et al*., 1970; Brock *et al*., 1972). Thermoacidophilic archaea isolated later were classified into the orders *Sulfolobales* and *Thermoplasmatale*s. They grow at a pH range of 1.0-5.0, optimally at pH 3.0.

Thermoplasma volcanium which belongs to *Thermoplasmatales* is more acidophilic. It grows at pH between 0.8 and 4 with an optimum at pH 1.0-2.0. The another genus of *Thermoplasmatales* is *Picrophilus* which has two different species; *Picrophilus torridus* and *Picrophilus oshimae* (Schleper *et al*., 1995). *P.torridus* and *P.oshimae* were isolated from solfataric hydrothermal fields in Hokkaido, Northern Japan (Schleper *et al*., 1995). *P. oshimae* is one of the most thermoacidophilic organism capable of surviving at very low pH, which grows optimally at pH 0.7 and at 60°C (Schleper *et al*., 1996). *P.oshimae* is the model organism used in this thesis project.

1.2.1. General Adaptation and Resistance Mechanisms to Acidic Environment

Acidophiles use several mechanims to resist low pH for providing pH homeostasis in the cells illustrated in Figure 1.5:

(i) Many acidophiles have highly impermeable cell membranes to restrict proton entry into the cell. Acidophiles reverse the membrane potential to reject proton entry by the help of potassium-transporting ATPases (Figure 1.5 i).

(ii) Proton entry can also be decreased by the generation of a inside positive membrane potential produced by Donnan potential. Donnan potential is the difference in electrical potential that is produced when the entry of potassium ions is more excess than the outflow of protons (Fütterer *et al*., 2004) (Figure 1.5 ii).

(iii) Another mechanism for pH homeostasis is the removal of the excess protons from the cytoplasm (Figure 1.5iii). Transporters export protons to maintain pH gradient. The pH gradient is produced by active proton pumping, via both primary and secondary transporters. The genome sequence analysis has demonstrated that acidophiles have a large amount of the genes encoding for secondary transporters (Baker-Austin and Dopson, 2007).

(iv) In addition, the buffering capacity of the cytoplasm by use of secondary transporters to seize or deliver protons might be an adaptation mechanism for pH homeostasis (Figure 1.5 iv).

(v) Specific enzymes or small molecules such as amino acids (histidine, arginine and lysine) that are able to seize protons contribute to such buffering capacity (Zychlinsky and Matin, 1983) (Figure 1.5 v). For instance, the decarboxylation of arginine and glutamate in *E.coli* is associated with the cell buffering through consuming protons that are then removed from the cell (Krulwich *et al*, 1985; Rius and Loren, 1996).

(vi) DNA and proton repair systems might be needed as an adaptation mechanism to survive at acidic environments (Figure 1.5 vi). Comparative genome analysis proposed that many acidophiles such as *Picrophilus torridus* have a multitude of DNA and protein repair genes in their genomes (Crossman *et al*., 2004; Fütterer *et al*.,2004 and Schäfer *et al*., 2004).

(vii) Organic acids that act as uncouplers in acidophiles can be degraded by acidophiles (Figure 1.5 vii). Uncouplers are synthetic, uncharged compounds that diffuse bilayers easily. Organic acids such as lactic acid or acetic acid damage the acidophiles since they act as uncouplers of respiratory chain at low pH. Thus, for the maintenance of pH homeostasis, organic acid degradation mechanisms might be used by the acidophiles (Ciaramella *et al*., 2005).

On the other hand, the genomes of acidophiles have a numerous pyrimidine codons. These pyrimidine codons are less sensitive to acid hydrolysis. This also makes cell membrane more durable for acidic environment (Paul *et al*., 2004; Baker-Austin and Dopson, 2007).

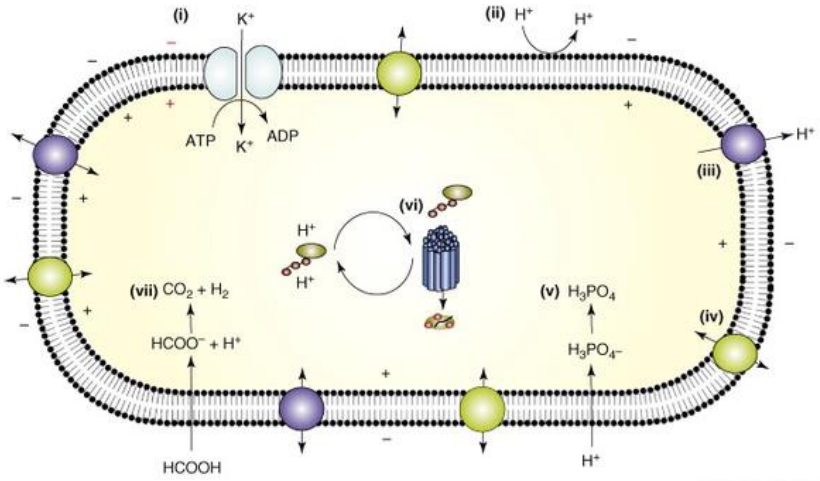

Figure 1.5. Mechanisms of pH homeostasis in acidophiles (Baker-Austin and Dopson,2007)

1.2.2. Protein Adaptations in Acidophilic Archaea

Acidophiles and thermophiles are clustered together since they share genome similarities, and most acidic environments are also hot (Reed *et al*., 2013). As a result, acidophilic proteins also display thermophilic adaptations (Sharma *et al*., 2012). Hydrophobicity has an important role in protein stability and protein folding at high temperature. Tight packing of hydrophobic core might be considered as an adaptation mechanism for also most acidophiles due to their thermophilic features (Reed *et al*., 2013).

Many polar charged aminoacids are protonated at acidic pH. This might cause the disruption of structural interactions and misfolding of the protein. So, acidophilic proteins should have adaptations to acidic pH. Increased basic residues on the protein surface and buried acidic residues inside create a highly positive surface charge. It has been suggested that this might be a structural adaptation for low pH conditions (Francois *et al*., 2006). Proteomic studies on acidophiles have revealed that an increase in hydrophobic residues on the protein surface might support their acid stability (Ciaramella *et al*., 2005). On the other hand, their activities at low pH seems

to be referred to the frequency of acidic (negatively charged at a neutral pH) amino acids on the surface of these acidophilic proteins (Reed *et al*., 2013).

Comparison of genomes of the genera *Picrophilus*, *Thermoplasma* and *Sulfolobus* has disclosed that several features contribute to their ability to survive at high temperature and low pH. These organisms have some enzymes which show high activity at pH less than 3 and above 80°C. For example, a highly acidophilic and thermophilic endo-β-glucanase from *S.solfataricus* has been observed to be optimally active at pH 1.8 and 80°C (Huang *et al*., 2005). The α-glucosidase from *Ferroplasma acidiphilum* is another example for low pH activity with optimum activity at pH 3 (Golyshina and Timmis, 2005).

However, all proteins of acidophiles do not show stability at low pH since the intracellular pH is not as low as external environment. For example, ATP-dependent DNA ligase from *F. acidarmanus* shows optimum activity at more neutral (pH 6-7) environment. This might be associated with the substrate of the enzyme; DNA has reduced the stability at low pH.

In addition, iron proteins which are found in high amount are also contributory to acid stability since they behave as iron rivet and protect the secondary structure of proteins at low pH (Baker-Austin and Dopson, 2007). The proteome of *Ferroplasma acidiphilum* have high proportion of iron proteins which might be associated with tolerance to live at low pH (Ferrer *et al*., 2007).

1.2.3. The Properties of Archaeal Membranes

The archaeal membrane lipids have different properties from bacterial and eucaryal membranes. Ether linkages available in archaeal membranes are less sensitive to acid hydrolysis when compared to the ester linkages in bacterial membranes.

An essential feature of acidophilic archaea including *P.oshimae* is that the membrane layer comprises of almost 100% glyceroldialkyl-glycerol-tetraether lipids which built a strong membrane monolayer (Macalady *et al*., 2004). There is a strong

association between tetraether lipids and tolerance to acid gradients (Golyshina *et al*., 2005). Elferink *et al*. (1994) have studied liposomes derived from glyceroldialkyl-glycerol-tetraether and showed that monolayer membranes are highly impermeable to protons. Cyclopentane rings that enhance the durability of membrane are also components of monolayer membranes of thermoacidophilic archaea and might be associated with acidophibicity (Schleper *et a*l. 1995; Macalady *et al*. 2004). Chugunov *et al*. (2014) demonstrated that methyl groups provide higher permeability to membrane with respect to the membrane spanning lipids withouth methyl groups. This may explain why membrane spanning tetraether lipids do not exist in the most acidophilic bacteria (Chugunov *et al*., 2014; Siliakus *et al*., 2017).

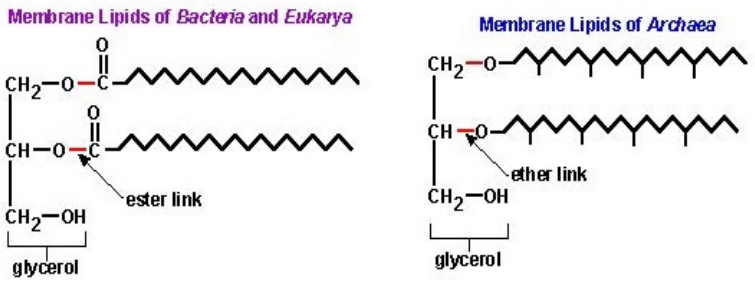

Figure 1.6. Membrane lipids of bacteria, eukarya and archaea. Bacterial and Eukaryotic membranes comprises of unbrached fatty acid chains bound to glycerol by ester bonds. Archaeal membranes have branched hydrocarbon chains bound to glycerol by ether bonds.

Also, it has been shown that a large isoprenoid core that contains ether bounds with glycerol contributes to the low proton permeability of archaeal membrane (van de Vossenberg *et al*., 1998; Yamauchi *et al*., 1993). In addition to it, their membrane structures are kept together by noncovalent bonds such as van der Waals and coulombic interactions which might be important for the impermeability of cell membranes (van de Vossenberg *et al*., 1998). These characteristics make archaeal membrane more durable to be able to survive at extreme conditions.

Besides above mentioned features of the acidophilic archaea, pore size of the membrane channels is also important for maintenance of pH homeostasis. It has been observed that the membrane channels have smaller pore size in acidophiles (Amaro *et al*., 1991).

1.2.4. The Properties of Picrophilus species

Thermoacidophiles are only inhabited in Archaea. The thermoacidophilic archaeon *Picrophilus torridus* and *Picrophilus oshimae* belong to the order of *Thermoplasmatales* within the kingdom of *Euryarchaeota* (Schleper *et al*., 1996).

P.torridus and *P.oshimae* were isolated from two distinct solfataric hydrothermal fields in Hokkaido, Northern Japan. Both species are the most thermoacidophilic organisms capable of surviving at very extreme conditions. They can grow in 1.2 M sulfuric acid and their optimum growth temperature is 60°C & pH 0.7. They keep the internal pH at 4.6 while the outside pH ranging from 0.5 to 5 (Van de Vossenberg *et al*. 1998). When compared to the other acidophiles, this pH value is low, since the internal pH is above 6 in other extreme acidophiles (Peeples and Kelly,1995).

P.oshimae and *P.torridus* are heterotrophic microorganisms. Schleper *et al.* (1995) reported that *P.oshimae* grew heterotrophically and aerobically on 0.1 to 0.5% (optimally 0.2%) yeast extract which is utilized as carbon source, yielding cell densities of approximately $5x10^8$/ml. The addition of 1% glucose, sucrose or lactose led to a slight decrease in growth, however cultures reached higher cell densities around 10^9/ml having an increased viability. Thus, 1% glucose was added to yeast extract for continuous cultivations. Once the cultures reached higher cell densities, the addition of glucose, lactose, sucrose or casamino acids did not stimulate growth anymore. Under optimal conditions, their generation time was 6 hours (Scheleper *et al*., 1995).

16S rRNA is highly conserved during evolution and shows functional stability. Because of these features, 16S rRNA has been a significant phylogenetic marker to

specify the three domains of life (Woese *et al*., 1990). The phylogenetic tree of 16S rRNA from Archaea is shown in Figure 1.7. Analysis of 16S rRNA sequences have revealed that the closest neighbour of *P.oshimae* and *P.torridus* is *Thermoplasma acidophilum*. There is 9.5% difference between the 16S rRNA sequences of Picrophilus species and *Thermoplasma acidophilum*. 16S rRNA sequence of *Picrophilus oshimae* is about 3% different from the sequence of *Picrophilus torridus.*

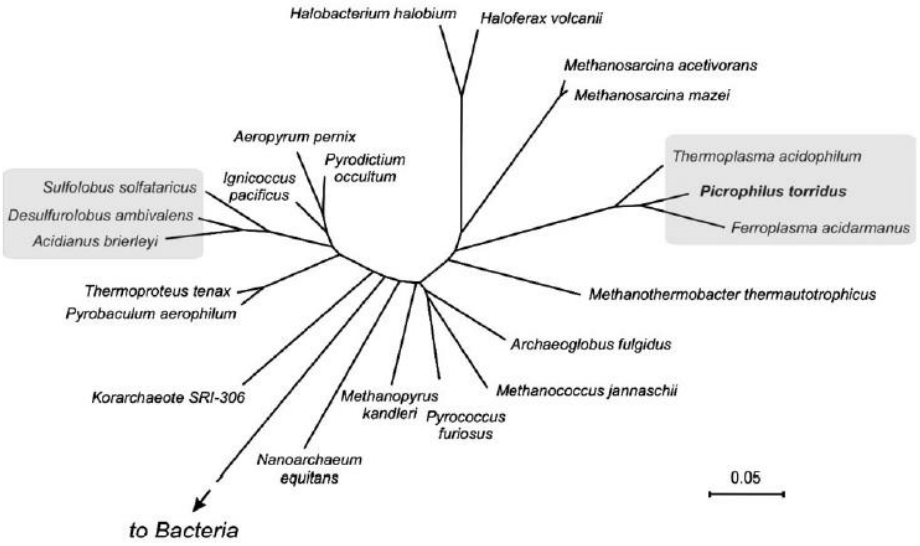

Figure 1.7. The phylogenetic tree of 16S rRNA from Archaea. Two groups of thermoacidophiles are highlighted. Data from Fütterer *et al*., 2004

1.2.4.1. Morphology of Cells

The cells are disorganized cocci with a diameter of around 1 to 1.5 µm diameter, like *Thermococcus* and *Pyrococcus* cells. In exponentially growing cultures, various duplex and triplex formations of cells were observed as shown in Figure 1.8B. In electrograph of thin segments, large gaps which are similar to vacuoles were observed in the cells (Figure 1.8A).

P.oshimae and *P.torridus* share similar physiological characteristics and they cannot be distinguished morphologically. The cells have an envelope which forms a S-layer located on top of the cytoplasmic membrane. This S-layer consists of an outer compact segment and almost empty inner segment. It has tetragonal crystal structure which resembles a filigree with a pattern of openwork (or wirework). S-layer probably contains long polysaccharide chains on the outside. There is no flagella or pili observed (Schleper *et al*., 1995) (Figure 1.8C).

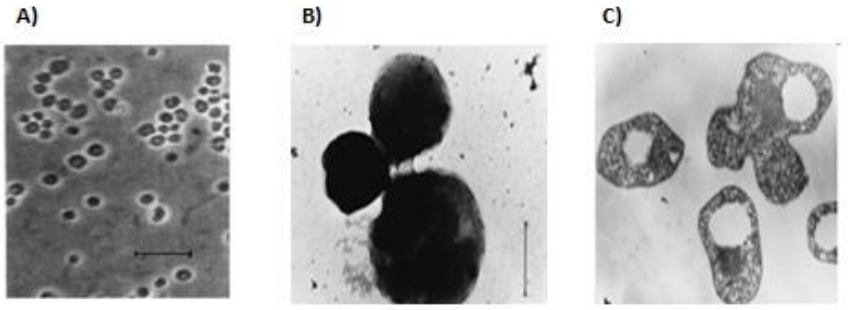

Figure 1.8. Morphology of *P.oshimae* cells. A) Phase contrast micrograph of *Picrophilus oshimae*. Bar = 5μm (Schleper *et al*.,1996). B) Electron micrographs of *P.oshimae*. Cells from a logarithmic culture, triplex formation. C) Thin part showing an S-layer and gaps buried. Bar = 1μm. (Schleper *et al*., 1995)

1.2.4.2. Genome Studies of Picrophilus Species

Originally *P.torridus* and *P.oshimae* were distinguished from each other by distinct *Eco*RI restriction patterns of their genomic DNA (Schleper *et al*., 1995).

P.oshimae contains a linear chromosome. Recently, the results of whole genome shotgun sequencing project has been published (J Varghese, 2017). Total genome size of *P.oshimae* is 1,534,155 bp. It has the smallest genome among the thermoacidophile groups. Its genome contains 1623 genes, 44 pseudogenes, 3 ribosomal RNAs, 46 transfer RNAs and 2 non-coding RNAs. The number of protein encoding gene sequences is 1530, of which enzymes, transmembrane proteins are constituting 36 and 22%, respectively. The GC content in the genome of *P.oshimae*

is 36 mol%, and the coding density is 93%. This data was obtained from online database of NCBI.

Two distinct plasmids were observed in the strains of *P.oshimae*. In the strain DSM 9789, these plasmids are approximately 8.3 kbp and 8.8 kpb in length and partially homologous plasmids. However, plasmids are not found in all strains (Schleper *et al*., 1995). pPO1 plasmid has been mobilized from *P.oshimae* by introducing origin-containing transposons. The whole sequencing of the pPO1 plasmid revealed that the pPO1 plasmid is a circular molecule with 7646 bp length (GenBank accession number JN032732). GC content of this plasmid is 30.5%. The nucleotide sequence of pPO1 plasmid did not have any homolog region to the *P.torridus* and to plasmids of the other archaea. Until the study of Angelov *et al*. (2011), Picrophilus species did not have any cloning or transformation method. Apparently, pPO1 plasmid encodes for the restriction and modification systems and recombinase enzyme. It was observed that the open reading frames of this restriction or modification system share homologs with the bacteria (Angelov *et al*., 2011).

1.2.4.3. Transport Systems

12% of all genome of (170 ORFs) *P.torridus* encodes transport proteins including both primary and secondary transporters. This gives a clue about that *P.torridus* is highly depended on transporters for the survival (Angelov and Liebl, 2006). Primary transporters also named as ABC (ATP-binding cassettes) transporters utilize ATP to drive transport while secondary transporters utilize the transmembrane potential. Sodium-proton pump (Na^+/H^+ pump) which is a secondary transporter transports Na^+ ions into the cell and H^+ out of the cell to drive transport. The common usage of the transmembrane proton gradient is predictable due to the presence of a large proton gradient in acidophiles. The another transport system, K^+-transporting ATPase which is an ABC transporter is associated with the lifestyle of *Picrophilus* species. The major function of this transport system is likely to keep intracellular pH near neutral and provide pH homeostasis. This is achieved by taking K^+ to

reverse membrane potential to inside positive (She *et al*., 2001). Transporters are involved in the detoxification of the cells and found for peptides, inorganic elements and sugars in *P.torridus*. 34 ORFs are required for the uptake of aminoacids and peptides while 32 ORFs are involved in uptake of sugars. 21 transporters are thought to be found in drug efflux system which is involved in drug resistance (Fütterer *et al*., 2004).

1.2.4.4. Energy Metabolism

P.torridus should produce large amount of metabolic energy to keep intracellular pH near neutral. It has been reported that only glucose and galactose could be respired by *P.oshimae* cells (van de Vossenberg *et al*., 1998).

Glucose is metabolized by a nonphosphorylated alternative of the Entner-Doudoroff pathway in *P.torridus* (Reher and Schönheit, 2006). In the first step of this pathway, glucose dehydrogenase oxidizes the glucose to gluconate. The following dehydration catalysed by gluconate dehydratase produces 2-keto-3-deoxy-gluconate. KDG is cleaved to pyruvate and glyceraldehyde. Then, a glyceraldehyde dehydrogenase reduces $NADP^+$ and glyceraldehyde is oxidized to glycerate. Glycerate is phosphorylated to 2-phosphoglycerate by a glycerate kinase. Further, an enolase converts 2-phosphoglycerate into phosphoenolypyruvate and then a pyruvate kinase converts it to pyruvate.

P.torridus seems to have genes for tricarboxylic acid cycle. Acetyl-CoA is produced from pyruvate by a NAD^+-dependent pyruvate dehydrogenase which reduces NAD^+ to NADH (Fütterer *et al*., 2004). After that, oxidative phosphorylation occurs, which leads to production of ATP.

Besides glucose, *P.torridus* employs this pathway for the usage of galactose. It has been considered that it can be valid for many archaea. There are some evidences which support this idea of dual specifity of glucose dehydrogenase from *P.torridus* (Angelov *et al*., 2005). Glucose dehydrogenase of *S.solfataricus* also catalyzes both

the oxidation of glucose to gluconate and galactose to galactonate (Lamble *et al*., 2003,2004).

In addition to carbohydrates, amino acids can be used as energy source by *P.oshimae*. It was reported that the highest respiration rate was observed in the presence of yeast extract or the mixture of amino acids, casamino acids or individual amino acids such as proline, leucine and glutamate (van de Vossenberg *et al*., 1998).

1.2.5. Extremozymes Purified from Picrophilus Species

Extremozymes are enzymes which are purified from extremophiles. The production of these heat- and acid-stable enyzmes are important in multiple industrial area including food, textile, cosmetic and pharmaceutical industries.

After complete genome analysis of *P.torridus*, genes encoding amylolytic enzymes, esterases and proteases were identified (Scheper *et al*., 2006; Hess *et al*., 2008).

A novel intracellular glucoamylase enzyme from *P. torridus* was purified and characterized (Schepers *et al*., 2006). Optimal enzyme activity was detected at 50°C and pH 5.0. Similarly, extracellular glucoamylases from *P.torridus* and *P.oshimae* were purified (Serour and Antranikian, 2002). These glucoamylases were active at 90°C and pH 2.0. Their enzymatic activity was observed even at 100°C and pH 1.0.

They were thermostable at high temperature with a half-life of 24 h at 90°C for *P.torridus* originated enzyme, and 20 h at 90°C for *P.oshimae* originated enzyme.

A trehalose synthase gene from *P.torridus* was cloned and its gene product was purified (Chen *et al*., 2006). In the genome of *P.torridus*, no trehalase gene or trehalose-hydrolyzing genes were annotated. The purified recombinant trehalose might have a regulatory role in the control of intracellular amount of trehalose itself in *P.torridus*. Optimal activity of the purified recombinant trehalose synthase of *P.torridus* was observed at 45°C and at pH 6.0. High activity and stability was maintained up to 60°C and pH 5.0 (Schiraldi *et al*., 2002).

A hydrolytic γ-glutamyl transpeptidase was also purifed from *P.torridus*. Optimal enzyme activity was observed at 55°C and pH 7.0 (Rajput *et al*., 2013).

Other enzymes purified from *P.torridus* are as follows: 4-hydroxyphenylpyruvate dioxygenase, a putative mevalonate diphosphate decarboxylase, extremely thermostable esterase, aspartate racemase, α-glucosidase, α-mannosidase and pantothenate kinase (Frick *et al*.,, 2014; Rossoni *et al*., 2015; Hess *et al*., 2008; Aihara *et al*., 2016; Angelov *et al*., 2006 and Takagi *et al*., 2010).

1.3. Scope and Aim of The Study

In this thesis study, we have aimed to analyze substrate binding activity of a small heat shock protein from a thermoacidophilic archaeon *Picrophilus oshimae.* The gene encoding HSP20 family protein (poHSP20) has been cloned in pQE2 vector and overexpressed in *E.coli* host cells. By use of site-directed mutagenesis, point mutations (K99E and K99G) were introduced to improve its chaperone activity.

Wild-type and mutant proteins have been purified by Ni-NTA affinity chromatography and HPLC. Structural characterizations has been accomplished by size-exclusion chromatography.

Finally, chaperone activities of both wild-type and mutant proteins has been studied by using citrate synthase chaperone activity and aggregation assays.

3-D structure model of the wild-type poHSP20 protein was generated by using online Modeling and Analysis tools.

CHAPTER 2

MATERIAL AND METHODS

2.1. Materials

2.1.1. Chemicals, Enzymes and Kits

All chemicals used during these experiments were molecular biology grade and highest purity available.

Agarose, ethidium bromide (Et-Br), pig heart citrate synthase (CS), ampicillin, Tris, tetramethylethylenediamine (TEMED), lysozyme, isopropyl β-D-1-thiogalactopyranoside (IPTG), acrylamide, ammonium per-sulfate (APS), potassium chloride (KCl), calcium chloride dihydrate ($CaCl_2 \cdot 2H_2O$) were purchased from Sigma Aldrich® (Missouri, USA).

Sodium dodecyl sulfate (SDS), ethylenediaminetetraacetic acid (EDTA), glycin, potassium dihydrogen phosphate (KH_2PO_4), magnesium sulfate heptahydrate ($MgSO_4 \cdot 7H_2O$), ammonium sulfate $(NH_4)_2SO_4$, casein hydrolysate, sodium chloride (NaCl), sodium hydroxide (NaOH), β-Mercaptoetanol, and tryptone were purchased from Merck (Darmstadt, Germany).

Powder imidazole and agar were from Fluka Chemie AG (Switzerland). Yeast extract was bought from Difco (Detroid, USA).

Ethanol, methanol, and acetic acid-glacial were from Reidel de Häen (Germany).

Restriction enzymes, T4 ligase, and molecular size markers were purchased from Thermo Scientific (Massachusetts, USA).

QuikChange II Site-Directed Mutagenesis Kit was from Agilent Companies (California, USA).

The QIA*expressionist*™ Kit, QIAprep Spin Miniprep Kit, QIAquick Spin Gel Extraction Kit was from Qiagen (Hilden, Germany).

GeneJET Plasmid Miniprep Kit and GeneArt® Site-Directed Mutagenesis PLUS Kit were from Thermo Scientific (Massachusetts, USA).

2.1.2. Buffer and Solutions

The preparations of buffers and solutions used during this study are given in Appendix A.

All buffers and solutions were prepared in ultrapure water and sterilized in autoclave (ALP Co. Ltd., Tokyo, Japan).

2.1.3. Molecular Size Markers and Plasmid Vector

The pQE2 vector was purchased from Qiagen (Hilden, Germany). The map of pQE2 vector is given in Appendix B.

The molecular size markers for DNA are Generuler 50 bp DNA Ladder, Generuler 100 bp DNA Ladder plus, O'RangeRuler 200 bp Ladder, O'Range Ruler 500 bp marker and O'Gene ruler DNA Ladder mix. The molecular weight marker for protein is PageRuler Prestained Protein Ladder. They were purchased from Thermo Scientific (Massachusetts, USA). The images of markers are shown in Appendix C.

2.2. Strains and Growth Media

2.2.1. Archaeal and Bacterial Strains

Thermoacidophilic archaea *Picrophilus oshimae* was used as a model organism in these experiments.

Escherichia coli TG1 strain was from our laboratory collection, One ShotR MAX EfficiencyR DH5α™-T1R *Escherichia coli* competent cells provided by GeneArt® Site-Directed Mutagenesis PLUS Kit and XL1-Blue supercompenent *Escherichia*

coli cells provided by QuikChange II Site-Directed Mutagenesis Kit were used as a host in the transformation experiments.

2.2.2. Growth Medium and Culture Conditions

Picrophilus oshimae cells were grown (pH_{opt} 0.7 and T_{opt} 60ºC) in a Picrophilus Standard Medium supplemented with 5% yeast extract as a carbon source. The *Picrophilus* liquid culture was subcultured in every week.

Recombinant *E.coli* TG1 and XL1-Blue wt and mutant strains were grown on LB agar containing ampicillin (100 µg/ml) at 37ºC. The cultures were subcultured in every 30 days.

2.3. Methods

2.3.1. Cloning of Picrophilus oshimae Small Heat Shock Protein 20 (po-sHSP20) Gene in pQE2 Vector

The gene encoding the po-sHSP20 gene of *P.oshimae* chromosomal DNA was cloned into pQE2 vector at *Nde*I and *Pst*I restriction enzyme sites. For this purpose, a PCR based strategy was followed as explained below.

2.3.1.1. Primer Design for PCR Amplification

Amplification primers were designed based on the homology between thermoacidopilic archaea *Picrophilus torridus*. The sequences of primers were given in Table 2.1.

Table 2.1. The sequences of forward and reverse primers for PCR amplification of the po-sHSP20 gene

The name of primer	**The sequence of primer**
Forward primer	5'-TGAGCATATGCAGATGTACAGACCATTAAAATTCTATTCG-3'
Reverse primer	5'-GGATATCAATGGATGCCTTGCAGAGAAGCTGCAGCTGA-3'

2.3.1.2. PCR Amplification of po-sHSP20 Gene

PCR amplification was performed with the forward and reverse primers, using *Picrophilus oshimae* chromosomal DNA as template. Total volume of reaction mixture was 100 µl. Reaction mixture was prepared with Taq buffer [$(NH_4)_2SO_4$-$MgCl_2$], 25 mM $MgCl_2$, 100 pmol of each primers and 10 mM deoxyribonucleoside triphosphate (dNTP) mixture. Sterile milli-q H_2O was used for completing total volume to 100 µl. Samples were pre-incubated at 94°C for 5 min. before adding Taq DNA polymerase. Reactions were performed with 30 cycles of amplifications in a thermal cycler (Techgene, Techne Inc. NJ. USA). The parameters of thermal cycling were given in Table 2.2. Temperature of storage was 4°C.

Table 2.2. *The parameters of thermal cycling*

Steps	**Temperature**	**Time**
Denaturation	94°C	1 min.
Annealing	55°C	2 min.
Extension	72°C	3 min.
Final extension	72°C	10 min.

2.3.1.3. Purification of DNA Fragments From Agarose Gel

After PCR amplification, QIAquick Spin Gel Extraction kit was used to purify the PCR products from 1% agarose gel, following the Manufacturer's protocol (Qiagen).

2.3.1.4. Digestion of PCR Amplicons and pQE2 Vector

Gel extracted PCR amplicons and pQE2 vector were digested with *Nde*I and *Pst*I restriction enzymes.

Firstly, PCR amplicons and pQE2 vector were double digested with *Nde*I and *Pst*I according to the instructions of Manufacturer. Then, digested products were purified by using QIAquick Gel Extraction Kit (Qiagen).

2.3.1.5. Ligation and Transformation into *E. Coli* TG1 Competent Cells

Purified PCR fragments and pQE2 vector were ligated by using T4 Ligase (Thermo Scientific). The ligation mixture was transferred into TG1 competent cells according to the TSS protocol (Chung *et al*., 1989).

Putative recombinant colonies were randomly picked up, their plasmids were isolated and characterized.

2.3.2. Plasmid Isolation

Plasmids were isolated by using QIAprep Spin Miniprep Kit (Qiagen, Germany) and a microcentrifuge. The plasmids were isolated according to the instructions of kit protocol.

First, the bacterial overnight cultures were centrifuged at 4.500 rpm for 15 min. The pellet was resuspended in 250 µl of Buffer P1. 250 µl of Buffer P2 was added, and mixed. The mixture was incubated at room temperature for 5 min, and then, 350 µl of Buffer N3 was added and mixed by inverting. After that, the sample was centrifuged for 10 min. at 13.000 rpm. 800 µl of supernatant was applied to the QIAprep spin column and centrifuged for 1 min. at 13.000 rpm. The flow-through was removed. The column was washed by 500 µl of Buffer PB and 750 µl of Buffer PE, respectively. The flow-through was discarded. To remove residual wash buffer, the sample was centrifuged once more. DNA from spin column was eluted by adding of 50 µl of Buffer EB.

GeneJET Plasmid Miniprep Kit from Thermo Scientific was also used for plasmid isolation in mutagenesis experiments and sequencing according to the Kit Protocol. The pellet was resuspended in 250 µl of Resuspension Solution and 250 µl of the Lysis Solution was added. After mixing, 350 µl of the Neutralization Solution was added and mixed by inverting. The sample was centrifuged for 10 min. Supernatant was transferred into the supplied GeneJET spin column, and then centrifuged for 1 min. The flow-through was discarded. Then, 500 µl of the Wash Solution was added

to the spin column. The sample was centrifuged for 1 min. After that, washing step was repeated. The flow-through was discarded. The sample was centrifuged again to remove residual wash buffer. DNA from spin column was eluted by adding of 50 µl of the Elution Buffer.

The concentrations and purities of plasmids were measured by picodrop (Picopet01, UK).

2.3.3. Plasmid Digestion by Restriction Endonucleases

Isolated plasmids were digested with various restriction endonucleases for checking the presence of cloned gene and characterization of it. *Nde*I and *Pst*I restriction enzymes were used for double digestion and *Hind*III and *Bgl*II enzymes were used for single digestion. Digestions were carried out according to the instructions of Manufacturer (Thermo Scientific).

2.3.4. Agarose Gel Electrophoresis

The DNA fragments were visualized on 1% agarose gel in 1X TAE buffer. The gel was supplemented with ethidium bromide (Et-Br 10 mg/ml). Samples were mixed with DNA loading dye at 1:10 ratio and loaded into gel. Electrophoresis was performed at 80 V and 80 mAmp (Bio-Rad 1000/500, Power Supply). The bands were visualized with Bio-Print imaging system (Vilber, France). The size markers used are given in Appendix C.

2.3.5. Site-Directed Mutagenesis by GeneArt® Site-Directed Mutagenesis Plus Kit

2.3.5.1. Designing of Mutant Primers

Mutagenic primers containing the desired mutation were designed according to the instructions of mutagenesis kit. Primer sequences for mutagenesis were listed in Table 2.3. Substitutions were indicated in bold.

Table 2.3. *The sequences of mutagenic primers*

The name of Primers	The sequence of mutagenic primers
K99G Forward Primer	5'-CCATCAAAGGTCTTT**GGG**AGGATACAGCTGCC-3'
K99G Reverse Primer	5'-GGCAGCTGTATCCT**CCC**AAAGACCTTTGATGG-3'
K99E Forward Primer	5'-CCATCAAAGGTCTTT**GAG**AGGATACAGCTGCC-3'
K99E Reverse Primer	5'-GGCAGCTGTATCCT**CTC**AAAGACCTTTGATGG-3'

2.3.5.2. The Synthesis of Mutant Strand

Firstly, reaction mixture containing 6 µl of 10X AccuPrime™ *Pfx* reaction buffer, 6 µl of 10X Enhancer, 20-25 ng of plasmid DNA, 1.2 µl of DNA methylase (4 U/µl), 2.4 µl of of 25X SAM and 1.5 units AccuPrime™ *Pfx* was prepared. Afterwards, the reaction mixture was divided into two PCR tubes on which 1 µl of the mutagenic primer mix were added.

After addition of primer mix, the methylation and amplification were carried out at the same time in a thermal cycler (Techgene, Techne Inc. NJ. USA) according to the parameters given in the kit. The conditions were optimized according to the length of plasmid.

Amplified PCR products were mixed in a recombination reaction mixture containing 2 µl of PCR products, 8 µl of PCR water and 10 µl of GeneArt 2X Enzyme Mix. They were mixed and incubated at room temperature for 15 min. Then, the reaction was stopped by addition of 1 µl of 0.5 M EDTA. They were kept on ice and immediately continued with transformation into DH5α™-T1R *E. Coli* cells.

2.3.5.3. Transformation into DH5α™-T1R *E. Coli* cells

Two 50 µl vial of One ShotR MAX EfficiencyR DH5α™-T1R competent cells were thawed on ice and 3 µl of each recombination mixtures was directly transfered into each vial of cells and mixed by tapping. Then, they were kept on ice for 15 min. Afterwards, they were incubated on 42ºC water bath for 30 seconds. After heat shock, they were kept on ice for 2 min. 250 µl of pre-warmed SOC medium was put

into test tubes and then, transformation mixtures were added into these test tubes. Aliquotes of mixtures were spread on LB agar plates containing ampicillin.

Then, the plates were incubated for overnight at 37°C. Next day, putative mutant colonies were counted and transformation efficiencies were calculated. Randomly picked up colonies were streaked on LB (+amp) agar for further characterization.

2.3.6. Site-Directed Mutagenesis by QuikChange II Site-Directed Mutagenesis Kit

Same primers listed in Table 2.3 were used for introduction of intended mutations into po-sHSP20 gene.

Mutant strand was synthesized with a thermal cycler (Techgene, Techne Inc. NJ. USA). Reaction mixtures were prepared with 5 µl of 10X Reaction buffer, 5-50 ng of plasmid dsDNA, 2.6 µl of each forward and reverse primers (125 ng) and 1 µl of dNTP mix. Total volumes of reactions were completed to 50 µl with ddH_2O. Then, 1 µl of *Pfu*Ultra HF DNA Polymerase (2.5 U/ µl) was added to each reactions. Thermal cycling was carried out using the suggested parameters in the kit's protocol.

After thermal cycling, amplification mixes were kept on ice for 2 min. And then, 1 µl of *Dpn*I enzyme was added to each reactions for digestion of parental dsDNA at 37˚C for 1 hour.

Then, 1 µl of *Dpn*I-digested DNA from each reactions were transferred into XL1-Blue supercompetent cells. After incubation on ice, transformation mixtures were kept at 42˚C water bath for 45 seconds. After that, they were kept on ice for 2 min. Then, we added 0.5 ml of NZY^+ broth to the transformation reaction mixtures. Transformation mixtures were incubated at 37°C for 1 hour with shaking at 250 rpm.

100 µl of each transformation reactions were spread on LB agar plates containing ampicillin (100 µg/ml). And then, plates were incubated at 37˚C for overnight. Next day, putative mutant colonies were counted and transformation efficiencies were calculated. Randomly selected colonies were then used in plasmid isolation.

2.3.7. Preparation of Cell Extract and Expression of po-sHSP20 Protein

The QIA*expressionist*™ kit from QIAGEN was used for the study of expression of the recombinant protein.

Firstly, cell extracts were prepared. The overnight cultures were added to 50 ml of prewarmed LB medium containing 100 μg/ml ampicillin. Then, they were grown at 37ºC with shaking at 300 rpm, until the optical density (OD600) had reached to 0.6 (Shimadzu UV-1601, Japan).

Then, IPTG was added to a final concentration of 1 mM into the culture to induce expression. The cultures were incubated for 5 hour at 37ºC with shaking at 300 rpm. After incubation, the cells were harvested by centrifugation at 4000x g for 20 min (Sigma 3K30, UK).

The pellets were solved in 6-8 ml of lysis buffer and incubated on ice for 30 min. Then, solutions were sonicated to lyse the cells by using a microtube probe and a sonicator (Jencons, USA). Afterwards, the lysates were centrifuged at 10.000 xg at 4ºC for 30 min (Sigma 3K30, UK), to obtain cell-free extracts.

2.3.8. Purification of Protein by Ni-NTA Affinity Chromatography

Since po-sHSP20 gene was cloned into pQE2 expression vector which introduced histidine tags to N-terminus, Ni-NTA affinity chromatography was performed in order to isolate pure protein.

As a preparation for purification, 2 ml of lysis buffer containing 10 mM imidazole, 2 ml of cell lysate, and 1 ml of 50% Ni-NTA agarose were mixed.

After incubation, the mixture was applied into the column. When the column set, flow through was collected in 1.5 ml eppendorf tubes. Then, the column was washed for 2 times with 4 ml of wash buffer. Protein was eluted six times with 0.5 ml elution buffer. Eluents were kept at -20°C.

Amicon® Ultra-4 Centrifugal Filter Units (Millipore) with a 10-kDa cutoff were used in order to concentrate the eluted protein.

2.3.9. Purification of Protein by High Performance Liquid Chromatography

Affinity chromatography was also performed by HPLC *Ä*KTA Prime System (Amersham Pharmacia Biotech, UK) using HisTrap FF 1 ml column. Firstly, the cell extract was filtrated by using 0.45 μm filtrate and 0.22 μm filtrate, respectively. At the beginning, the system was washed with 20% ethanol for 3 times. Then, ethanol was flushed out by System Wash Method and double-distilled water. This step was repeated for 7 times. Then, manual run was performed for cleaning the sample loop with ddH_2O for 6 min. Then, the HisTrap FF 1 ml column was connected and washed with ddH_2O until obtaining a straight line. After the column was washed, the column was equilibrated until obtaining a stable baseline. Flow was passed through the column. Afterwards, 10 ml of binding buffer was injected and 2 ml of sample was loaded. For the following steps of purification, ‘‘Method Template’’ program was used.

2.3.10. Heat Treatment of Cell Lysates

The cell lysates were incubated in water bath at 60-70ºC for 15 min in order to eliminate unstable host proteins. After heat shock, they were kept on ice for 30 min and then centrifuged at 25.000xg for 30 min (Sigma 3K30, UK). The supernatant was stored at -20ºC.

2.3.11. Size Exclusion Chromatography

Size exclusion chromatography was performed with Sephacryl S300 15/50 column in order to analyze the oligomeric state of po-sHSP20.

Firstly, the concentrations of pooled, filtrated proteins were measured by picodrop (Picopet01, UK). The column has already been equilibrated with sodium phosphate buffer. Then, 710 μl (0.142 mg) sample was applied into the column. By using sodium phosphate buffer as running buffer and a peristaltic pump, samples (0.88 ml)

were collected in total of 70 eppendorf tubes. The absorbance of each tube while fractions were being collected was recorded with UV spectrophotometer at 280 nm (Shimadzu UV-1601, Japan). After elution was completed, the column was washed with one column volume (53 ml) of sodium phosphate buffer and one column volume of 20% ethanol, respectively.

2.3.12. SDS-PAGE Gel Electrophoresis

Polyacrylamide gel electrophoresis was carried out with 12% separating and 5% stacking gels (Laemmli, 1970). PageRuler^{TM} prestained protein ladder from Thermo Scientific was used as a molecular weight marker. 10 µl of 2X SDS loading dye was mixed with 10 µl of sample. The mixture was incubated in boiling water for 5 min. to denature the protein. Then sample was kept on ice. Samples and 7 µl of molecular weight marker were loaded into the gel. Then, the running was performed by using Bio-Rad 1000/500 Power Supply, US.

Proteins were visualized by staining with Coomassie Brilliant Blue. Then, the gel was washed with destaining solution for removal of excess staining solution. The gel was visualized by Chemidoc^{TM} MP Imaging System, Bio-Rad (California, USA).

2.3.13. Enzymatic Assays for Determination of Chaperone Activity

Chaperone activities of both wild-type and mutant po-sHSP20 proteins were measured at 412 nm by using pig heart citrate synthase enzyme (CS) as a model substrate. Citrate synthase is a mesophilic enzyme whose activity is strongly decreased at 47˚C. The citrate synthase activity was determined by Srere *et al.* (1963). It catalyzes the conversion of oxaloacetic acid and acetyl-coenzyme A into citrate and coenzyme A. When the acetyl CoA is hydrolyzed, it forms CoA with a thiol group (CoaA-SH) which reacts with the 5-5'-dithiobisnitrobenzoate (DTNB) in the reaction mixture. This reaction results in the formation of 5-thio-2-nitrobenzoic acid (TNB) which was measured at 412 nm using UV/visible spectrophotometer with a temperature controlled cell holder (Shimadzu l601 UV/Visible Spectrophotometer, Shimadzu Analytical Co., Kyoto, Japan).

The activity assay was carried out at 35˚C, in the presence and absence of the sHSP as described before (Kocabiyik *et al*., 2012). Heat-denaturation of CS was achieved by incubating at 47˚C for 10 min in the presence (tests) and absence (negative control) of po-sHSP20 variants. As positive control, CS activity was measured without heat-treatment. The assays were run in replicates and repeated at least two times.

In order to determine effect of pre-heating on chaperone activity of the wild-type and mutant po-sHSP20 proteins, above mentioned assay was performed with chaperones preheated at 65˚C for 10 min. After preheat treatment, chaperone activity assay was carried out with CS at 47°C as described above.

2.3.14. Thermal Aggregation Assay For Determination of Chaperone Activity

CS thermal aggregation was monitored by measuring the light scattering at 320 nm at 45°C for 2 hours by using 96-well Microplate Corning 3631 and Multiskan GO Microplate Spectrophotometer (Thermo Scientific). The reaction mixture in each well contained 1.4 μM CS together with different volumes of po-sHSP20 protein with a molar ratio of 1:7 and 1:35 (CS:po-sHSP20) in 50 mM HEPES buffer. Experiments were run in replicates and repeated at least two times.

2.3.15. Bioinformatic Analysis of Gene and Protein Sequence

Restriction Mapper Version 3 was used for determination of cutting positions of restriction enzymes for both gene and pQE2 vector.

The cloned wild-type and mutant gene sequences were verified by DNA sequencing (GenScript, USA). The gene and aminoacid sequences of po-sHSP20 were obtained from NCBI (National Center for Biotechnology Information, US) for multiple sequence alignment.

3-D structure model of the wild-type po-sHSP20 protein was generated by using Modeling and Analysis online tools.

In order to analyze sequencing results, pair-wise and multiple sequence alignments were performed using Clustal Omega Program (https://www.ebi.ac.uk).

CHAPTER 3

RESULTS

3.1. po-sHSP20 Primary & 3-D Structure Analysis

The model was generated by using *Sulfolobus tokodaii* template. The 3D structure models of po-sHSP20 monomer and po-sHSP20 dimer are shown in Figure 3.1 and Figure 3.2, respectively. The structure was refined at a resolution of 2.40Å.

As revealed by, the model structure of po-sHSP20 monomer is a typical sHSP monomer which is composed of an alpha crystallin domain (colored by pink), a N-terminal domain (colored by red) and a C-terminal domain (colored by blue). Beta strands from β2 to β9 was illustrated with pink (Figure 3.1).

This predicted monomer contains nine β-strands in two antiparallel sheets which built the α-crystallin core domain. The ACD consists of a typical compact β-sandwich. One of β-sheet has β2, β3, β8 and β9 strands, the other β-sheet has β4, β5 and β7 strands. The β-sheets are connected by an inter-domain loop. β6-strand has been observed in a long exchange loop (connecting β5- and β7-strands) extending from the β-sandwich. N-terminal domain has a long and straight α-helix structure and C-terminal domain has a shorter coil structure. N-terminal α-helix (residues 1-44) has 44 aminoacids. The ACD (residues 44-127) comprises of 84 amino acids and C-terminal coil domain has 10 amino acids (residues 128-137). Figure 3.3 demonstrates a secondary structure prediction of po-sHSP20 dimer created by using *S.tokodaii* template. The length of N-terminal domain, ACD and C-terminal domain was determined. The residues of β-strands were shown in Figure 3.3.

A predicted dimer model is shown as a ribbon diagram in Figure 3.2. In order to differentiate two monomers, each po-sHSP20 monomers were illustrated with different colors. β-strands were labeled by starting from β2 to β9. Two po-sHSP20

monomers share same structure to form a symmetric dimer. All intermolecular hydrogen bonds, hydrophobic interactions and electrostatic interactions between two subunits of po-sHSP20 dimer are shown in Table 3.1 and Table 3.2. The ACD is involved in a homo-dimer formation by β6-strand exchanges between partner subunits. β6-strand of one monomer interacts with β2-strand of its equivalent monomer via hydrogen bonds to make a dimeric interface (Figure 3.2 and Table 3.1).

Table 3.1. *Intermolecular hydrogen bonds and hydrophobic interactions between two chains of po-sHSP20 dimer*

Intermolecular Hydrogen Bonds		**Intermolecular Hydrophobic Interactions**	
A chain	**B chain**	**A chain**	**B chain**
A:ARG80-B:ASP56(x2)	B:ARG80-A:ASP56(x2)	A:ARG93-B:PRO41	B:ARG93-A:PRO41
A:ARG93-B:ASP54(x2)	B:MET42-A:GLN92	A:TYR39-B:PRO41	B:TYR39-A:PRO41
A:MET42-B:GLN92	B:MET44-A:GLU90	A:PHE89-B:PRO104	B:PHE89-A:PRO104
A:MET44-B:GLU90	B:GLN46-A:THR87	A:PRO58-B:PRO58	
A:GLY59-B:ASP119	B:GLY59-A:ASP119	A:TYR45-B:LYS84	
A:PHE89- B:MET44	B:THR87-A:GLN46	A:PRO41-B:PRO94	
A:GLU90-B:MET44	B:PHE89-A:MET44		
A:GLN92-B:MET42	B:GLU90-A:MET44		
A:ARG93-B:ASP56	B:GLN92-A:MET42		
A:LYS99-B:GLN92	B:ARG93-A:ASP56		
A:TYR45-B:THR87	B:LYS99-A:GLN92		
A:ARG93-B:THR43	B:THR43-A:GLU90		
A:ARG93-B:ASP54	B:ARG93-A:ASP54		
	B:PRO94-A:ASP56		

Table 3.2. *Intermolecular electrostatic interactions between two chains of po-sHSP20 dimer*

Intermolecular Electrostatic Interactions			
A chain	**Type**	**B chain**	**Type**
A:ARG80-B:ASP56(x2)	Salt Bridge	B:ARG80-A:ASP56(x2)	Salt Bridge
A:ARG93-B:ASP54	Salt Bridge	B:LYS84- A:ASP54	Attractive Charge
A:ARG93-B:ASP56	Salt Bridge	B:ARG93- A:ASP54	Attractive Charge
A:ARG93-B:ASP56	Attractive Charge	B:ARG93- A:ASP56	Attractive Charge
A:ARG93-B:ASP54	Attractive Charge		

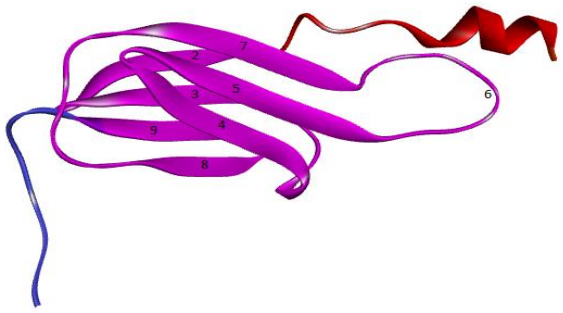

Figure 3.1. Three-Dimensional Structure of po-sHSP20 Monomer: Red color indicates N-terminal domain. Pink color indicates alpha-crystallin domain. Beta strands are labeled by starting from β2. Blue color indicates C-terminal domain.

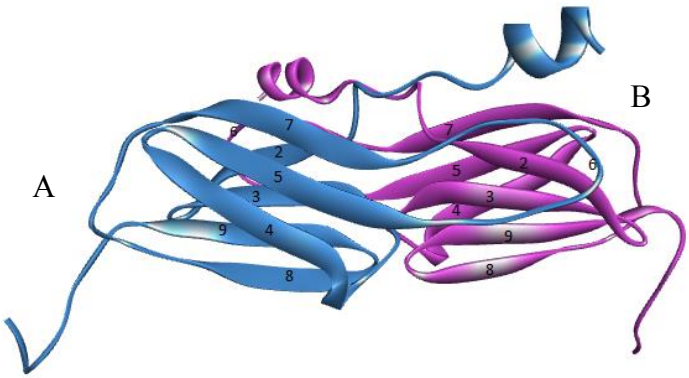

Figure 3.2. Three-Dimensional Structure of po-sHSP20 Dimer: A chain and B chain are colored by blue and pink. β-strands are labeled starting from β2 to β9. β6-strand places in the extended loop.

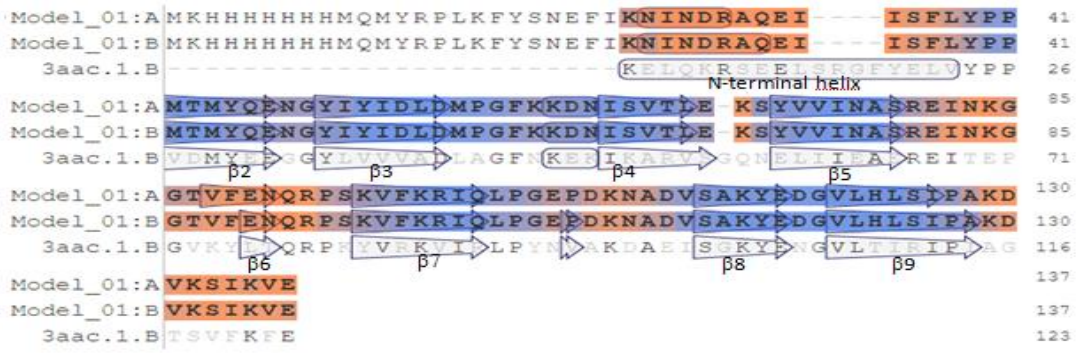

Figure 3.3. Secondary structure prediction of po-sHSP20 dimer. 3aac.1.B: *Sulfolobus tokodaii* template. Model_01:A: A chain of po-sHSP20 dimer. Model_01:B: B chain of po-sHSP20 dimer.

One of the residue in the ACD that contributes intermolecular hydrogen bonding is K99. Figure 3.4 demonstrates intermolecular hydrogen bond in the 3D model structure of po-sHSP20 dimer. Since, there are additional residues (11 residues) coming from pQE2 vector, K88 of *P.oshimae* sHSP without His-tag corresponds to K99 of po-sHSP20 with His-tag. In po-sHSP20 structure, Lys99 of one monomer makes hydrogen bond with Gln92 of other monomer (Figure 3.4).

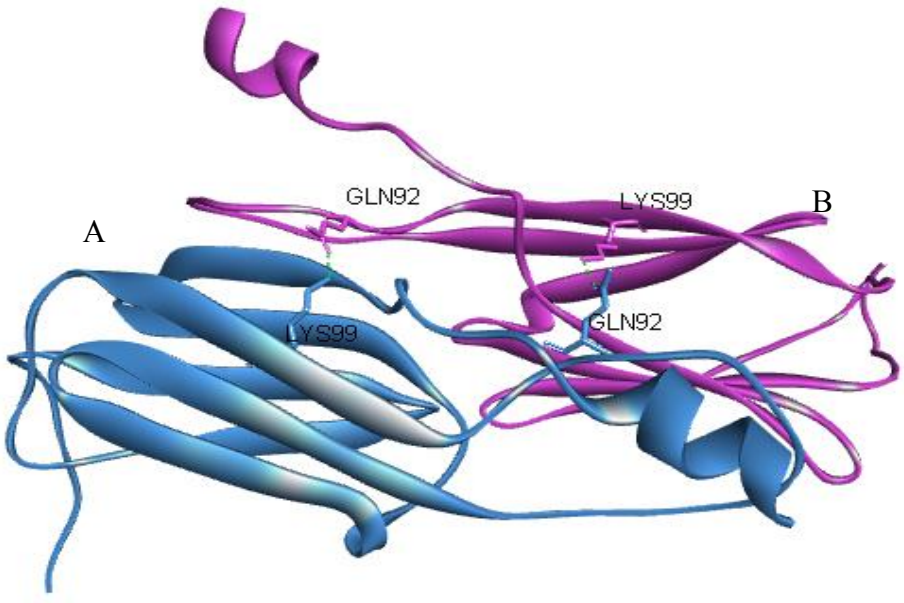

Figure 3.4. Intermolecular hydrogen bond between Lys99 of one chain and Gln92 of other chain.

Also, Lys99 makes intramolecular hydrogen bonds with Ile76 and Pro40 in A chain (Figure 3.5). On the other hand, in B chain, in addition to these bonds, there is an another intramolecular hydrogen bond of Lys99 with Leu38 (Figure 3.5).

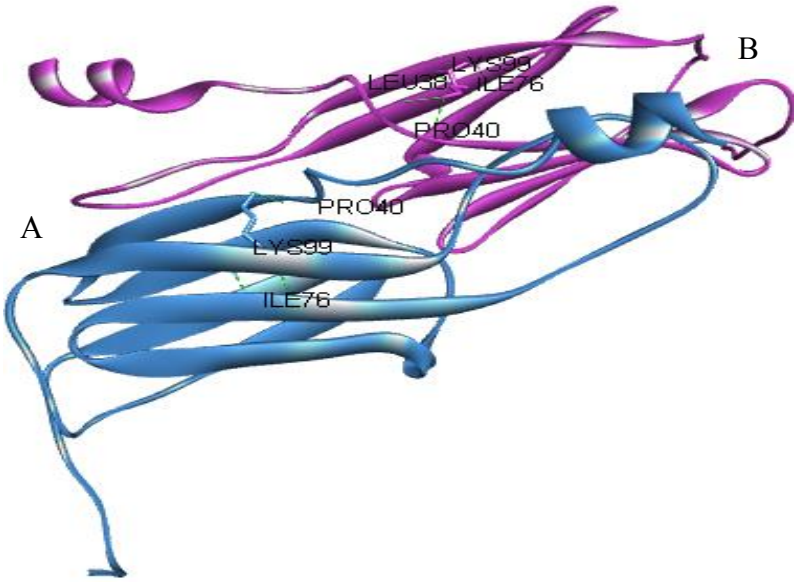

Figure 3.5. Intramolecular hydrogen bonds of Lys99 of po-sHSP20 in one chain

K99 also makes intramolecular hydrophobic interactions with Ile101 and Pro40 in A chain. In B chain, there is only one hydrophobic bond between Lys99 and Pro40 (Figure 3.6).

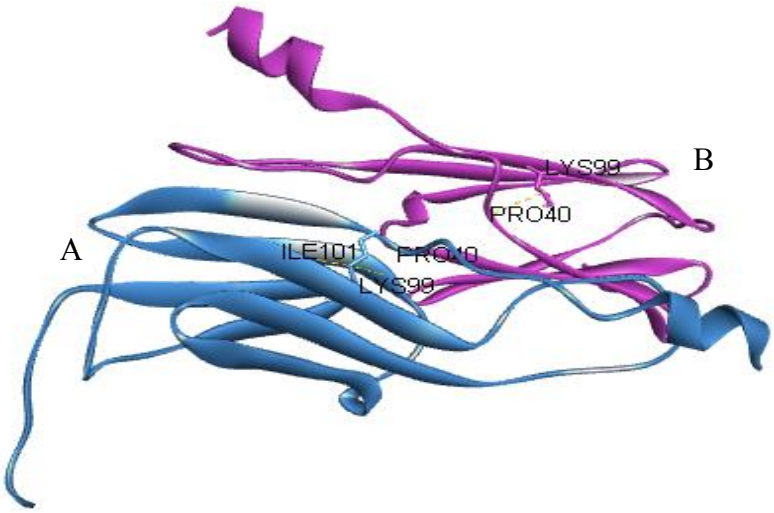

Figure 3.6. Intramolecular hydrophobic interactions of Lys99 of po-sHSP20 in one chain

3.2. Multiple Sequence Alignments

Multiple sequence alignments of amino acid sequence of po-sHSP20 protein among some archaeal sHSPs from different thermoacidophilic organisms were performed by Clustal Omega Programme. Amino acid sequences were obtained from online-database of NCBI.

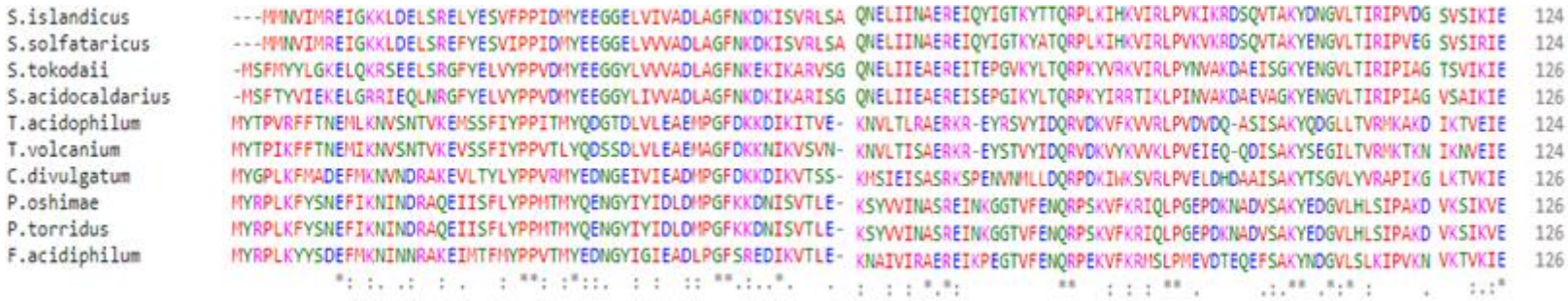

Figure 3.7. Multiple sequence alignment results of po-sHSP20 among the archaeal sHSPs sequences from different thermoacidophilic organisms. Coloring was performed by Clustal Omega automatically. The species names corresponding to each accession number are as given: **WP_012718226.1:** Hsp20/alpha crystallin family protein [Sulfolobus islandicus], **WP_009989320.1:** Hsp20/alpha crystallin family protein [Sulfolobus solfataricus], **WP_084742669.1:** Hsp20/alpha crystallin family protein [Sulfolobus tokodaii], **WP_011278477.1:** Hsp20/alpha crystallin family protein [Sulfolobus acidocaldarius], **WP_010901274.1:** Hsp20/alpha crystallin family protein [Thermoplasma acidophilum], **WP_010917033.1:** Hsp20/alpha crystallin family protein [Thermoplasma volcanium], **WP_077076822.1:** Hsp20/alpha crystallin family protein [Cuniculiplasma divulgatum], **SMD30368.1:** heat shock protein Hsp20 [Picrophilus oshimae DSM 9789], **AAT43324.1:** small heat shock protein hsp20 family [Picrophilus torridus DSM 9790], **WP_081141468.1:** Hsp20/alpha crystallin family protein [Ferroplasma acidiphilum]

Figure 3.8. Multiple sequence alignment results of po-sHSP20 among the eucaryal sHSP sequences from different eucaryotic organisms. Coloring was performed by Clustal Omega automatically. The species names corresponding to each accession number are as given: **AAA28635.1:** hsp22 [D. melanogaster], **AAA28638.1:** Hsp27 [D.melanogaster], **ACP18852.1:** αB-crystallin [H.sapiens], **AAA97523.1:** αA-crystallin [H.sapiens], **SMD30368.1:** Hsp20 [P.oshimae DSM 9789], **CAJ19361.1:** HSP20 [T.aestivum], **CAM12498.1:** small heat-shock protein [P.sativum], **CAA85016.1:** HSP26 [S.cerevisiae], **CAA19337.1:** Hsp20 [S.pombe]

The results of the multiple sequence alignment showed that lysine 88 of *P.oshimae* sHSP without His-tag (K99 of po-sHSP20 with His-tag) corresponds to arginine 120 of αB-crystallin from human and arginine 116 of αA-crystallin from human as seen in Figure 3.9. Amino acid sequences were obtained from online-database of NCBI. R116 mutation of αA-crystallin and R120 mutation in αB-crystallin are the most studied mutations in sHSPs of human. In this study, K88 was chosen for the amino acid substitution.

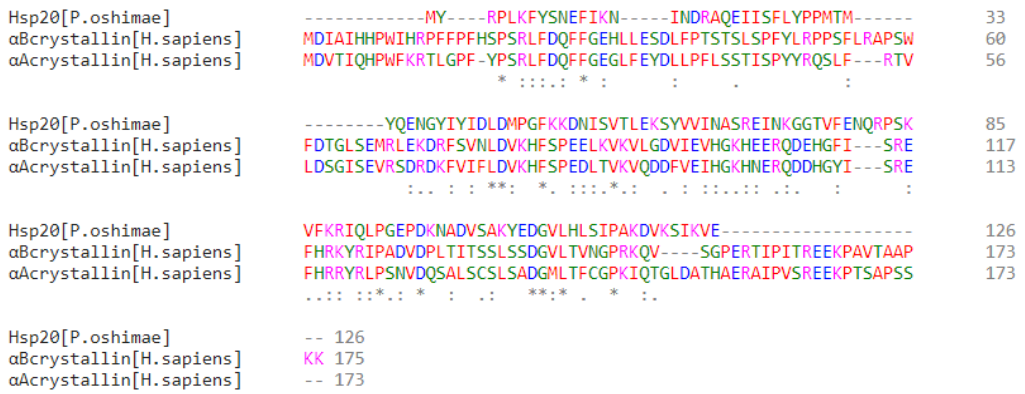

Figure 3.9. Multiple sequence alignment results of *P.oshimae* sHSP with αB-crystallin of human. The species names corresponding to each accession number are as given: SMD30368.1: po-sHSP20 [P. oshimae]. ACP18852.1: αB-crystallin [H. sapiens]. AAA97523.1: αA-crystallin [H.sapiens]

Evolutionary relationships between HSP20 family proteins from different organisms have been shown in phylogenetic tree cladogram (Figure 3.10). HSP20 family proteins of *P.oshimae* and *P.torridus* were found identical with the 100% amino acid sequence identity, as shown in Figure 3.7 and Table 3.3. According to the amino acid sequences of HSP20 family protein, the second highest homology was found between po-sHSP20 of *P.oshimae* and HSP20 of *F.acidiphilum* with the homology score of 63.49. The other homologs of po-sHSP20 of *P.oshimae* are HSP20 family proteins of *C.divulgatum* and *T.acidophilum* with the homology scores of 48.41 and 41.94, respectively (Table 3.3). *P.oshimae*, *P.torridus* and *F.acidiphilum* construct one phylogenetic group (Figure 3.10). The most distant

organisms to *P.oshimae* were *M.jannaschii* and *P.furiosus* with the homology scores of 19.17 and 21.77, respectively (Table 3.3), based on their amino acid sequences of HSP20 family protein.

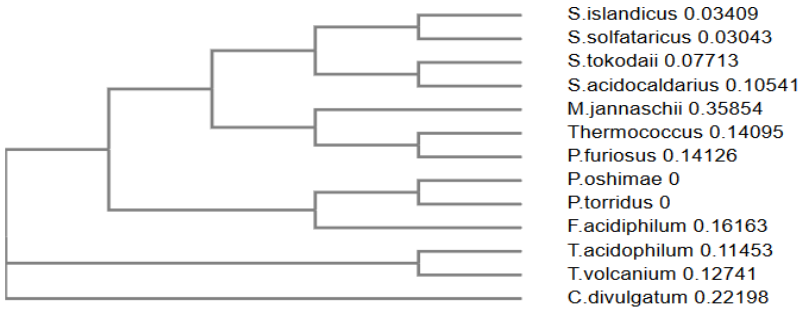

Figure 3.10. Phylogenetic tree based on the homology between sHSP amino acid sequences from different source organisms. The accession numbers of each species are as given: **SMD30368.1**: *Picrophilus oshimae*, **AAT43324.1:** *Picrophilus torridus,* **WP_077076822.1:** *Cuniculiplasma divulgatum*, **WP_010901274.1**: *Thermoplasma acidophilum*, **WP_012718226.1:** *Sulfolobus islandicus*, **WP_084742669.1:** *Sulfolobus tokodaii*, **WP_011278477.1:** *Sulfolobus acidocaldarius*, **WP_010917033.1:** *Thermoplasma volcanium*, **WP_081141468.1:** *Ferroplasma acidiphilum*, **WP_009989320.1:** *Sulfolobus solfataricus*, **BAB40930.1:** *Thermococcus* sp., **AAB98273.1:** *Methanocaldococcus jannaschii,* **AAF71367.1:** *Pyrococcus furiosus*

Table 3.3. *Homology scores between po-sHSP20 and several archaeal organisms obtained by multiple sequence alignment*

	1	2	3	4	5	6	7	8	9	10	11	12	13
(1) S.islandicus	100.00	93.55	60.48	58.87	33.06	33.88	37.40	39.02	39.02	37.40	24.79	28.21	27.27
(2) S.solfataricus		100.00	62.90	61.29	33.88	33.06	35.77	38.21	38.21	36.59	26.50	28.21	27.27
(3) S.tokodaii			100.00	81.75	35.77	34.15	37.60	34.40	34.40	38.40	26.05	29.41	28.46
(4) S.acidocaldarius				100.00	28.46	28.46	33.60	34.40	34.40	35.20	27.73	26.89	26.02
(5) T.acidophilum					100.00	75.81	50.81	41.94	41.94	45.97	22.69	26.05	25.20
(6) T.volcanium						100.00	50.00	40.32	40.32	43.55	20.17	24.37	25.20
(7) C.duvilgatum							100.00	48.41	48.41	54.76	21.67	24.17	25.81
(8) P.oshimae								100.00	100.00	63.49	19.17	23.33	21.77
(9) P.torridus									100.00	63.49	19.17	23.33	21.77
(10) F.acidiphilum										100.00	25.00	25.83	26.61
(11) M.jannaschii											100.00	29.66	32.19
(12) Thermococcus sp.												100.00	71.78
(13) P.furiosus													100.00

3.3. Cloning of po-sHSP20 Gene in pQE2 Vector

The po-sHSP20 gene was cloned into pQE2 vector as described in Material and Methods section.

As a first step for cloning, po-sHSP20 gene was amplified by PCR using primers with *Nde*I and *Pst*I cut sites at their ends. The size of amplified PCR fragments was estimated as 485 bp in length. Amplified PCR products were purified by QIAquick Spin Gel Extraction Kit. The bands of amplified and purified PCR fragments are given in Figure 3.11A

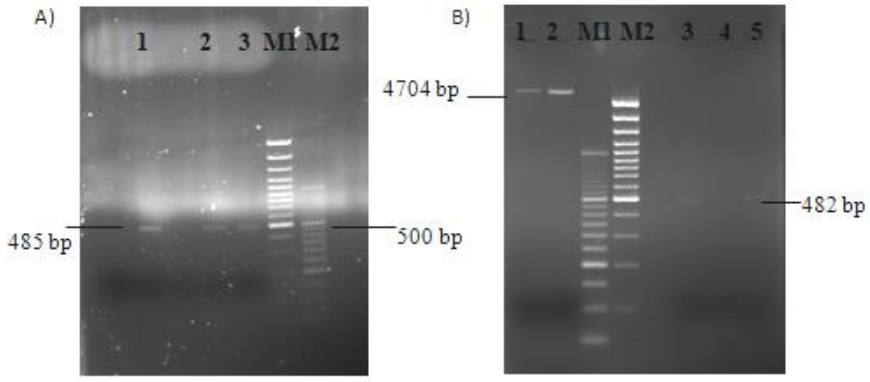

Figure 3.11. Agarose gel electrophoresis of PCR products of po-sHSP20 gene. **A)** PCR amplification of po-sHSP20 gene. **Lane 1**, **Lane 2** and **Lane 3:** Amplified and purified PCR products. **M1**: GeneRuler™, 100 bp DNA ladder. **M2:** GeneRuler™, 50 bp DNA Ladder. **B)** Agarose gel electrophoresis of digested PCR products and pQE2 vector by *Nde*I and *Pst*I. **Lane 1** and **Lane 2:** Double-digested pQE2 vector. **Lane 3, Lane 4 and Lane 5:** Double-digested PCR products. **M1**: GeneRuler™, 50 bp DNA ladder. **M2:** GeneRuler™, 100 bp DNA Ladder.

PCR fragments were eluted from gel. PCR fragments and pQE2 cloning expression vector were digested with *Nde*I and *Pst*I as described in Material Method section. The size of pQE2 vector is 4758 bp. After double digestion, the remaining sizes of vector and PCR product were calculated as 4704 bp and 482 bp, respectively which are seen in Figure 3.11B.

Then, *Nde*I and *Pst*I digested PCR fragments and pQE2 vector were ligated by T4 ligase, ligation mixture was transfered into *E.coli* TG1 competent cells for transformation. Plasmids from randomly selected transformed colonies were isolated and digested at the cut sites flanking the gene to verify the presence of the cloned po-sHSP20 gene. 8 recombinant clones were identified by this selection. Agarose gel bands of digested plasmids are shown in Figure 3.12 which were at expected positions.

The bands (4707 bp and 482 bp in length for vector and insert, respectively) are as expected when compared with size markers. This result confirmed that the cloning of the po-sHSP20 gene into pQE2 vector was succesful.

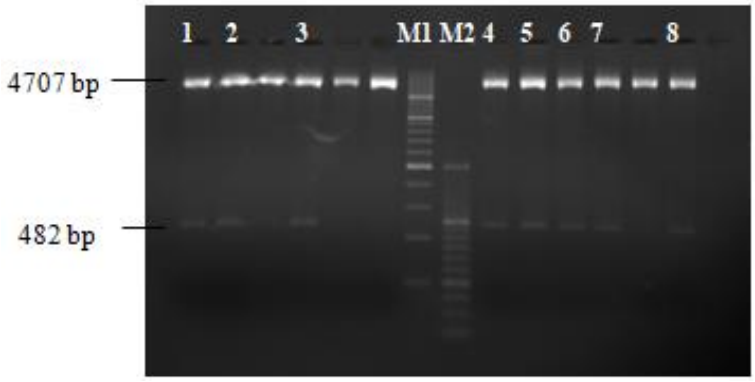

Figure 3.12. Agarose gel electrophoresis of isolated and digested plasmids by *Nde*I and *Pst*I. **Lane 1-Lane 8**: Isolated/digested recombinant plasmids. **M1:** O'RangeRuler^{TM}, 200bp DNA Ladder. **M2:** GeneRuler^{TM}, 50bp DNA Ladder

3.3.1. Characterization of Recombinant Plasmids by Restriction Mapping

The recombinant pQE2:po-sHSP20 plasmids were also digested by *Hind*III and *Bgl*II enzymes for further characterization. The cut positions of the restriction enzymes used are given in the Table 3.4. Accordingly, the digestion by *Hind*III produced two bands: larger band is 4781 and smaller band is 408 bp. *Bgl*II linearized the recombinant pQE2 vector giving rise to a 5189 bp single fragment. The digestion profiles in agarose gel are shown in Figure 3.13.

Table 3.4. *The cut positions of restriction endonucleases*

Restriction Enzymes	**Cut Positions**	
	Insert	**Vector**
*Nde*I	2	140
*Pst*I	484	190
*Hind*III	81	194
*Bgl*II	135	-

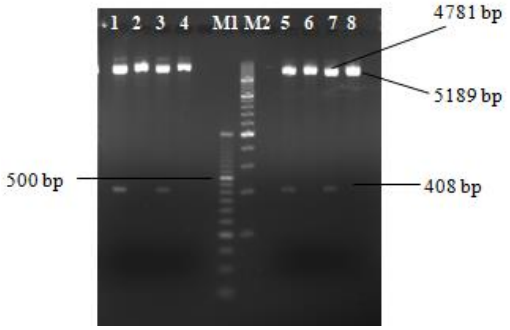

Figure 3.13. Agarose gel electrophoresis of digested plasmids. **Lane 1, Lane 3, Lane 5 and Lane 7:** Plasmids digested with *Hind*III. **Lane 2, Lane 4, Lane 6 and Lane 8:** Plasmids digested with *Bgl*II. **M1:** GeneRuler^{TM} 50 bp DNA Ladder **M2:** O'RangeRuler^{TM} 200 bp DNA Ladder

3.3.2. Verification of Cloning by DNA Sequencing

Isolated plasmids from po-sHSP20-1/10 and po-sHSP20-3/9 clones were digested with *Pst*I restriction enzyme and sent for sequencing to verify the cloned po-sHSP20 gene. *Pst*I digestion produced a 5189 bp single fragment. The concentrations and purity of plasmids were determined by PicoDrop measurements. The concentrations of plasmids (Lane 1 and Lane 2, in Figure 3.14) were measured as 71.6 ng/µl and 84.7 ng/µl, respectively and their purities ($A_{260/280}$) were determined as 1.941 and 1.955, respectively. The results of sequencing were analyzed by pairwise sequence alignments with the original sequence of po-sHSP20 gene obtained from online-database of NCBI. The sequences of cloned po-sHSP20 genes were found as same with the original sequence of po-sHSP20 gene (Figure 3.15 and Figure 3.16).

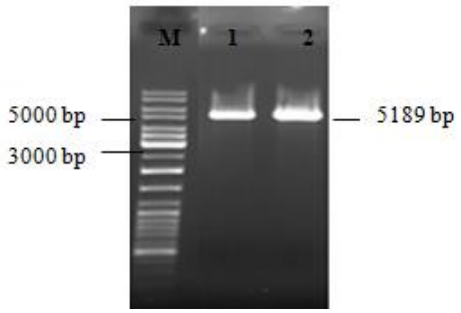

Figure 3.14. Agarose gel electrophoresis of plasmids digested with *Pst*I enzyme. **M**: O' Gene ruler DNA Ladder mix. **Lane 1** and **Lane 2**: Digested DNA fragments

```
po-sHsp20 (NCBI) ATGTACAGACCATTAAAATTCTATTCGAATGAATTTATTAAGAATATAAATGATAGGGCG   60
WT plasmid       ATGTACAGACCATTAAAATTCTATTCGAATGAATTTATTAAGAATATAAATGATAGGGCG   60
                 ************************************************************

po-sHsp20 (NCBI) CAGGAGATAATAAGCTTTTTATACCCTCCAATGACGATGTACCAGGAAAATGGCTATATA   120
WT plasmid       CAGGAGATAATAAGCTTTTTATACCCTCCAATGACGATGTACCAGGAAAATGGCTATATA   120
                 ************************************************************

po-sHsp20 (NCBI) TACATAGATCTTGACATGCCGGGATTTAAAAAGGATAACATCTCTGTTACACTGGAGAAA   180
WT plasmid       TACATAGATCTTGACATGCCGGGATTTAAAAAGGATAACATCTCTGTTACACTGGAGAAA   180
                 ************************************************************

po-sHsp20 (NCBI) TCATACGTTGTTATAAATGCAAGCAGGGAGATAAACAAAGGCGGAACAGTCTTTGAGAAC   240
WT plasmid       TCATACGTTGTTATAAATGCAAGCAGGGAGATAAACAAAGGCGGAACAGTCTTTGAGAAC   240
                 ************************************************************

po-sHsp20 (NCBI) CAGAGGCCATCAAAGGTCTTTAAGAGGATACAGCTGCCTGGAGAGCCAGATAAAAACGCT   300
WT plasmid       CAGAGGCCATCAAAGGTCTTTAAGAGGATACAGCTGCCTGGAGAGCCAGATAAAAACGCT   300
                 ************************************************************

po-sHsp20 (NCBI) GATGTCTCTGCAAAATATGAGGACGGCGTTCTGCATCTATCAATACCTGCAAAGGATGTA   360
WT plasmid       GATGTCTCTGCAAAATATGAGGACGGCGTTCTGCATCTATCAATACCTGCAAAGGATGTA   360
                 ************************************************************

po-sHsp20 (NCBI) AAATCCATAAAGGTTGAATAA  381
WT plasmid       AAATCCATAAAGGTTGAATAA  381
                 *********************
```

Figure 3.15. Pairwise sequence alignment of the nucleotide sequence of the wild-type plasmid with that of the original sequence of po-sHSP20 obtained from online-database of NCBI.

```
po-sHsp20 (NCBI)   MYRPLKFYSNEFIKNINDRAQEIISFLYPPMTMYQENGYIYIDLDMPGFKKDNISVTLEK  60
WT plasmid         MYRPLKFYSNEFIKNINDRAQEIISFLYPPMTMYQENGYIYIDLDMPGFKKDNISVTLEK  60
                   ************************************************************
po-sHsp20 (NCBI)   SYVVINASREINKGGTVFENQRPSKVFKRIQLPGEPDKNADVSAKYEDGVLHLSIPAKDV  120
WT plasmid         SYVVINASREINKGGTVFENQRPSKVFKRIQLPGEPDKNADVSAKYEDGVLHLSIPAKDV  120
                   ************************************************************

po-sHsp20 (NCBI)   KSIKVE  126
WT plasmid         KSIKVE  126
                   ******
```

Figure 3.16. Pairwise sequence alignment of the amino acid sequence of the wild-type plasmid with that of the original sequence of po-sHSP20 obtained from online-database of NCBI.

3.4. Site-Directed Mutagenesis

Site-directed mutagenesis was first performed with GeneArt® Site-Directed Mutagenesis Plus Kit using mutagenic primers for K99G and K99E mutations as described in the Materials and Methods.

For transformation control, 50 pg of the control plasmid, pUC19 (provided with the kit) was transformed into One ShotR MAX EfficiencyR DH5α™-T1R competent cells. Transformed colonies were counted after overnight incubation. Transformation efficiencies were calculated as ranging from $4x10^8$ cfu/μg to $2x10^9$ cfu/μg.

Mutagenesis reaction mixtures were prepared by using about 26 ng of plasmid DNA. The reaction mixtures were transformed into One ShotR MAX EfficiencyR DH5α™-T1R competent cells. After overnight incubation, putative mutant colonies were counted. Transformation efficiencies were calculated according to the formula of cfu/μg of transforming DNA and the results are shown in Table 3.5.

Table 3.5. *Transformation Efficiencies of Mutated Plasmids*

Mutation	Transformation efficiency (cfu/μg)
K99G	$9x10^7$
K99E	$1x10^8$

3.4.1. Characterization and Verification of Mutations

Plasmids from randomly selected 3 colonies for each mutation were isolated. The isolated plasmids were digested by *Hind*III restriction enzyme. The digestion produced two bands which are 4781 bp and 408 bp, as expected. Figure 3.17 shows the agarose gel image of putative mutant po-sHSP20 gene. The concentrations and purity of the plasmids were determined by Picodrop measurements (Table 3.6). These plasmids were sent for sequencing to see whether they contain expected mutation or not. Amino acid replacements were controlled by pairwise sequence

alignments of the mutant gene (without His-tag) with that of the wild-type gene sequence without His-tag. The analysis of the results showed that the targeted residue was substituted as expected for only one of the K99E mutant plasmid. However, in addition to the desired mutation, there were additions and deletions of nucleotide sequences observed in all three K99G and two of the K99E putative mutant plasmids. Since K99G mutant was not obtained, the mutagenesis was repeated using an another mutagenesis kit, i.e., QuickChangeII Site-Directed Mutagenesis Kit.

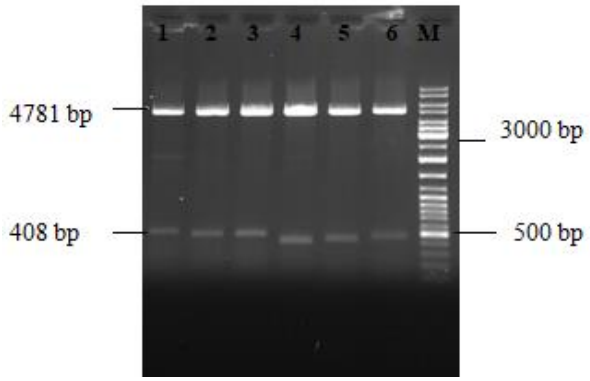

Figure 3.17. Agarose gel electrophoresis of putative mutant plasmids after *Hind*III digestion. **Lane 1, Lane 2 and Lane 3:** Isolated and *Hind*III-digested DNA fragments of K99G mutant. **Lane 4, Lane 5 and Lane 6**: Isolated and *Hind*III-digested DNA fragments of K99E mutant. **M:** O'GeneRuler DNA Ladder Mix

Table 3.6. *Concentrations and Purities of Plasmids*

K99G mutant plasmids	**Concentration (ng/µl)**	**A 260/280**
K99G1 (Lane 1)	40 ng/ µl	1.947
K99G2 (Lane 2)	50 ng/ µl	1.962
K99G3 (Lane 3)	54 ng/ µl	1.963
K99E mutant plasmids		
K99E1 (Lane 4)	70 ng/ µl	1.987
K99E2 (Lane 5)	46 ng/ µl	1.992
K99E3 (Lane 6)	36 ng/ µl	1.853

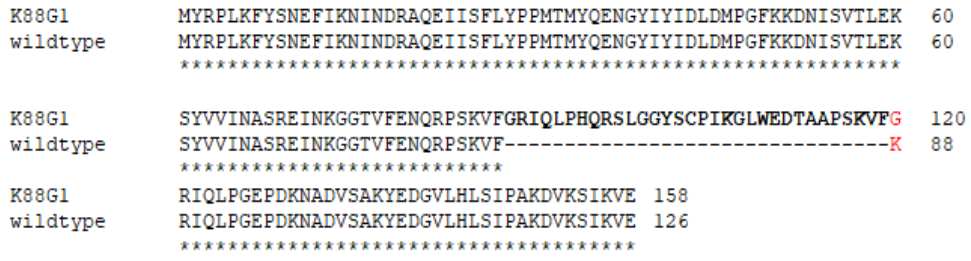

Figure 3.18. Pairwise sequence alignment of aminoacid sequence of K88G1 mutant plasmid with that of the wild-type sequence. Expected mutation was emphasized with red color. Unexpected insertions were shown in bold.

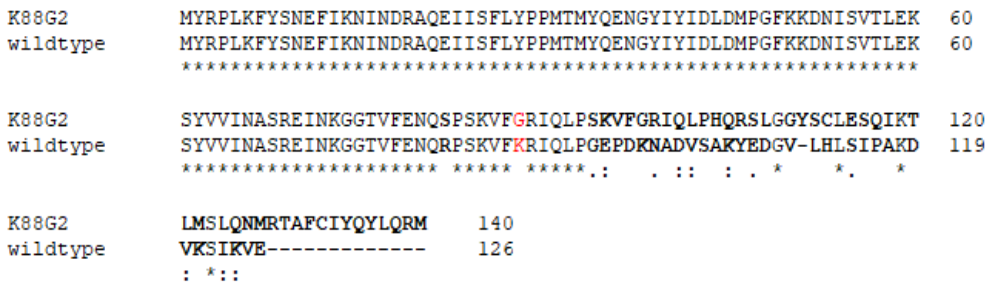

Figure 3.19. Pairwise sequence alignment of aminoacid sequence of K88G2 mutant plasmid with that of the wild-type sequence. Expected mutation was emphasized with red color. Unexpected insertions and substitutions were shown in bold.

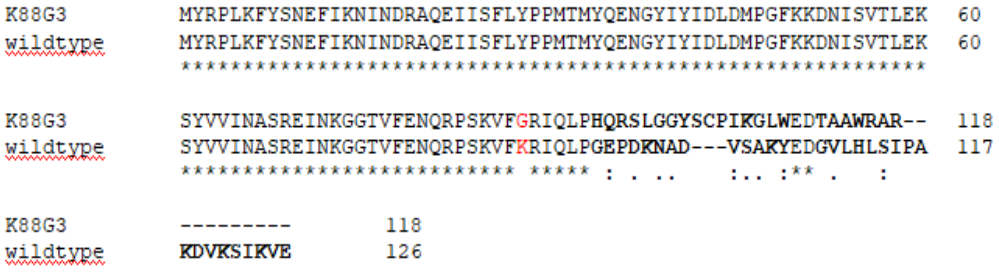

Figure 3.20. Pairwise sequence alignment of aminoacid sequence of K88G3 mutant plasmid with that of the wild-type sequence. Expected mutation was emphasized with red color. Unexpected mutations (insertions, deletions and substitutions) were shown in bold.

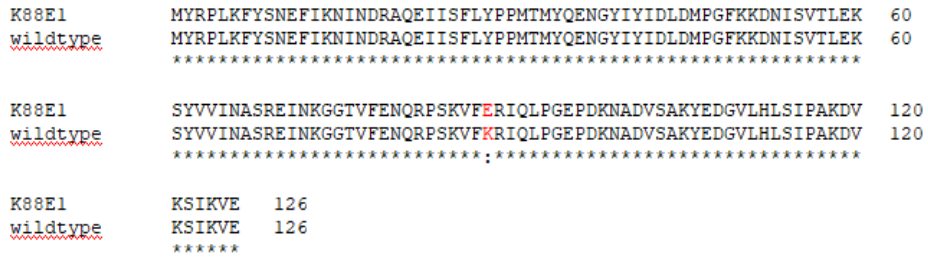

Figure 3.21. Pairwise sequence alignment of aminoacid sequence of K88E1 mutant plasmid with that of the wild-type sequence. Expected mutation was emphasized with red color.

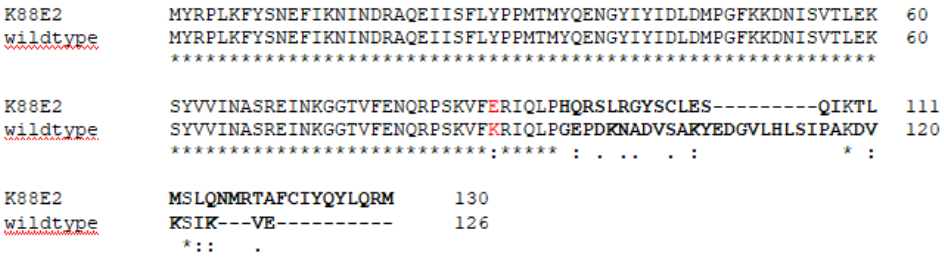

Figure 3.22. Pairwise sequence alignment of aminoacid sequence of K88E2 mutant plasmid with that of the wild-type sequence. Expected mutation was emphasized with red color. Unexpected mutations (insertions, deletions and substitutions) were shown in bold.

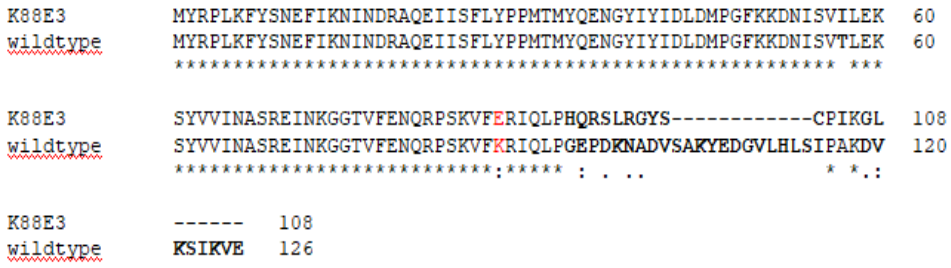

Figure 3.23. Pairwise sequence alignment of aminoacid sequence of K88E3 mutant plasmid with that of the wild-type sequence. Expected mutation was emphasized with red color. Unexpected mutations (insertions, deletions and substitutions) were shown in bold.

The QuikChange II Site-Directed Mutagenesis Kit Protocol was followed using the mutagenic primers for K99G and K99E mutations which were designed as described.

After mutagenesis reaction was completed, positive selection of the mutated plasmids were achieved by cutting the plasmids in the mutagenesis mixture with *Dpn*I enzyme. This enzyme cuts parental methylated and hemimethylated DNA. The transformation efficiencies were calculated by the formula of cfu/µg of transforming DNA. Transformation efficiencies for K99G and K99E mutant plasmids were found as $2x10^5$ cfu/µg and $8x10^5$ cfu/µg, respectively.

3.4.2. Characterization and Verification of Mutations

After transformation of mutated plasmids into XL1-Blue supercompetent cells and overnight growth, colonies were picked up randomly and their plasmids were isolated. Isolated plasmids were digested with *Hind*III for checking and characterization of the insert. The digestion yielded two bands which are 4781 bp and 408 bp, as expected. The concentrations and purity of the three plasmids (Table 3.7) for each mutation were determined by PicoDrop and sent for sequencing to verify the desired mutation. The results of sequencing were analyzed and the desired aminoacid replacements were verified by pairwise sequence alignments.

The results of sequence alignments showed that each plasmids of putative K99E mutation were correctly mutated. While, only one plasmid of putative K99G mutation contained the desired amino acid substitution.

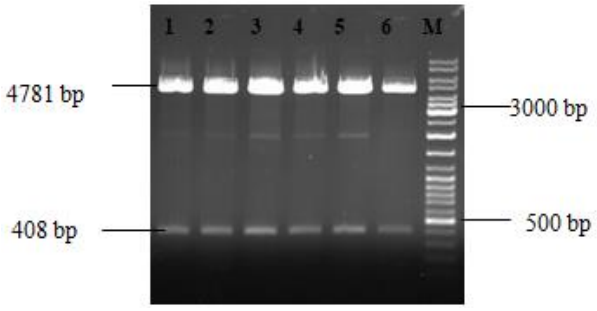

Figure 3.24. Agarose gel electrophoresis of putative mutant plasmids after *Hind*III digestion. **Lane 1-Lane 3**: Isolated and *Hind*III-digested DNA fragments of K99G mutant. **Lane 4-Lane 6**: Isolated and *Hind*III-digested DNA fragments of K99E mutant. **M:** 0'GeneRuler, DNA Ladder Mix

Table 3.7. *Concentrations and Purities of Plasmids*

K99G mutant plasmids	**Concentration (ng/µl)**	**A 260/280**
K99G1 (Lane 1)	67 ng/µl	1.952
K99G2 (Lane 2)	85 ng/µl	2.027
K99G3 (Lane 3)	107 ng/µl	1.985
K99E mutant plasmids		
K99E1 (Lane 4)	81 ng/µl	1.964
K99E2 (Lane 5)	101 ng/µl	1.935
K99E3 (Lane 6)	59 ng/µl	1.918

```
wildtype        -----------MYRPLKFYSNEFIKNINDRAQEIISFLYPPMTMYQENGYIYIDLDMPGF  49
K88G1           ---------MQMYRPLKFYSNEFIKNINDRAQEIISFLYPPMTMYQENGYIYIDLDMPGF  51
                          **************************************************

wildtype        KKDNISVTLEKSYVVINASREINKGGTVFENQRPSKVFKRIQLPGEPDKNADVSAKYEDG  109
K88G1           KKDNISVTLEKSYVVINASREINKGGTVFENQRPSKVLGGYSCLESQIKTLMSLQNMRTA  111
                ************************************:   .   .  *.     : . .

wildtype        VLHLSIPAKDVKSIKVE       126
K88G1           FCIYQY----LQRM---       121
                .   .     :: :
```

Figure 3.25. Pairwise sequence alignment of aminoacid sequence of K88G1 mutant plasmid with that of the wild-type sequence. Expected mutation was emphasized with red color. Unexpected mutations (insertions, deletions and substitutions) were shown in bold.

```
K88G2           ---------MQMYRPLKFYSNEFIKNINDRAQEIISFLYPPMTMYQENGYIYIDLDMPGF   51
wildtype        -----------MYRPLKFYSNEFIKNINDRAQEIISFLYPPMTMYQENGYIYIDLDMPGF   49
                          **************************************************

K88G2           KKDNISVTLEKSYVVINASREINKGGTVFENQRPSKVFKRIQLPGEPDKNADVSAKYEDG   111
wildtype        KKDNISVTLEKSYVVINASREINKGGTVFENQRPSKVFKRIQLPGEPDKNADVSAKYEDG   109
                ************************************************************

K88G2           VLHLSIPAKDVKSIKVE       128
wildtype        VLHLSIPAKDVKSIKVE       126
                *****************
```

Figure 3.26. Pairwise sequence alignment of aminoacid sequence of K88G2 mutant plasmid with that of the wild-type sequence. There was no substitution observed.

```
K88G3          ---------MQMYRPLKFYSNEFIKNINDRAQEIISFLYPPMTMYQENGYIYIDLDMPGF   51
wildtype       -----------MYRPLKFYSNEFIKNINDRAQEIISFLYPPMTMYQENGYIYIDLDMPGF   49
                          **************************************************

K88G3          KKDNISVTLEKSYVVINASREINKGGTVFENQRPSKVFGRIQLPGEPDKNADVSAKYEDG   111
wildtype       KKDNISVTLEKSYVVINASREINKGGTVFENQRPSKVFKRIQLPGEPDKNADVSAKYEDG   109
               ************************************ **********************

K88G3          VLHLSIPAKDVKSIKVE       128
wildtype       VLHLSIPAKDVKSIKVE       126
               *****************
```

Figure 3.27. Pairwise sequence alignment of aminoacid sequence of K88G3 mutant plasmid with that of the wild-type sequence. Expected mutation was emphasized with red color.

```
K88E1          ---------MQMYRPLKFYSNEFIKNINDRAQEIISFLYPPMTMYQENGYIYIDLDMPGF   51
wildtype       -----------MYRPLKFYSNEFIKNINDRAQEIISFLYPPMTMYQENGYIYIDLDMPGF   49
                          **************************************************

K88E1          KKDNISVTLEKSYVVINASREINKGGTVFENQRPSKVFERIQLPGEPDKNADVSAKYEDG   111
wildtype       KKDNISVTLEKSYVVINASREINKGGTVFENQRPSKVFKRIQLPGEPDKNADVSAKYEDG   109
               ************************************:**********************

K88E1          VLHLSIPAKDVKSIKVE       128
wildtype       VLHLSIPAKDVKSIKVE       126
               *****************
```

Figure 3.28. Pairwise sequence alignment of aminoacid sequence of K88E1 mutant plasmid with that of the wild-type sequence. Expected mutation was emphasized with red color.

```
K88E2          ---------MQMYRPLKFYSNEFIKNINDRAQEIISFLYPPMTMYQENGYIYIDLDMPGF   51
wildtype       -----------MYRPLKFYSNEFIKNINDRAQEIISFLYPPMTMYQENGYIYIDLDMPGF   49
                          **************************************************

K88E2          KKDNISVTLEKSYVVINASREINKGGTVFENQRPSKVFERIQLPGEPDKNADVSAKYEDG   111
wildtype       KKDNISVTLEKSYVVINASREINKGGTVFENQRPSKVFKRIQLPGEPDKNADVSAKYEDG   109
               ************************************:**********************

K88E2          VLHLSIPAKDVKSIKVE       128
wildtype       VLHLSIPAKDVKSIKVE       126
               *****************
```

Figure 3.29. Pairwise sequence alignment of aminoacid sequence of K88E2 mutant plasmid with that of the wild-type sequence. Expected mutation was emphasized with red color.

```
K88E3          ---------MQMYRPLKFYSNEFIKNINDRAQEIISFLYPPMTMYQENGYIYIDLDMPGF   51
wildtype       -----------MYRPLKFYSNEFIKNINDRAQEIISFLYPPMTMYQENGYIYIDLDMPGF   49
                          **************************************************

K88E3          KKDNISVTLEKSYVVINASREINKGGTVFENQRPSKVFERIQLPGEPDKNADVSAKYEDG   111
wildtype       KKDNISVTLEKSYVVINASREINKGGTVFENQRPSKVFKRIQLPGEPDKNADVSAKYEDG   109
               ************************************ **********************

K88E3          VLHLSIPAKDVKSIKVE       128
wildtype       VLHLSIPAKDVKSIKVE       126
               *****************
```

Figure 3.30. Pairwise sequence alignment of aminoacid sequence of K88E3 mutant plasmid with that of the wild-type sequence. Expected mutation was emphasized with red color.

Figure 3.31. Pairwise sequence alignment of nucleotide sequences of the wild-type (WT) and K88E2 (Lane 5 in Figure 3.24) mutant po-sHSP20. AAG is changed to GAG (Base substitution is showed in bold and underlined).

Figure 3.32. Pairwise sequence alignment of nucleotide sequences of the wild-type (WT) and K88G3 (Lane 3 in Figure 3.24) mutant po-sHSP20. AAG is changed to GGG (Base substitution is showed in bold and underlined).

3.5. Expression and Purification of Wild-type and Mutant po-sHSP20

3.5.1. Expression of po-sHSP20

Wild-type and mutant po-sHSP20 genes were expressed by IPTG induction under the control of lacZ promoter. Then, the cell lysates were prepared and the soluble po-sHSP20 samples were analyzed on 12% polyacrylamid gel. Protein bands were visualized by staining with Coomassie Brillant Blue.

Firstly, cell lysate was prepared in lysis buffer containing lysozyme by sonication. The molecular weight of His-tagged protein monomer was calculated as approximately 16.02 kDa by using Expasy protpram bioinformatic tool. The molecular weight of lysozyme is 14.3 kDa. Since the molecular weight of lysozyme (14.3 kDa) is close to the po-sHSP20, their bands overlapped as shown in Figure 3.33. For this reason, cell lysate was again obtained by sonication but with lysis buffer which does not contain lysozyme. The expression profile of po-sHSP20 is as shown on Figure 3.33. As expected a single strong band corresponding to po-sHSP20 protein was obtained. Rest of the bands belong to *E.coli* host proteins. SDS-PAGE gel electrophoresis has revealed the presence of expression of po-sHSP20 gene product. The recombinant po-sHSP20 proteins obtained from two strains were named as po-sHSP20-1/10 and po-sHSP20-3/9.

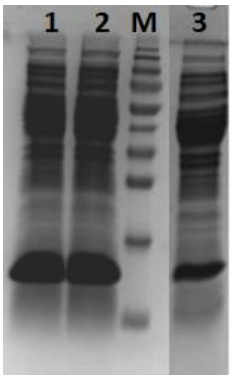

Figure 3.33. SDS-PAGE gel electrophoresis of po-sHSP20 protein. **Lane 1:** Cell extract of po-sHSP20-1/10**. Lane 2**: Cell extract of po-sHSP20-3/9. **M:** PageRuler^{TM} Prestained Protein Ladder. **Lane 3**: Cell extract of po-sHSP20-1/10 (no lysozyme).

Since, *P.oshimae* is a thermoacidophilic archaeon, its sHSP is expected to be heat stable as well. Therefore, as a first step for purification, heat sensitive host proteins could be eliminated by heat treatment**.** For this purpose, cell extracts were incubated at 65˚C-70˚C for 15 min. Denatured proteins were precipitated by centrifuge. Most of the *E.coli* proteins were lost after heat treatment at 65ºC shown in Figure 3.34. When temperature was increased to 70°C, better removal of heat-labile host proteins was achieved (Figure 3.34).

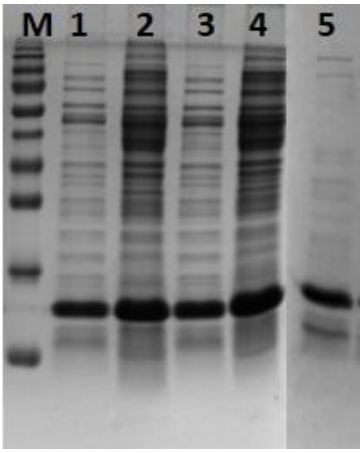

Figure 3.34. SDS-PAGE gel electrophoresis of the wild-type po-sHSP20 before and after heat treatment. **Lane 1 and 3**: The po-sHSP20-3/9 after heat treatment at 65ºC. **Lane 2 and 4**: The non-heated po-sHSP20-3/9 . **Lane 5**: The po-sHSP20-3/9 after heat treatment at 70ºC. **M:** PageRuler^{TM} Prestained Protein Ladder.

There after, the lysates of mutant po-sHSP20 proteins were prepared without using lysozyme for cell lysis. Figure 3.35A shows the protein bands of the mutant po-sHSP20s on 12% polyacrylamide gel. Mutant po-sHSP20 proteins were named as po-sHSP-K99E 3/9 and po-sHSP-K99G 3/12.

Mutant cell extracts were also incubated at 60ºC-70ºC for 15-20 min to eliminate the host proteins. Heat treatment at 60ºC was not sufficient for elimination of the host proteins (Figure 3.35A). Heat treatment at 65ºC was more effective for removal of

host proteins (Figure 3.35B). But, when temperature was increased to 70°C, better removal of heat-labile host proteins was achieved (Figure 3.35C).

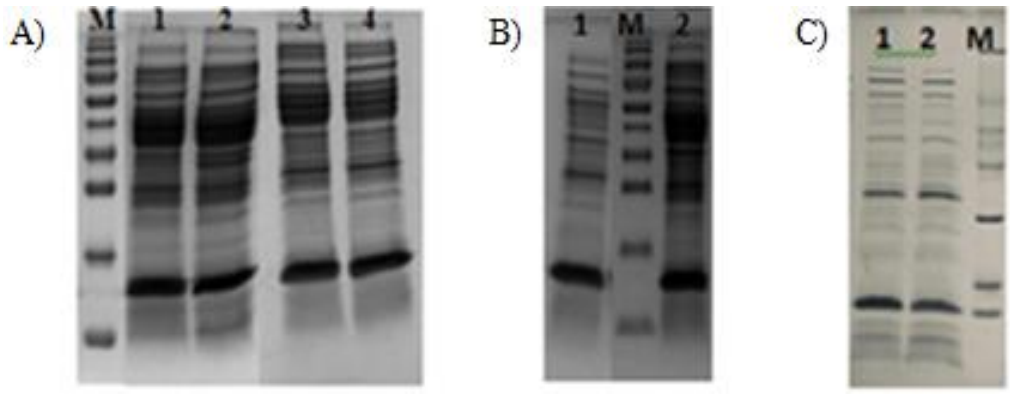

Figure 3.35. SDS-PAGE gel electrophoresis of K99E and K99G mutant proteins. **A) Lane 1:** po-sHSP-K99G 3/12. **Lane 2:** po-sHSP-K99E 3/9. **Lane 3:** po-sHSP-K99G 3/12 after heat treatment at 60ºC. **Lane 4:** po-sHSP-K99E 3/9 after heat treatment at 60ºC. **M:** PageRuler^{TM} Prestained Protein Ladder. **B) Lane 1**: po-sHSP-K99E 3/9 after heat treatment at 65ºC. **Lane 2**: po-sHSP-K99E 3/9. **M:** PageRuler^{TM} Prestained Protein Ladder. **C) Lane 1:** po-sHSP-K99G 3/12 after heat treatment at 70ºC. **Lane 2:** po-sHSP-K99E 3/9 after heat treatment at 70ºC. **M:** The Unstained Protein Molecular Weight Marker (Fermentas)

3.5.2. Purification of po-sHSP20

N-terminal 6xHis-tagged recombinant proteins expressed in *E.coli* cells and cleared cell lysates were prepared under native conditions as explained in Material and Methods. Then two different methods were used for affinity purification:

1. Batch purification by using Ni-NTA Agarose loaded column,

Cell extracts of wild-type were applied into the column before heat treatment. Firstly, flow-through was collected. After that, the column was washed with wash buffer and wash fractions were collected. Then, protein was eluted six times with 0.5 ml of elution buffer. SDS-PAGE gel electrophoresis of elution fractions of po-sHSP20-1/10 and po-sHSP20-3/9 are shown in Figure 3.36 and Figure 3.37, respectively.

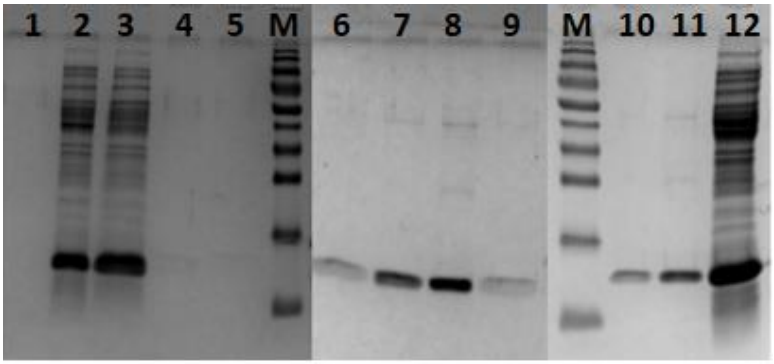

Figure 3.36. The elution profile of po-sHSP20-1/10 on 12% polyacrylamid gel. **Lane 1 and Lane 2:** Fractions from washing step (wash2-4 and wash1-1). **Lane 3:** Flow-through 1. **Lane 4-Lane 11:** The elution fractions of po-sHSP20-1/10. **(4)**: EL5. **(5)**: EL6. **(6)**: EL4. **(7 and 10)**: EL3. **(8 and 11)**: EL2. **(9)**: EL1. **Lane 12:** Cell extract of po-sHSP20-1/10. **M:** PageRuler^{TM} Prestained Protein Ladder

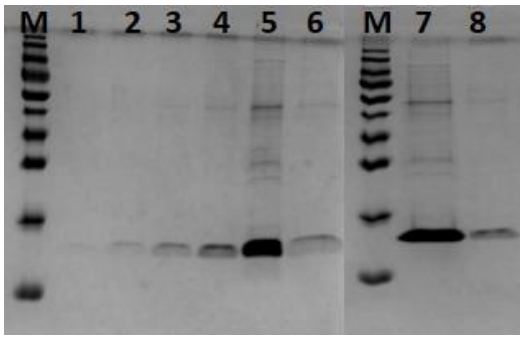

Figure 3.37. SDS-PAGE gel electrophoresis of elutions of po-sHSP20-3/9 and filtrated sample. **Lane 1-Lane 6:** Elution 6 to elution 1, respectively. **Lane 7:** Filtrated po-sHsp20-3/9. **Lane 8:** Elution mixture (1 to 6) before ultrafiltration. **M:** PageRuler^{TM} Prestained Protein Ladder.

After Ni-NTA affinity purification, elutions (EL1 to EL5) shown in Figure 3.36 and elutions (EL1 to EL6) shown in Figure 3.37 were concentrated by ultrafiltration using Amicon® Ultra-4 Centrifugal Filter Units (Millipore) of 10-kDa cutoff. Afterwards, filtrated sample was used in size-exclusion chromatography.

The mutant po-sHSP20 proteins were also purified by Ni-NTA affinity chromatography. Mutant cell extracts were applied into the column after heat

treatment. SDS-PAGE gel electrophoresis of elution fractions of the mutant po-sHSP20 proteins is shown in Figure 3.38.

After Ni-NTA purification, elutions (EL1 to EL3) of each mutants shown in Figure 3.38 were ultrafiltrated by using Amicon® Ultra-4 Centrifugal Filter Unit. Ultrafiltration result of these proteins are shown in Figure 3.39.

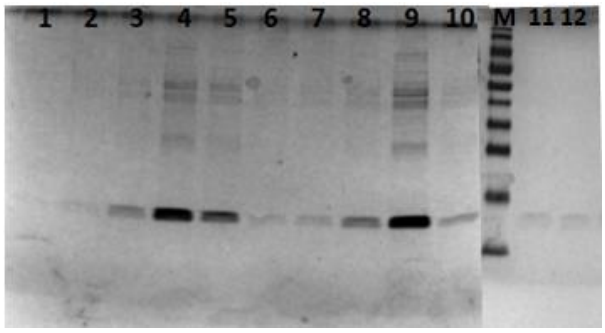

Figure 3.38. SDS-PAGE gel electrophoresis of purified K99E and K99G mutants by Ni-NTA chromatography. **Lane 1-Lane 5:** The elution fractions of po-sHSP-K99G 3/12. Elution 5 to elution 1, respectively. **Lane 6-Lane 10:** The elutions of po-sHSP20-K99E 3/9. Elution 5 to elution 1, respectively. **Lane 11:** Elution 6 of po-sHSP-K99G 3/12. **Lane 12:** Elution 6 of po-sHSP-K99E 3/9. **M:** PageRuler™ Prestained Protein Ladder

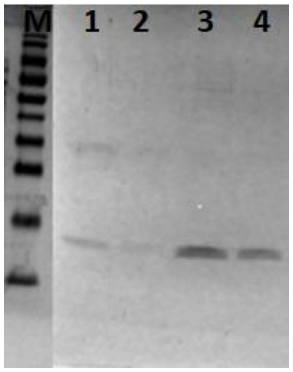

Figure 3.39. SDS-PAGE gel electrophoresis of K99E and K99G mutant proteins. **Lane 1**: Filtrated po-sHSP-K99E 3/9. **Lane 2:** Filtrated po-sHSP-K99G 3/12. **Lane 3:** Elution mixture (1 to 3) of po-sHSP-K99E 3/9 before ultrafiltration. **Lane 4:** Elution mixture (1 to 3) of po-sHSP-K99G 3/12 before ultrafiltration. **M:** PageRuler™ Prestained Protein Ladder.

2.Purification by High Performance Liquid Chromatography (HPLC)

In order to purify the wild-type protein by HPLC, 2 ml of po-sHSP20-3/9 protein was applied onto a HisTrap FF 1ml column (GE Healthcare). A single peak that indicates the elution fraction of the po-sHSP20-3/9 has been obtained by elution with imidazole. The graph of po-sHSP20-3/9 purification is shown in Figure 3.40.

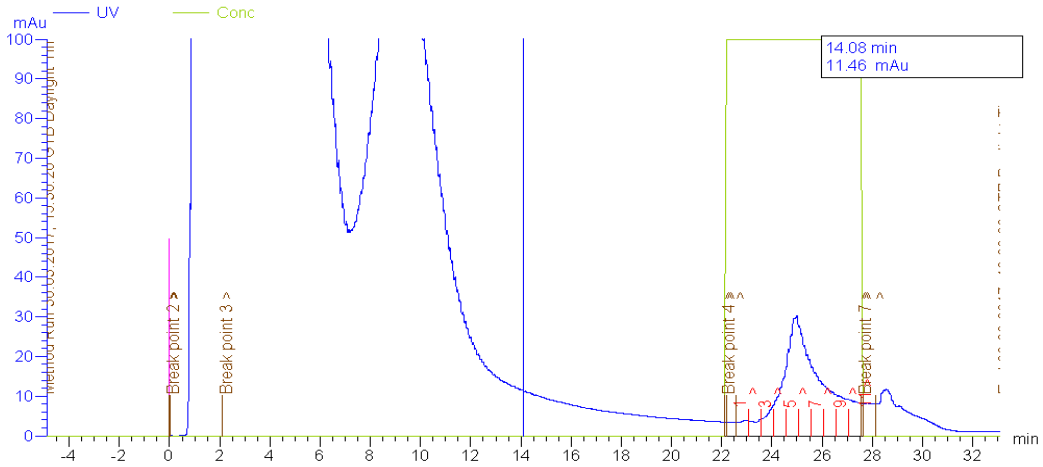

Figure 3.40. The graph of purified wild-type po-sHSP20 by HPLC. Peak 6 includes the highest amount of the eluted po-sHSP20-3/9.

SDS-PAGE gel electrophoresis of the elution fractions of the po-sHSP20 protein by HPLC is shown in Figure 3.41.

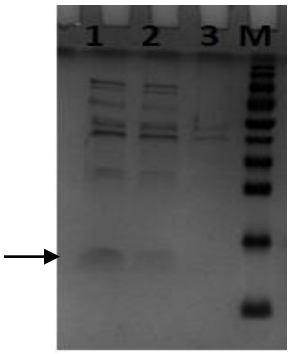

Figure 3.41. SDS-PAGE gel electrophoresis of elution fractions of the po-sHSP20-3/9 by HPLC on 12% polyacrylamid gel. **Lane 1:** Elution fraction 7. **Lane 2:** Elution fraction 6. **Lane 3:** Elution fraction 5. The po-sHSP20 band is indicated by arrow. **M:** PageRuler^{TM} Prestained Protein Ladder

3.6. Structural Characterization of Wild-type po-sHSP20 by SEC

In order to determine the oligomeric structure of po-sHSP20 protein, size exclusion chromatography was performed by using a Sephacryl S300 15/50 column at the flow rate of 0.5 ml/min with absorbance monitored at 280 nm. Column was calibrated with the low molecular weight calibration kit proteins (aprotinin 6,5 kDa, ribonuclease A 13,7 kDa and carbonic anhydrase 29 kDa). The volume of column (V_C) is 53 ml. The void volume (V_o) of the column was determined by dextran blue (2000 kDa) as 19,35 ml. Proteins were separated on the column in sodium-phosphate buffer and the elution volume of each sample was used for the estimation of the molecular weight.

The po-sHSP20 protein was eluted from the column in two combined major peaks; 20,24, 22,88 ml and ≥43,12 ml elutions which correspond to 18-mer, 12-mer and dimeric/monomeric units, respectively. Thus, size exclusion chromatography of wild-type po-sHSP20 demonstrated that the po-sHSP20 protein formed mostly large homo-oligomers consisting of 18 and 12 subunits. The SEC profile of po-sHSP20 is shown in Figure 3.42.

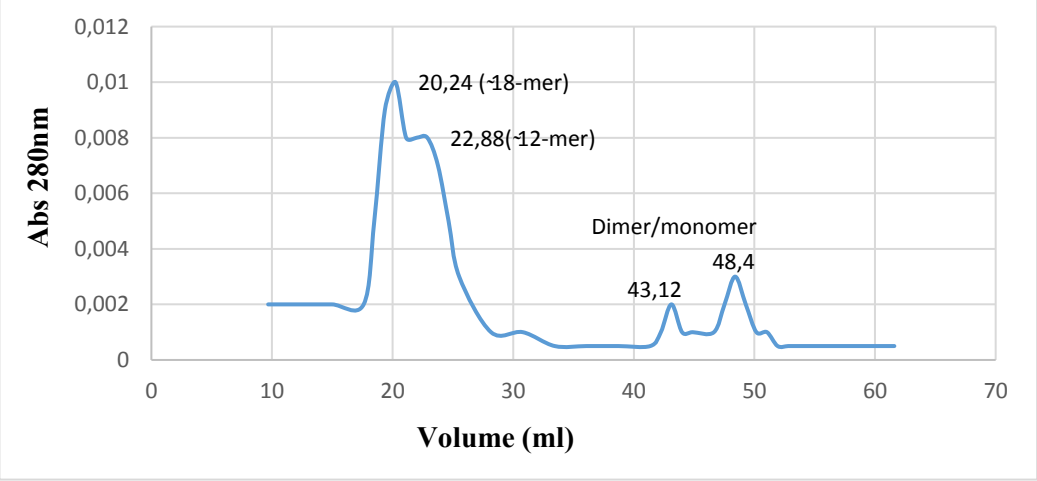

Figure 3.42. Size exclusion chromatography profile of concentrated po-sHSP20 protein. SEC analysis was performed on Sephacryl S300 15/50 column at the flow rate of 0.5 ml/min. with absorbance monitored at 280 nm. Two major combined peaks are corresponding to large oligomers (~18-mer and 12-mer) and small monomeric/dimeric units, respectively.

3.7. Determination of Chaperone Activities of Wild-type and Mutant po-sHSP20s

Chaperone activity assay was performed for both wild-type and mutant proteins. In this assay, pig heart citrate synthase enzyme (CS) was used as the model substrat. Citrate synthase which is a mesophilic enzyme loses its activity at 47˚C. Enzyme activity was measured in the presence and absence of po-sHSP20 variants under optimal and denaturing temperatures as described in Materials and Methods.

The results showed that wild-type po-sHSP20 and both variants of po-sHSP20 could protect CS activity at 47°C. Figure 3.43 shows one representative citrate synthase assay result. The chaperone activity of K99E mutant was observed to be the highest one. The protection by K99G mutant sHSP was less than that of the K99E mutant sHSP, but higher than the wild-type sHSP (Table 3.8). Thus, the results have revealed that the two point mutations increased the chaperone activity, with respect to wild-type sHSP activity.

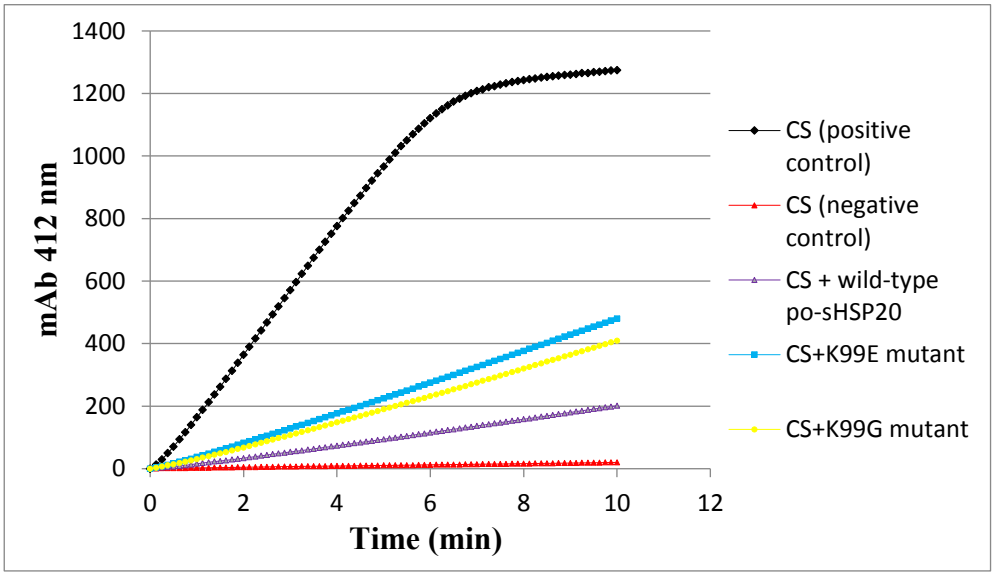

Figure 3.43. Citrate synthase activity: CS heated at 47ºC in all experiments, either in the presence (tests) or absence (negative control) of sHSP, except positive control.

In order to obtain better protection, wild-type and mutant chaperones were preheated at 65°C before carrying out activity assay. After preheating, chaperone activity assay was performed with CS as described before. It was observed that preheating of the sHSPs resulted in slightly increase in their chaperone activity. Figure 3.44 shows the result of one representative experiment performed following preheating of the chaperones. After preheating, the protection of CS from heat inactivation by K99E mutant was better while there has been only slight increase in the chaperone activities of K99G and wild-type sHSPs (Table 3.8).

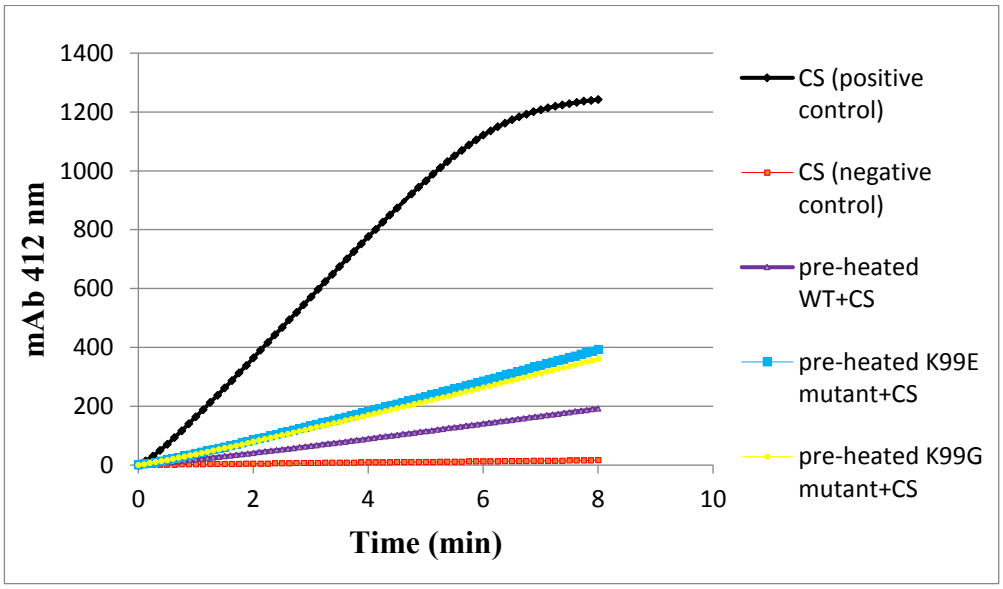

Figure 3.44. Citrate synthase activity after preheating of chaperones: CS alone incubated at 35°C (positive control). CS alone incubated at 47°C (negative control). CS incubated at 47°C in the presence of preheated wild-type chaperone. CS incubated at 47ºC in the presence of preheated K99E mutant chaperone. CS incubated at 47ºC in the presence of preheated K99G mutant chaperone.

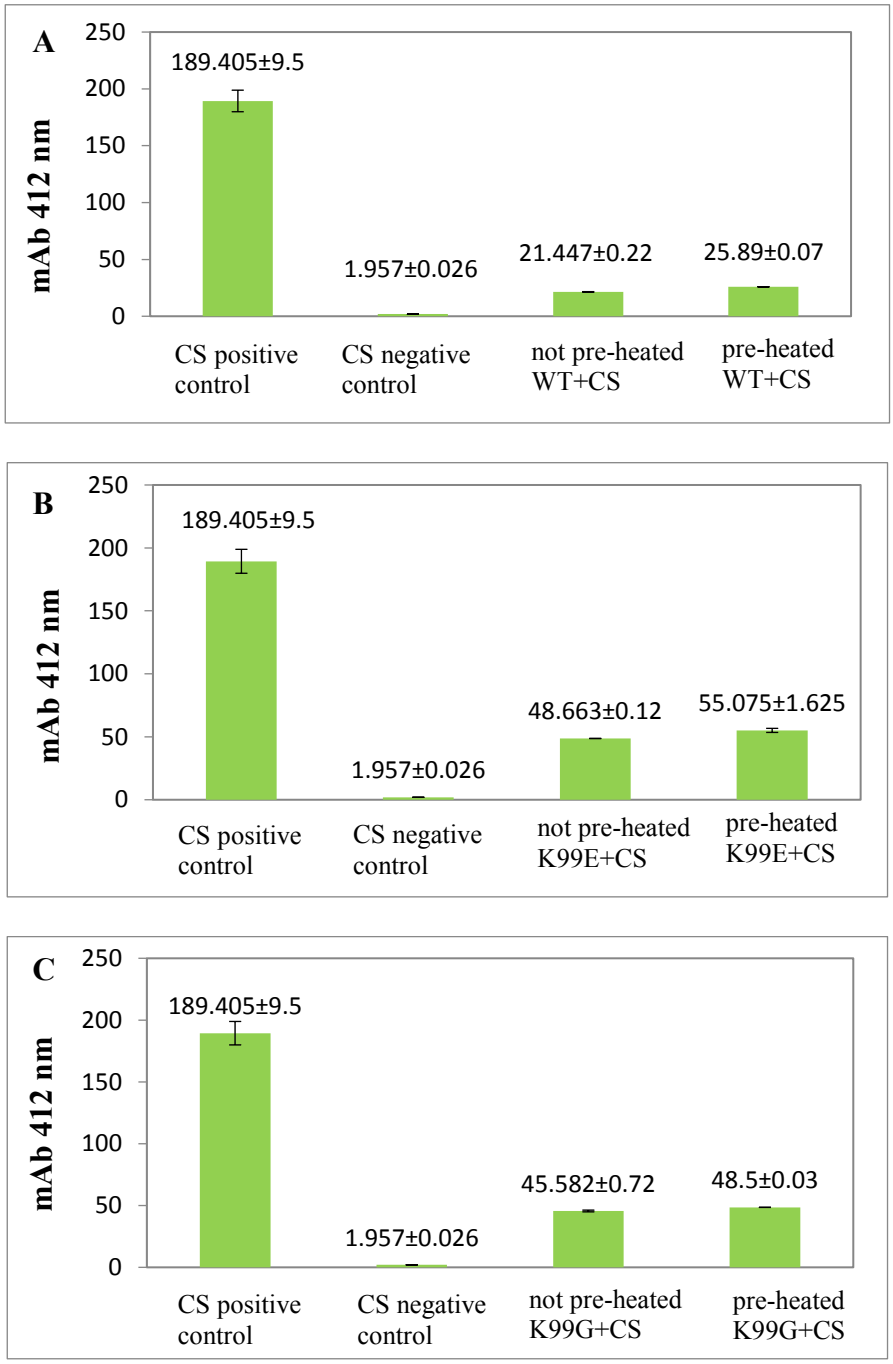

Figure 3.45. Chaperone activities of wild-type and mutant po-sHSP20s before and after heat treatment. A) Chaperone activity of wild-type po-sHSP20 before and after heat treatment. B) Chaperone activity of K99E mutant po-sHSP20 before and after heat treatment. C) Chaperone activity of K99G mutant po-sHSP20 before and after heat treatment. The values on top of each bar represents the mean ± standart deviation of results obtained in 3 independent experiments.

Table 3.8. *Mean activity (as mAbs/min) of po-sHSPs with and without preheat treatment*

CS under different conditions	**Mean activity of chaperones (as mAbs/min)**
CS incubated at 35ºC (positive control)	189.405 ± 9.5
CS incubated at 47ºC (negative control)	1.957 ± 0.026
CS incubated at 47ºC with WT	21.447 ± 0.22
CS incubated at 47ºC with K99E	48.663 ± 0.12
CS incubated at 47ºC with K99G	45.582 ± 0.72
CS incubated at 47ºC with preheated WT	25.89 ± 0.07
CS incubated at 47ºC with preheated K99E	55.075 ± 1.625
CS incubated at 47ºC with preheated K99G	48.5 ± 0.03

3.8. Thermal Aggregation Assay for Citrate Synthase by Light Scattering

Chaperone activities of wild-type and mutant proteins were also studied by thermal aggregation assay. The CS begins to form insoluble aggregates at 45ºC which were detected by measuring the absorbance at 320 nm in a time dependent manner.

Under experimental conditions, all po-sHSP20 wild-type and mutant proteins could prevent thermal aggregation of CS with a molar ratio of both 1:7 and 1:35 (CS:chaperone). The aggregation curves of each chaperones were plotted as shown in Figure 3.46 to Figure 3.51. As a control, CS aggregation was measured in the absence of chaperones. The blank contained only the buffer.

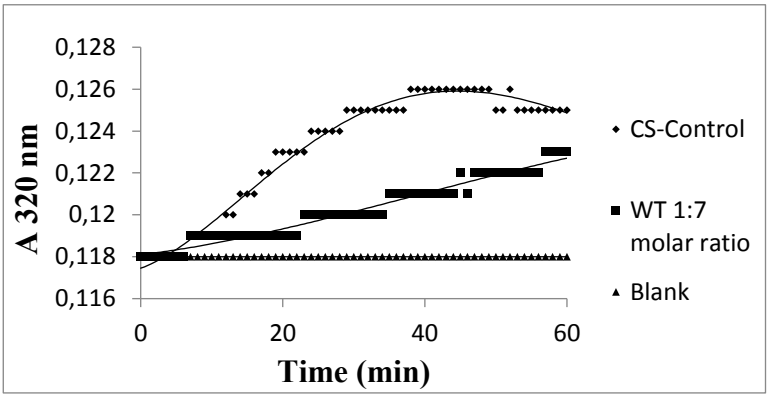

Figure 3.46. Thermal aggregation of CS with wild-type chaperone at a 1:7 molar ratio. Absorbance was measured at 320 nm.

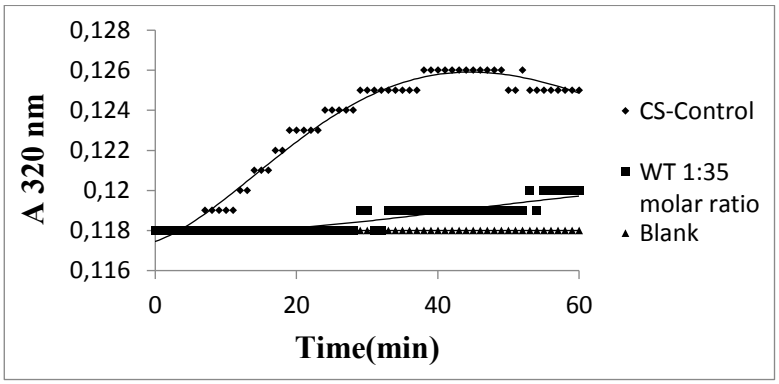

Figure 3.47. Thermal aggregation of CS with wild-type chaperone at a 1:35 molar ratio. Absorbance was measured at 320 nm.

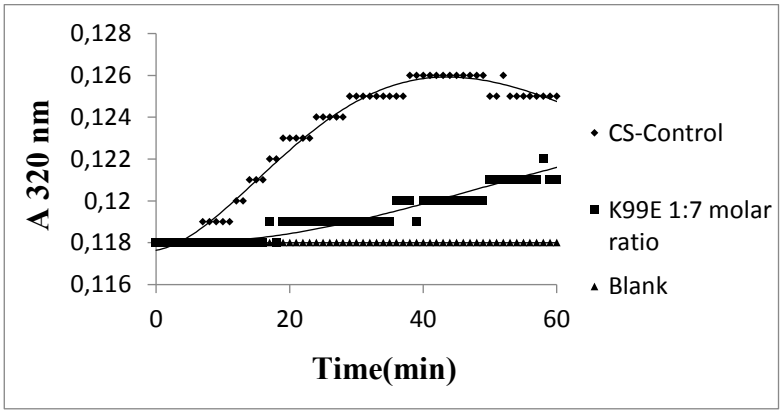

Figure 3.48. Thermal aggregation of CS with K99E mutant at a 1:7 molar ratio. Absorbance was measured at 320 nm.

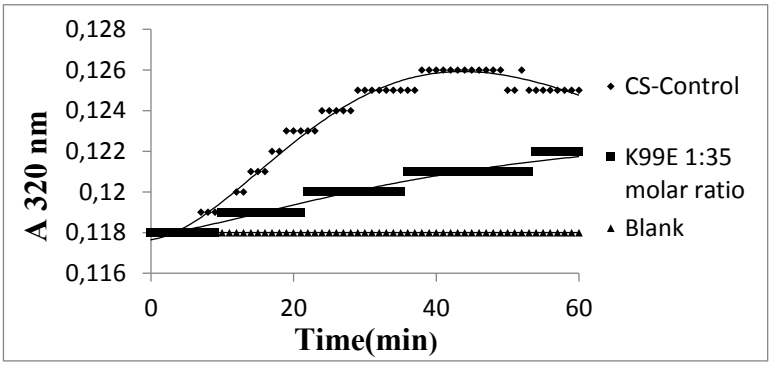

Figure 3.49. Thermal aggregation of CS with K99E mutant at a 1:35 molar ratio. Absorbance was measured at 320 nm.

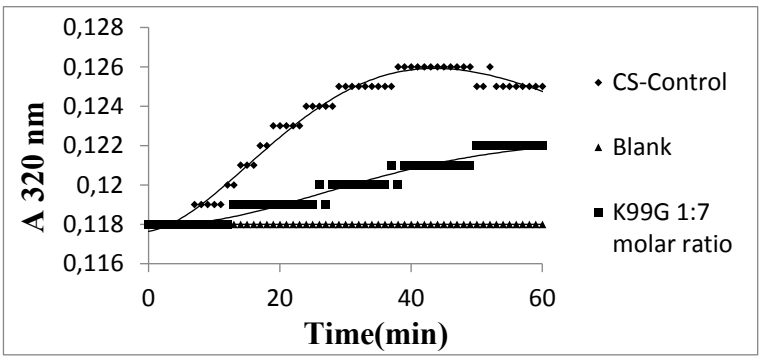

Figure 3.50. Thermal aggregation of CS with K99G mutant at a 1:7 molar ratio. Absorbance was measured at 320 nm.

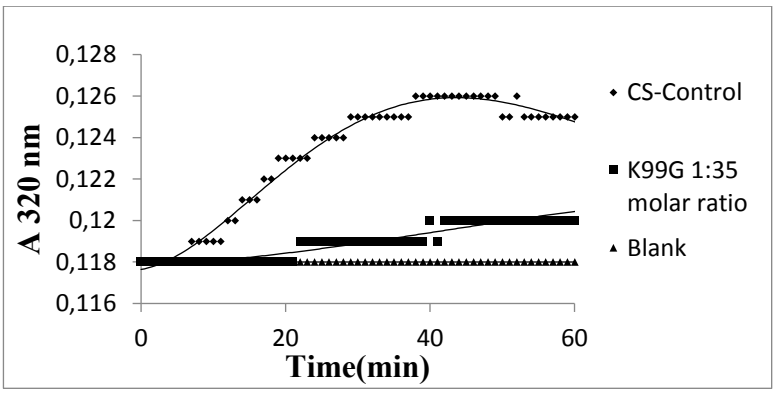

Figure 3.51. Thermal aggregation of CS with K99G mutant at a 1:35 molar ratio. Absorbance was measured at 320 nm.

All chaperone variants, including wild-type and mutant sHSPs, showed same effect on prevention of CS aggregation at a molar ratio of 1:7 (CS:chaperone). In the absence of chaperones (control), aggregation rate was detected as 100%. In the presence of each chaperones (molar ratio of 1:7), aggregation rate was found to be decreased to 20% (Figure 3.52).

When CS:chaperone molar ratio was 1:35, CS aggregation rate was decreased to 12.5% in the presence of wild-type and K99G mutant chaperones. On the other hand, in the presence of K99E mutant chaperone, aggregation rate was 17.5% (Figure 3.53). This result shows that wild-type and K99G mutant prevented CS aggregation more efficiently when compared to K99E mutant at a molar ratio of 1:35. Overall, all po-sHSP20 variants provided better protection of CS from heat aggregation in excess amounts (i.e., 1:35 molar ratio) (Figure 3.52 and Figure 3.53).

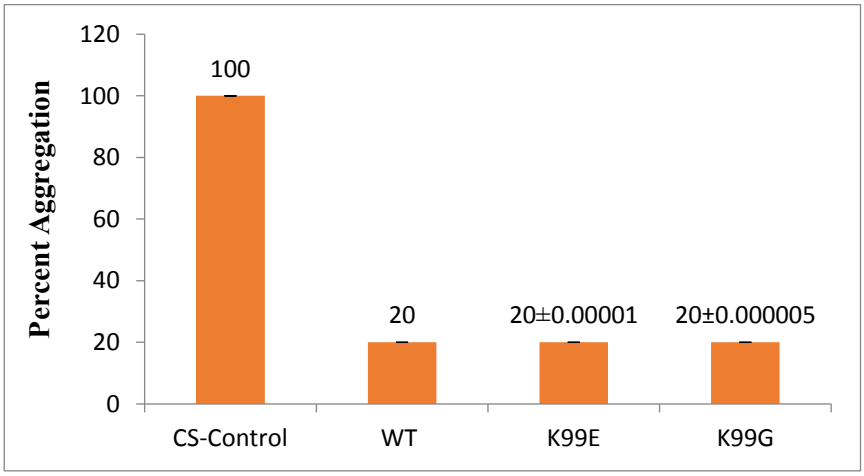

Figure 3.52. Percentage aggregation in the presence of chaperones with a molar ratio of 1:7. The values on top of each bar represents the mean ± standart deviation of results obtained in 3 independent experiments.

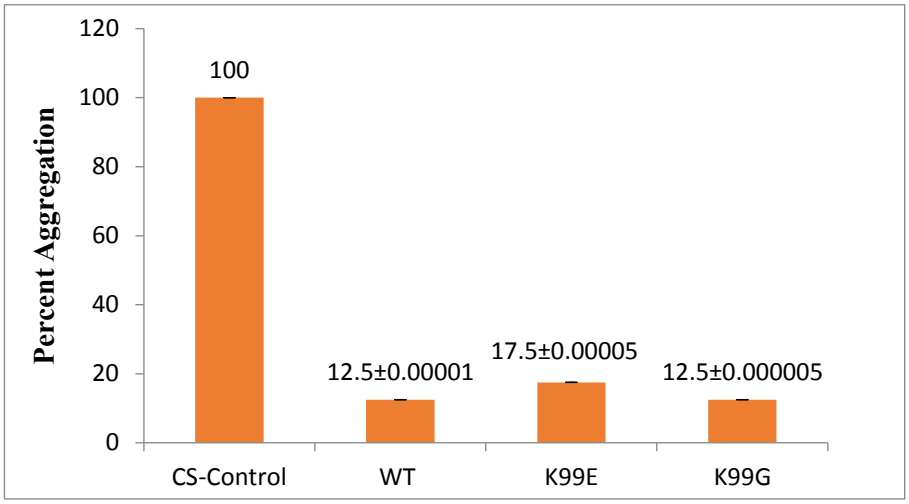

Figure 3.53. Percentage aggregation in the presence of chaperones with a molar ratio of 1:35. The values on top of each bar represents the mean ± standart deviation of results obtained in 3 independent experiments.

CHAPTER 4

DISCUSSION

Small heat shock proteins are widespread family of molecular chaperones involved in prevention of aggregation of unfolded proteins during stress by refolding of them in an ATP-independent manner. sHSPs are ubiquitous, found in all living organisms (Archaea, Bacteria, and Eucarya) and cyanobacterial phages (Bourelle-Langlois et al., 2016; Maaroufi and Tanguay 2013). They bind hydrophobic sites of unfolded proteins and keep them in folding state (Richter *et al*., 2010). They are associated with many cellular events including cell death, differentiation and cell cycle, stress tolerance, the conservation of cytoskeletal integrity, signal transduction and development (Bakthisaran *et al*., 2015). sHSPs such as αB-crystallin and Hsp27 have anti-apoptotic and anti-inflammatory properties. sHSP in human are also involved in cardioprotection and neuroprotection (Arrigo *et al*., 2007). Some other have roles in immunomodulation and anti-platelet aggregation properties (Bakthisaran *et al*., 2015). Therefore, mutations in the sHSP genes change their structure or chaperone activity and further cause several diseases such as cancer, cataract or neurodegenerative disorders (Cara *et al*., 2017). For example, R120G mutation in αA-crystallin results in eye lens cataract and myopathies in human (Clark *et al*., 2011 and Andley *et al*., 2011). R157H and G154S mutations in αB-crystallin cause dilated cardiomyopathies in human (Inagaki *et al*., 2006).

Up to date, different sHSPs from different organisms, including various thermophilic archaea such as *Sulfolobus solfataricus*, *Sulfolobus tokodaii* strain 7, *Methanococcus jannaschii, Thermococus sp*. strain KS-1 and *Pyrococcus furiosus* were studied functionally and structurally (Li *et al*., 2011; Abe *et al*., 2011; Kim *et al*., 1998; Usui *et al*., 2001 and Laksanalamai *et al*., 2001). This is the first report of cloning of

sHSP gene from a hyperacidophilic and thermophilic archaeon *Picrophilus oshimae* and over-expression of its recombinant protein in *E.coli* TG1 cells.

In the first part of this study, PCR-based strategy have been used for cloning and expression of po-sHSP20 gene in the pQE2 vector. Cloning was confirmed by restriction mapping and further verified by sequencing. Total 485 bp amplicon was cloned. Of which 381 bp sequence belongs po-sHSP20 gene.

In the second step of this study, overexpression of po-sHSP20 in *E.coli* was induced by IPTG under the control of lacZ operon. Our recombinant protein contains 6xHis-tag at its N-terminal. Thus, Ni-NTA agarose which is the affinity chromatography matrix was used for the purification of 6xHis-tagged po-sHSP20 protein. In addition, the recombinant protein was also purified by HPLC using HisTrap FF column. Isolated po-sHSP20 was analyzed on 12% SDS-PAGE gel. The recombinant protein revealed a protein band of 16 kDa molecular mass as estimated by bioinformatic tool. The batch purification by Ni-NTA affinity chromatography was found to be more effective to purify recombinant po-sHSP20 protein when compared to HPLC purification, in terms of yield and purity. Mostly elution 2 and elution 3 fractions of Ni-NTA column gave pure protein band on 12% polyacrylamid gel. When purification was performed by HPLC, the concentrations of elutions (elution 6 and elution 7) was apparently less compared to the elutions (elution 2 and elution 3) obtained by Ni-NTA chromatography (Figure 3.41).

After heat-treatment at 60 to 70°C, the po-sHSP20 protein bands on 12% SDS-PAGE gel were comparable in strength to that of untreated protein. This result indicated that po-sHSP20 is highly heat resistant, that might be related to thermophilic nature of the source organism. Similar results have been also reported in different studies with other thermophilic archaeal sHSPs. For example, cell extracts of Hsp20.1 and Hsp14.1 from *S.solfataricus* were heated at 75ºC for 30 min. While host proteins were removed at this temperature, Hsp20.1 and Hsp14.1 could resist this much high temperature (Liu *et al*., 2015). Similarly, cell extracts of *pfu-*

sHSP in *E.coli* were heated at 105ºC for 20-40 min. SDS-PAGE analysis of heated and non-heated cell extracts of pfu-sHSP showed that after heat treatment, bands of *E.coli* proteins became weak indicating the removal of host proteins (Laksanalamai *et al*., 2001). When cell extracts of MjHsp16.5 were heated up to 100ºC, it has been observed that MjHsp16.5 was heat-stable even at 100ºC (Kim *et al*., 1998). A sHSP from *Thermococcus* sp. was also heated at 75ºC for 30 min and was found so stable after heat treatment (Usui *et al*., 2001).

Our size-exclusion chromatography yielded two major combined peaks representing oligomers with a molecular mass of about 285 kDa and 201 kDa, implicating a 18-mer and a 12-mer complexes, and a smaller mass of ~24 and ~12 kDa, implicating dimeric/monomeric units. The molecular weight of po-sHSP20 is about 16 kDa. The results demonstrated that the po-sHSP20 protein under physiological conditions mostly forms large homo-oligomers consisting of about 12 and 18 subunits. Most of archaeal sHSPs consist of 12 to more than 32 subunits in their oligomeric state (Haslbeck *et al*., 2015). MjHsp16.5 was eluted from SEC column as a single peak with ~ 440 kDa corresponding to 24 monomers (Kim *et al*., 1998). Similarly, Hsp20.2 from *A.fulgidus* was isolated as a large oligomer of approximately 400 kDa representing the 24 subunits and a monomer of 16,537 kDa (Haslbeck *et al*., 2008). The oligomeric state of *S.tokodaii* Hsp14.0 was determined as 24-mer with the molecular mass of 364 kDa (Takeda *et al*., 2011). Also, *S.solfataricus* Hsp20.1 was isolated as an approximately 480 kDa implicating a 24-mer complex. SEC results of the purified sHSP of *Thermococcus* sp. have revealed that it also exits as 24-mer complex with the molecular weight of 478.6 kDa. Another example is an eukaryotic sHSP (Hsp16.9) isolated from *Triticum aestivum.* SEC profile of Hsp16.9 has indicated that it forms 12-mer complex (van Montfort *et al*., 2001).

In the third step of our study, lysine amino acid at position 99 of the recombinant po-sHSP20 was mutated. This residue of HSP20 from *Picrophilus oshimae* is equivalent to arginine 116 in αA-crystallin and arginine 120 in αB-crystallin of human. R116 in αA-crystallin and R120 in αB-crystallin are the most studied highly

conserved residues among sHSPs and associated with many diseases in human including eye lens cataract, various types of cancer, desmin-related myophaty and neurodegenerative diseases such as Alzheimer's disease, Parkinson's disease and Huntington's disease (Bova *et al*., 1999; Clark *et al*., 2011; Carra *et al*., 2017 and Treweek *et al*., 2015). The study of Bova *et al*. showed that R120G mutation in αB-crystallin resulted in loss of chaperone activity and increase in the oligomer size. R120G αB-crystallin became irregular in structure which might be associated with the disruption of the formation of β-sheet structure. R120G mutant had less amount of β-sheet structure according to the wild-type αB-crystallin (Bova *et al*., 1999). Panda *et al*. also showed R120G mutant αB-crystallin had larger oligomer size with decreased thermal stability as compared to wild-type protein. This instability caused loss in chaperone activity (Panda *et al*., 2016). Another report on R116 mutation in αA-crystallin showed that R116C mutation in αA-crystallin has been related to congenital cataract (Litt *et al*., 1998). R116C mutation also caused decrease in chaperone activity of αA-crystallin to prevent lens epithelial cell apoptosis. It also resulted in increase in oligomer size when compared to wild-type αA-crystallin and structural rearrangement in the subunits (Kumar *et al*., 1999). Therefore, structural changes and loss of surface hydrophobicity in R116C mutant were expected to be associated with the decrease in chaperone activity (Andley *et al*., 2002).

We have substituted K99 of the po-sHSP20 protein by G and E. In the first mutagenesis, positively charged polar amino acid lysine was replaced with glycine which is a hydrophobic amino acid (K99G). In the second mutagenesis, lysine was replaced with glutamic acid which is a negatively charged polar amino acid (K99E).

Chaperone activities of both wild-type and mutant po- sHSP20s were measured by using citrate synthase enzyme as a model substrate. Citrate synthase is a mesophilic enzyme and loses its activity at 47˚C. Our results showed that the wild-type and both mutant po-sHSP20s protected CS from heat denaturation. CS activity was observed to be the highest (25%) in the presence of K99E mutant sHSP. In the presence of K99G mutant sHSP, CS activity was relatively low (23%). In the presence of wild-

type sHSP, CS activity was the lowest (11%) when compared to mutant sHSPs. In order to obtain better protection, the wild-type and both variants were preheated at 65°C before performing activity assay. Preheating at 65°C resulted in even more increase in protection of CS from thermal inactivation by all po-sHSP20 variants. Many sHSPs exhibit enhanced chaperone activity after preheating (Haslbeck *et al*., 1999; Kim *et al*., 2003). The surface hydrophobicity of Hsp16.5 was increased by heat-stimulated conformational alterations of it. It has been shown that the chaperone activity of Hsp16.5 from *Methanococcus jannaschii* significantly increased after preheating at 85ºC (Cao *et al*., 2008). This is consistent with our results. We have observed a slight increase in protection of CS activity after preheat treatment at 65°C.

The increased chaperone activity of K99G might be explained due to the substitution of hydrophilic residue to hydrophobic residue. In the previous study of our laboratory, K87 in Hsp14.3 from *Thermoplasma volcanium* was replaced with isoleucine (hydrophobic) to search the effects of these mutations on chaperone activity (Kocabıyık *et al*., 2014). The increased chaperone activity of K87I was explained by the increase in hydrophobicity. K87 of *Tpv* Hsp14.3 is equivalent to K99 of po-sHSP20. Therefore, K99G mutation may result in the increased chaperone activity as a result of increased hydrophobicity. Likewise, R107 of MjHsp16.5 corresponding to K99 of po-sHSP20 was substituted by glycine and this mutation resulted in higher chaperone activity of MjHsp16.5 (Quinlan *et al*., 2013).

K99E mutant po-sHSP20 also resulted in higher chaperone activity relative to wild-type po-sHSP20. Lysine and glutamic acid have opposite charges. In the other charge reversal mutagenesis experiment (positive to negative), in αA-crytallin of human, R116D mutation resulted in decreased chaperone activity and significant change in structure including increased oligomer mass and loss of chaperone activity (Bera *et al*., 2002 and Simon *et al*. 2007). But, in our case, that mutation in equivalent position (K99E) resulted in increased chaperone activity. Therefore, the mutations at equivalent residues in the primary structures of different sHSPs from

different organisms, might have different structural and functional effects due to their particular positioning and interactions in 3-D structure.

On the other hand, arginine residues in ACD of sHSPs have important roles in the formation of oligomeric complexes of sHSPs and their chaperone activities (Moutaoufik *et al*., 2017). The positive charge on guadinine group of Arg residue is involved in the formation of salt bridges (Dabbaghizadeh *et al*., 2017). Modeling studies on HSP16.5 from *M.jannaschii* showed that R107 (K99 equivalent of po-sHSP20) is buried in hydrophobic patch of protein and makes a salt bridge with G41 (Ijssell *et al*., 1999). The replacement of R107 with glycine abolished electrostatic interaction in the dimer between R107 in one monomer and E98 in an neighbouring monomer to make more flexible ACD loop and caused changes in dimer interface. This mutation resulted in increased chaperone activity (Quinlan *et al*., 2013). In a similar study, R135 of *D.melanogaster* corresponding to K99 of po-sHSP20 was substituted by glycine. R135G mutation caused a slight change in its surface charge as compared to its wild-type. Because of this slight change, chaperone activity of R135G was found almost same with wild-type (Moutaoufik *et al*., 2017).

Chen *et al*. (2006) studied chaperone activity of a sHSP from *Pyrococcus furiosus*. They showed that after preheating at 97ºC, *Taq* DNA polymerase lost its enzyme activity. However, together with *pfu*-sHSP, *Taq* DNA polymerase could produce PCR product. This result indicated that chaperone activity of *pfu*-sHSP could protect the enzyme activity of *Taq* DNA polymerase under PCR conditions (Chen *et al*., 2006). Similarly, the activity of *Hind*III restriction enzyme was also protected after heat treatment at 60ºC by the addition of pfu-sHSP (Chen *et al*., 2006). The other chaperone activity assay was performed with sHSPs of *D.melanogaster* by using luciferase. When luciferase was heated at 42ºC, its activity was strongly decreased (2%). In the presence of Hsp22 and Hsp27, luciferase activity was determined as 54.9% and 42.8%, respectively (Morrow *et al*., 2006). Dabbaghizadeh *et al*. has also reported that Hsp22 of *D.melanogaster* increased the luciferase activity in human cells at 46ºC. Luciferase lost its activity after heat shock at 44ºC and 46ºC. They

showed that luciferase recovered 5% of its activity after the addition of Hsp22. When Hsp22 was heated at 44ºC and 46ºC, luciferase activity was increased to 12% and 10%, respectively (Dabbagizadeh *et al*., 2018). In consistent with the above observations, the wild-type po-sHSP20 and its two mutant variants are capable of protecting mesophilic pig heart citrate synthase effectively from heat-inactivation.

Thermal aggregation of CS was monitored by measuring the light scattering at 320 nm at 45°C. Solution in 50 mM HEPES buffer contained CS alone and CS at a molar ratio of 1:7 and 1:35 (CS:chaperone). It has been observed that all chaperones suppressed the aggregation of CS significantly. The presence of the wild-type and K99G at a molar ratio of 1:35 separately, resulted in better prevention of aggregation. The aggregation was suppressed more efficiently in the presence of wild-type po-sHSP20 and K99G mutant po-sHSP20 (12.5%) as compared to K99E mutant po-sHSP20 (17.5%).

In different thermal aggregation studies with various substrates and archaeal sHSPs, it has also been shown that sHSPs function in prevention of protein aggregation and unfolding under denaturing conditions. For example, Usui *et al*. showed that *T*.sHSP protected CS from thermal aggregation at a molar ratio of 1:40 (CS to chaperone). When molar ratio was 1:80, higher protection was observed (Usui *et al*., 2001). Hsp20.1 of *S.solfataricus* also could prevent thermal aggregation of MDH at a 1:24 molar ratio at 50ºC (Liu *et al*., 2015). Haslbeck *et al*. showed that Hsp20.2 of *A.fulgidus* up to a molar ratio of 1:8 (CS:Hsp20.2) prevented heat aggregation of CS (Haslbeck *et al*., 2008). The study of Kim *et al*. has revealed that 1:40 molar ratio of CS:MjHsp16.5 was required for inhibition of thermal aggregation at 40ºC, while 1:1 molar ratio of SCM (single-chain monellin):MjHsp16.5 was enough to prevent the client thermal aggregation at 80ºC (Kim *et al*., 1998). StHsp14.0 could completely prevented heat-induced aggregation of IPMDH at a 1:24 molar ratio (IPMDH:chaperone) at 87ºC (Usui *et al*.,2003). Morris *et al*. showed that HspB8 from human protected (50%) CS from thermal aggregation at a molar ratio of 1:4. Similar protection with Hsp27 was observed at a ratio of 1:1. (Morris *et al*., 2005).

In an another study, heat induced aggregates of lysozyme was decreased, when it is mixed with different concentrations of *pfu*-sHSP (Chen *et al*., 2006). In our study, thermal aggregation of pig heart CS was prevented by wild-type and mutant po-sHSP20 variants at 1:7 molar ratio. At higher molar ratio (1:35), aggregation of CS was inhibited even more efficiently.

Our molecular modelling results revealed that the predicted po-sHSP20 model structure resembles to the structure of other archaeal sHSPs (*M.jannaschii* Hsp16.5 Kim *et al*., 1998; wheat Hsp16.9 van Monfort *et al*., 2001; *S.tokodaii* Hsp14.0 Takeda *et al*., 2011; *S.solfataricus* Hsp14.1 Liu *et al*., 2015). The 3-D model of the po-sHSP20 monomer structure consists of an ACD flanked by a N-terminal α-helix and C-terminal coiled structure. Like a conventional ACD, it has an ACD of a compact β-sandwich which consists of two antiparallel β-sheets. One β-sheet has three strands, other β sheet has four strands. This β-sandwich resembles to an immunoglobulin fold. β6-strand is found in an extended loop which connects these two β-sheets. The dimer of po-sHSP20, similar to MjHsp16.5 and StHsp14.0 dimers, is formed by interaction of β6-strand of one monomer with β2-strand of other monomer and thus dimer interface is built (Takeda *et al*., 2011; McHaourab *et al*., 2012). However, ACD dimer of *S.solfataricus* Hsp20.1 is a little different from other archeal sHSPs and po-sHSP20. *S.solfataricus* Hsp20.1 does not contain a distinct β6-strand, it still makes a dimer via charged or polar residues of ACD (Liu *et al*., 2015).

Since, there are additional residues (11 residues) coming from pQE2 vector, K88 of *P.oshimae* sHSP corresponds to K99 of recombinant po-sHSP20. In po-sHSP20 structure, Lys99 of one monomer makes hydrogen bond with Gln92 of other monomer. Also, there are intramolecular hydrogen bonds between Lys99 and Ile76, Lys99 and Pro40 in A chain. On the other hand, in B chain, there is an intramolecular hydrogen bond between Lys99 and Leu38, in addition to hydrogen bonds between Lys99 and Ile76, Lys99 and Pro40.

In K99G mutant po-sHSP20 dimer, intermolecular hydrogen bond (in wild-type, K99 of one chain-Gln92 of other chain) was not observed, and only intramolecular hydrogen bond of K99 retained was with Ile76 in both chains. Other hydrophobic interactions and hydrogen bonds that K99 participates were lost as compared to wild-type po-sHSP20 structure. On the other hand, in K99E mutant po-sHSP20 dimer, intermolecular hydrogen bond (in wild-type, between K99 of one monomer and Gln92 of other monomer) was also lost. There are still intramolecular hydrogen bonds of Glu99 with Ile76 and Pro40. Intramolecular hydrophobic interactions of Glu99 with Ile101 and Pro40 were also lost as compared to wild-type po-sHSP20 structure. Overall, both mutant po-sHSP20 dimers lost intermolecular hydrogen bond of K99 with Gln92 and other intramolecular hydrophobic interactions of the K99 as well.

K99 is a residue in the ACD of po-sHSP20 that imparts subunit-subunit interaction by formation of a hydrogen bond with Gln92. The loss of this bond together with intramolecular hydrophobic bonds as a result of mutations may cause changes in the dimer/monomer structure and may also cause some change in the surface charges. This may affect the interaction of the mutant variants with the client protein (i.e., CS).

CHAPTER 5

CONCLUSION

1. In this study, for the first time we have cloned po-sHSP20 gene of *P.oshimae* and expressed its recombinant protein in *E.coli*.

2. Overexpressed recombinant protein that has N-terminal 6xHis-tag was purified by Ni-NTA affinity chromatography to homogeneity. The purified protein was stable to heat-denaturation at high temperature, i.e., 70ºC.

3. The oligomeric structures of the recombinant po-sHSP20 was studied by using SEC. The results showed that po-sHSP20 protein exists mostly as 18-mer and~12-mer oligomers together with some dimeric/monomeric units.

4. When highly conserved K99 residue was exchanged by hydrophobic Gly and Glu, chaperone activity of the po-sHSP20 increased as compared to wild-type protein. K99E and K99G mutant po-sHSP20 were more effective (2.3- and 2-fold, respectively) than wild-type po-sHSP20 to protect CS from heat inactivation at 47ºC. In accordance with this result, thermal aggregation of the client protein at 45ºC was significantly reduced by K99E and K99G mutant variants as compared to control.

5. The 3D model structure of the po-sHSP20 monomer as in other sHSPs consists of an ACD flanked by a N-terminal α-helix and C-terminal coiled structure. It has an ACD of a compact β-sandwich which consists of two antiparallel β-sheets. Dimer interface is built via the interactions of β6-strand of one monomer with β2-strand of other monomer, that is a characteristic feature of non-metazoan sHSPs. 3D model analysis of the mutant po-sHSP20 showed that Gly and Glu substitutions at position 99 resulted in loss of an intermolecular hydrogen bond, and an intramolecular hydrophobic interaction. Also, these mutations caused alterations or loss of some of the intramolecular hydrogen bonds that K99 residue forms. Overall changes in

bonding properties of the po-sHSP20 by point mutations, may alter surface exposed charges and interaction of the sHSPs with its client protein.

6. Due to their exceptional capacity for substrate binding and protection from heat denaturation, there might be several potential uses for po-sHSP20 and its mutant variants in industry and medical therapy (chaperonotherapy).

REFERENCES

Abe, T., Oka, T., Nakagome, A., Tsukada, Y., Yasunaga, T., & Yohda, M. (2011). StHsp14. 0, a small heat shock protein of Sulfolobus tokodaii strain 7, protects denatured proteins from aggregation in the partially dissociated conformation. The Journal of Biochemistry, 150(4), 403-409.

Aihara, T., Ito, T., Yamanaka, Y., Noguchi, K., Odaka, M., Sekine, M., & Yohda, M. (2016). Structural and functional characterization of aspartate racemase from the acidothermophilic archaeon Picrophilus torridus. Extremophiles, 20(4), 385-393.

Albers, S. V., Van de Vossenberg, J. L. C. M., Driessen, A. J., & Konings, W. N. (2000). Adaptations of the archaeal cell membrane to heat stress. Frontiers in Bioscience, 5, 813-820.

Andley, U. P., Hamilton, P. D., Ravi, N., & Weihl, C. C. (2011). A knock-in mouse model for the R120G mutation of αB-crystallin recapitulates human hereditary myopathy and cataracts. Public Library of Science One, 6(3), e17671.

Angelov, A., Voss, J., & Liebl, W. (2011). Characterization of Plasmid pPO1 from the Hyperacidophile Picrophilus oshimae. Archaea, 2011.

Aquilina, J. A., Benesch, J. L., Ding, L. L., Yaron, O., Horwitz, J. & Robinson, C. V. (2005). Subunit Exchange of polydisperse proteins: mass spectrometry reveals consequences of alphaA-crystallin truncation. Journal of Biological Chemistry 280, 14485–14491.

Arrigo, A. P., Simon, S., Gibert, B., Kretz-Remy, C., Nivon, M., Czekalla, A., & Vicart, P. (2007). Hsp27 (HspB1) and αB-crystallin (HspB5) as therapeutic targets. Federation of European Biochemical Societies Letters, 581(19), 3665-3674.

Bagneris, C., Bateman, O. A., Naylor, C. E., Cronin, N., Boelens, W. C., Keep, N. H., & Slingsby, C. (2009). Crystal structures of α-crystallin domain dimers of αB-crystallin and Hsp20. Journal of Molecular Biology, 392(5), 1242-1252.

Baker-Austin, C., & Dopson, M. (2007). Life in acid: pH homeostasis in acidophiles. Trends in Microbiology, 15(4), 165-171.

Bakthisaran, R., Tangirala, R., & Rao, C. M. (2015). Small heat shock proteins: role in cellular functions and pathology. Biochimica et Biophysica Acta (BBA)-Proteins and Proteomics, 1854(4), 291-319.

Baldwin, A. J., Hilton, G. R., Lioe, H., Bagnéris, C., Benesch, J. L., & Kay, L. E. (2011). Quaternary dynamics of αB-crystallin as a direct consequence of localised tertiary fluctuations in the C-terminus. Journal of Molecular Biology, 413(2), 310-320.

Basha, E., Friedrich, K. L., & Vierling, E. (2006). The N-terminal arm of small heat shock proteins is important for both chaperone activity and substrate specificity. Journal of Biological Chemistry, 281(52), 39943-39952.

Basha, E., Jones, C., Blackwell, A. E., Cheng, G., Waters, E. R., Samsel, K. A., & Vierling, E. (2013). An unusual dimeric small heat shock protein provides insight into the mechanism of this class of chaperones. Journal of Molecular Biology, 425(10), 1683-1696.

Bukach, O. V., Seit-Nebi, A. S., Marston, S. B., & Gusev, N. B. (2004). Some properties of human small heat shock protein Hsp20 (HspB6). European Journal of Biochemistry, 271(2), 291-302.

Bera, S., Thampi, P., Cho, W. J., & Abraham, E. C. (2002). A positive charge preservation at position 116 of αA-crystallin is critical for its structural and functional integrity. Biochemistry, 41(41), 12421-12426.

Binger, K. J., Ecroyd, H., Yang, S., Carver, J. A., Howlett, G. J., & Griffin, M. D. (2013). Avoiding the oligomeric state: αB-crystallin inhibits fragmentation and induces dissociation of apolipoprotein C-II amyloid fibrils. The Federation of American Societies for Experimental Biology, 27(3), 1214-1222.

Bourrelle-Langlois, M., Morrow, G., Finet, S., & Tanguay, R. M. (2016). In vitro structural and functional characterization of the small heat shock proteins (sHSP) of the Cyanophage S-ShM2 and its host, Synechococcus sp. WH7803. Public Library of Science One, 11(9), e0162233.

Brady, J. P., Garland, D., Duglas-Tabor, Y., Robison, W. G., Groome, A., & Wawrousek, E. F. (1997). Targeted disruption of the mouse αA-crystallin gene induces cataract and cytoplasmic inclusion bodies containing the small heat shockprotein αB-crystallin. Proceedings of the National Academy of Sciences, 94(3), 884-889.

Brock, T. D., Brock, K. M., Belly, R. T., & Weiss, R. L. (1972). Sulfolobus: a new genus of sulfur-oxidizing bacteria living at low pH and high temperature. Archiv für Mikrobiologie, 84(1), 54-68.

Carra, S., Alberti, S., Arrigo, P. A., Benesch, J. L., Benjamin, I. J., Boelens, W., & Carver, J. A. (2017). The growing world of small heat shock proteins: from structure to functions. Cell Stress and Chaperones, 22(4), 601-611.

Carver, J. A., Grosas, A. B., Ecroyd, H., & Quinlan, R. A. (2017). The functional roles of the unstructured N-and C-terminal regions in αB-crystallin and other mammalian small heat-shock proteins. Cell Stress and Chaperones, 22(4), 627-638.

Chen, Y. S., Lee, G. C., & Shaw, J. F. (2006). Gene cloning, expression, and biochemical characterization of a recombinant trehalose synthase from Picrophilus torridus in Escherichia coli. Journal of Agricultural and Food Chemistry, 54(19), 7098-7104.

Cheng, G., Basha, E., Wysocki, V. H., & Vierling, E. (2008). Insights into small heat shock protein and substrate structure during chaperone action derived from hydrogen/deuterium exchange and mass spectrometry. Journal of Biological Chemistry, 283(39), 26634-26642.

Ciaramella, M., Napoli, A., & Rossi, M. (2005). Another extreme genome: how to live at pH 0. Trends in Microbiology, 13(2), 49-51.

Clark, A. R., Lubsen, N. H., & Slingsby, C. (2012). sHSP in the eye lens: crystallin mutations, cataract and proteostasis. The International Journal of Biochemistry & Cell Biology, 44(10), 1687-1697.

Clark, A. R., Naylor, C. E., Bagneris, C., Keep, N. H., & Slingsby, C. (2011). Crystal structure of R120G disease mutant of human αB-crystallin domain dimer shows closure of a groove. Journal of Molecular Biology, 408(1), 118-134.

Cox, D., Whiten, D. R., Brown, J., Horrocks, M. H., San Gil, R., Dobson, C. M., & Ecroyd, H. (2018). The small heat shock protein Hsp27 binds α-synuclein fibrils, preventing elongation and cytotoxicity. Journal of Biological Chemistry, jbc-M117.

Cao, A., Wang, Z., Wei, P., Xu, F., Cao, J., & Lai, L. (2008). Preheating induced homogeneity of the small heat shock protein from Methanococcus jannaschii. Biochimica et Biophysica Acta (BBA)-Proteins and Proteomics, 1784(3), 489-495.

Chen, H., Chu, Z., Zhang, Y., & Yang, S. (2006). Over-expression and characterization of the recombinant small heat shock protein from Pyrococcus furiosus. Biotechnology Letters, 28(14), 1089-1094.

Chowdary, T. K., Raman, B., Ramakrishna, T., & Rao, C. M. (2004). Mammalian Hsp22 is a heat-inducible small heat-shock protein with chaperone-like activity. Biochemical Journal, 381(2), 379-387.

Dabbaghizadeh, A., Finet, S., Morrow, G., Moutaoufik, M. T., & Tanguay, R. M. (2017). Oligomeric structure and chaperone-like activity of Drosophila melanogaster mitochondrial small heat shock protein Hsp22 and arginine mutants in the alpha-crystallin domain. Cell Stress and Chaperones, 22(4), 577-588.

Dabbaghizadeh, A., Morrow, G., Amer, Y. O., Chatelain, E. H., Pichaud, N., & Tanguay, R. M. (2018). Identification of proteins interacting with the mitochondrial small heat shock protein Hsp22 of Drosophila melanogaster: Implication in mitochondrial homeostasis. Public Library of Science One, 13(3), e0193771.

Darland, G., Brock, T. D., Samsonoff, W., & Conti, S. F. (1970). A thermophilic, acidophilic mycoplasma isolated from a coal refuse pile. Science, 170(3965), 1416-1418.

Das, K. P., & Surewicz, W. K. (1995). Temperature-induced exposure of hydrophobic surfaces and its effect on the chaperone activity of α-crystallin. Federation of European Biochemical Societies Letters, 369(2-3), 321-325.

Delbecq, S. P., & Klevit, R. E. (2013). One size does not fit all: the oligomeric states of αB crystallin. Federation of European Biochemical Societies Letters, 587(8), 1073-1080.

Elferink, M. G., de Wit, J. G., Driessen, A. J., & Konings, W. N. (1994). Stability and proton-permeability of liposomes composed of archaeal tetraether lipids. Biochimica et Biophysica Acta (BBA)-Biomembranes, 1193(2), 247-254.

Eyles, S. J., & Gierasch, L. M. (2010). Nature's molecular sponges: small heat shock proteins grow into their chaperone roles. Proceedings of the National Academy of Sciences, 107(7), 2727-2728.

Ferrer, M., Golyshina, O. V., Beloqui, A., Golyshin, P. N., & Timmis, K. N. (2007). The cellular machinery of Ferroplasma acidiphilum is iron-protein-dominated. Nature, 445(7123), 91

Francois, J. A., Starks, C. M., Sivanuntakorn, S., Jiang, H., Ransome, A. E., Nam, J. W., & Kappock, T. J. (2006). Structure of a NADH-insensitive hexameric citrate synthase that resists acid inactivation. Biochemistry, 45(45), 13487-13499.

Frick, E., Spatzal, T., Gerhardt, S., Krämer, A., Einsle, O., & Hüttel, W. (2014). Structural and functional characterization of 4-hydroxyphenylpyruvate dioxygenase from the thermoacidophilic archaeon Picrophilus torridus. Extremophiles, 18(4), 641-651.

Fu, X., Zhang, H., Zhang, X., Cao, Y., Jiao, W., Liu, C., & Chang, Z. (2005). A dual role for the N-terminal region of Mycobacterium tuberculosis Hsp16. 3 in self-

oligomerization and binding denaturing substrate proteins. Journal of Biological Chemistry, 280(8), 6337-6348.

Fütterer, O., Angelov, A., Liesegang, H., Gottschalk, G., Schleper, C., Schepers, B., & Liebl, W. (2004). Genome sequence of Picrophilus torridus and its implications for life around pH 0. Proceedings of the National Academy of Sciences of the United States of America, 101(24), 9091-9096.

Garcia-Moreno, B. (2009). Adaptations of proteins to cellular and subcellular pH. Journal of Biology, 8(11), 98.

Ghosh, J. G., Shenoy, A. K., & Clark, J. I. (2006). N-and C-terminal motifs in human αB crystallin play an important role in the recognition, selection, and solubilization of substrates. Biochemistry, 45(46), 13847-13854.

Golyshina, O. V., & Timmis, K. N. (2005). Ferroplasma and relatives, recently discovered cell wall-lacking archaea making a living in extremely acid, heavy metal-rich environments. Environmental Microbiology, 7(9), 1277-1288.

Goswami, K., Arora, J., & Saha, S. (2015). Characterization of the MCM homohexamer from the thermoacidophilic euryarchaeon Picrophilus torridus. Scientific Reports, 5, 9057.

Gómez-Puertas, P., Martín-Benito, J., Carrascosa, J. L., Willison, K. R., & Valpuesta, J. M. (2004). The substrate recognition mechanisms in chaperonins. Journal of Molecular Recognition, 17(2), 85-94.

Haley DA, Bova MP, Huang QL, McHaourab HS, Stewart PL (2000) Small heat-shock protein structures reveal a continuum from symmetric to variable assemblies. Journal of Molecular Biology 298(2):261–272.

Haley DA, Horwitz J, Stewart PL (1998) The small heat-shock protein, aB-crystallin, has a variable quaternary structure. Journal of Molecular Biology 277(1):27–35.

Han, M. H., Hwang, S. I., Roy, D. B., Lundgren, D. H., Price, J. V., Ousman, S. S., & Grinnell, B. W. (2008). Proteomic analysis of active multiple sclerosis lesions reveals therapeutic targets. Nature, 451(7182), 1076.

Han, T., Zeng, F., Li, Z., Liu, L., Wei, M., Guan, Q., & Zhang, S. (2013). Biochemical characterization of a recombinant pullulanase from Thermococcus kodakarensis KOD1. Letters in Applied Microbiology, 57(4), 336-343.

Haslbeck, M., & Vierling, E. (2015). A first line of stress defense: small heat shock proteins and their function in protein homeostasis. Journal of Molecular Biology, 427(7), 1537-1548.

Haslbeck, M., Franzmann, T., Weinfurtner, D., and Buchner, J. (2005). Some like it hot: the structure and function of small-heat shock proteins. Nature Structural&Molecular Biology 12, 842–846.

Haslbeck, M., Kastenmüller, A., Buchner, J., Weinkauf, S., & Braun, N. (2008). Structural dynamics of archaeal small heat shock proteins. Journal of Molecular Biology, 378(2), 362-374.

Hess, M., Katzer, M., & Antranikian, G. (2008). Extremely thermostable esterases from the thermoacidophilic euryarchaeon Picrophilus torridus. Extremophiles, 12(3), 351-364.

Hilton, G. R., Hochberg, G. K., Laganowsky, A., McGinnigle, S. I., Baldwin, A. J., & Benesch, J. L. (2013). C-terminal interactions mediate the quaternary dynamics of αB-crystallin. Philopshical Transactions of the Royal Society B, 368(1617), 20110405.

Horwitz, J. (1992). Alpha-crystallin can function as a molecular chaperone. Proceedings of the National Academy of Sciences, 89(21), 10449-10453.

Houlden, H., Laura, M., Wavrant–De Vrièze, F., Blake, J., Wood, N., & Reilly, M. M. (2008). Mutations in the HSP27 (HSPB1) gene cause dominant, recessive, and sporadic distal HMN/CMT type 2. Neurology, 71(21), 1660-1668.

Huang, Y., Krauss, G., Cottaz, S., Driguez, H., & Lipps, G. (2005). A highly acid-stable and thermostable endo-β-glucanase from the thermoacidophilic archaeon Sulfolobus solfataricus. Biochemical Journal, 385(2), 581-588.

Ikeda, Y., Abe, A., Ishida, C., Takahashi, K., Hayasaka, K., & Yamada, M. (2009). A clinical phenotype of distal hereditary motor neuronopathy type II with a novel HSPB1 mutation. Journal of the Neurological Sciences, 277(1), 9-12.

Ikeda, Y., Abe, A., Ishida, C., Takahashi, K., Hayasaka, K., & Yamada, M. (2009). A clinical phenotype of distal hereditary motor neuronopathy type II with a novel HSPB1 mutation. Journal of the Neurological Sciences, 277(1), 9-126.

Ito, H., Kamei, K., Iwamoto, I., Inaguma, Y., Nohara, D., & Kato, K. (2001). Phosphorylation-induced change of the oligomerization state of αB-crystallin. Journal of Biological Chemistry, 276(7), 5346-5352.

Jay, Z. J., & Inskeep, W. P. (2015). The distribution, diversity, and importance of 16S rRNA gene introns in the order Thermoproteales. Biology Direct, 10(1), 35.

Jiao, Q., Sanbe, A., Zhang, X., Liu, J. P., & Minamisawa, S. (2014). αB-Crystallin R120G variant causes cardiac arrhythmias and alterations in the expression of Ca2+-handling proteins and endoplasmic reticulum stress in mice. Clinical and Experimental Pharmacology and Physiology, 41(8), 589-599.

Jiao, W., Hong, W., Li, P., Sun, S., Ma, J., Qian, M., & Chang, Z. (2008). The dramatically increased chaperone activity of small heat-shock protein IbpB is retained for an extended period of time after the stress condition is removed. Biochemical Journal, 410(1), 63-70.

Jovcevski, B., Aquilina, J. A., Benesch, J. L., & Ecroyd, H. (2018). The influence of the N-terminal region proximal to the core domain on the assembly and chaperone activity of αB-crystallin. Cell Stress and Chaperones, 1-10.

Kim, J. W., Flowers, L. O., Whiteley, M., & Peeples, T. L. (2001). Biochemical confirmation and characterization of the family-57-like α-amylase of Methanococcus jannaschii. Folia Microbiologica, 46(6), 467-473.

Kim, R., Lai, L., Lee, H. H., Cheong, G. W., Kim, K. K., Wu, Z., & Kim, S. H. (2003). On the mechanism of chaperone activity of the small heat-shock protein of Methanococcus jannaschii. Proceedings of the National Academy of Sciences, 100(14), 8151-8155.

Kumar, M. S., Kapoor, M., Sinha, S., & Reddy, G. B. (2005). Insights into hydrophobicity and the chaperone-like function of αA-and αB-crystallins. Journal of Biological Chemistry, 280(23), 21726-21730.

Laksanalamai, P., Maeder, D. L., & Robb, F. T. (2001). Regulation and mechanism of action of the small heat shock protein from the hyperthermophilic archaeon Pyrococcus furiosus. Journal of Bacteriology, 183(17), 5198-5202.

Lambert, W., Koeck, P. J., Ahrman, E., Purhonen, P., Cheng, K., Elmlund, D., & Emanuelsson, C. (2011). Subunit arrangement in the dodecameric chloroplast small heat shock protein Hsp21. Protein Science, 20(2), 291-301.

Lee, G. J., & Vierling, E. (2000). A small heat shock protein cooperates with heat shock protein 70 systems to reactivate a heat-denatured protein. Plant Physiology, 122(1), 189-198

Li, D. C., Yang, F., Lu, B., Chen, D. F., & Yang, W. J. (2012). Thermotolerance and molecular chaperone function of the small heat shock protein HSP20 from hyperthermophilic archaeon, Sulfolobus solfataricus P2. Cell stress and Chaperones, 17(1), 103-108.

Liu, L., Chen, J., Yang, B., & Wang, Y. (2015). Crystal structure and function of an unusual dimeric Hsp20. 1 provide insight into the thermal protection mechanism of small heat shock proteins. Biochemical and Biophysical Research Communications, 458(2), 429-434

Lindner, R. A., Kapur, A., Mariani, M., Titmuss, S. J., & Carver, J. A. (1998). Structural alterations of α-crystallin during its chaperone action. European Journal of Biochemistry, 258(1), 170-183.

Maaroufi, H., & Tanguay, R. M. (2013). Analysis and phylogeny of small heat shock proteins from marine viruses and their cyanobacteria host. Public Library of Science One, 8(11), e81207.

Mainz A, Peschek J, Stavropoulou M et al (2015) The chaperone αB-crystallin uses different interfaces to capture an amorphous and an amyloid client. Nature Structural& Molecular Biology 22(11):898–905. doi:10.1038/nsmb.3108.

Mangold, S., Rao Jonna, V., & Dopson, M. (2013). Response of Acidithiobacillus caldus toward suboptimal pH conditions. Extremophiles, 17(4), 689-696.

Mani, N., Bhandari, S., Moreno, R., Hu, L., Prasad, B. V., & Suguna, K. (2016). Multiple oligomeric structures of a bacterial small heat shock protein. Scientific reports, 6, 24019.

McGreal, R. S., Kantorow, W. L., Chauss, D. C., Wei, J., Brennan, L. A., & Kantorow, M. (2012). αB-crystallin/sHSP protects cytochrome c and mitochondrial function against oxidative stress in lens and retinal cells. Biochimica et Biophysica Acta (BBA)-General Subjects, 1820(7), 921-930.

Mchaourab, H. S., Godar, J. A., & Stewart, P. L. (2009). Structure and mechanism of protein stability sensors: chaperone activity of small heat shock proteins. Biochemistry, 48(18), 3828-3837.

Mchaourab, H. S., Lin, Y. L., & Spiller, B. W. (2012). Crystal structure of an activated variant of small heat shock protein Hsp16. 5. Biochemistry, 51(25), 5105-5112.

Michaux, C., Pouyez, J., Mayard, A., Vandurm, P., Housen, I., & Wouters, J. (2010). Structural insights into the acidophilic pH adaptation of a novel endo-1, 4-β-xylanase from Scytalidium acidophilum. Biochimie, 92(10), 1407-1415.

Mishra, S., Chandler, S. A., Williams, D., Claxton, D. P., Koteiche, H. A., Stewart, P. L., & Mchaourab, H. S. (2018). Engineering of a polydisperse small heat-Shock protein reveals conserved motifs of oligomer plasticity. bioRxiv, 247288.

Morrow, G., Heikkila, J. J., & Tanguay, R. M. (2006). Differences in the chaperone-like activities of the four main small heat shock proteins of Drosophila melanogaster. Cell stress & Chaperones, 11(1), 51.

Morrow, G., & Tanguay, R. M. (2012). Small heat shock protein expression and functions during development. The International Journal of Biochemistry & Cell Biology, 44(10), 1613-1621.

Ñancucheo, I., & Johnson, D. B. (2010). Production of glycolic acid by chemolithotrophic iron-and sulfur-oxidizing bacteria and its role in delineating and sustaining acidophilic sulfide mineral-oxidizing consortia. Applied and Environmental Microbiology, 76(2), 461-467.

Pras E, Frydman M, Levy-Nissenbaum E, Bakhan T, Raz J, Assia EI, Goldman B, Pras E (2000). A nonsense mutation (W9X) in CRYAA causes autosomal recessive cataract in an inbred Jewish Persian family. Invest Ophthalmol & Visual Science 41(11):3511–3515.

Rajput, R., Verma, V. V., Chaudhary, V., & Gupta, R. (2013). A hydrolytic γ-glutamyl transpeptidase from thermo-acidophilic archaeon Picrophilus torridus: binding pocket mutagenesis and transpeptidation. Extremophiles, 17(1), 29-41.

Raju, I., Oonthonpan, L., & Abraham, E. C. (2012). Mutations in human αA crystallin/sHSP affect subunit exchange interaction with αB-crystallin. Public Library of Science One, 7(2), e31421.

Ratajczak, E., Ziętkiewicz, S., & Liberek, K. (2009). Distinct activities of Escherichia coli small heat shock proteins IbpA and IbpB promote efficient protein disaggregation. Journal of Molecular Biology, 386(1), 178-189.

Reed, C. J., Lewis, H., Trejo, E., Winston, V., & Evilia, C. (2013). Protein adaptations in archaeal extremophiles. Archaea, 2013.

Reddy, G. B., Das, K. P., Petrash, J. M., & Surewicz, W. K. (2000). Temperature-dependent chaperone activity and structural properties of human αA-and αB-crystallins. Journal of Biological Chemistry, 275(7), 4565-4570

Reher, M., & Schönheit, P. (2006). Glyceraldehyde dehydrogenases from the thermoacidophilic euryarchaeota Picrophilus torridus and Thermoplasma acidophilum, key enzymes of the non-phosphorylative Entner–Doudoroff pathway, constitute a novel enzyme family within the aldehyde dehydrogenase superfamily. Federation of European Biochemical Societies Letters, 580(5), 1198-1204.

Reilly, M. M. (2008) Mutations in the HSP27 (HSPB1) gene cause dominant, recessive, and sporadic distal HMN/CMT type 2. Neurology 71(21):1660–1668.

Richter, K., Haslbeck, M., & Buchner, J. (2010). The heat shock response: life on the verge of death. Molecular Cell, 40(2), 253-266.

Roman, S. G., Chebotareva, N. A., & Kurganov, B. I. (2017). Anti-aggregation activity of small heat shock proteins under crowded conditions. International Journal of Biological Macromolecules, 100, 97-103.

Rossoni, L., Hall, S. J., Eastham, G., Licence, P., & Stephens, G. (2015). The putative mevalonate diphosphate decarboxylase from Picrophilus torridus is in reality a mevalonate-3-kinase with high potential for bioproduction of isobutene. Applied and Environmental Microbiology, 81(7), 2625-2634.

Rothschild, L. J., & Mancinelli, R. L. (2001). Life in extreme environments. Nature, 409(6823), 1092.

Saji, H., Iizuka, R., Yoshida, T., Abe, T., Kidokoro, S. I., Ishii, N., & Yohda, M. (2008). Role of the IXI/V motif in oligomer assembly and function of StHsp14. 0, asmall heat shock protein from the acidothermophilic archaeon, Sulfolobus tokodaii strain 7. Proteins: Structure, Function, and Bioinformatics, 71(2), 771-782.

Santhosh Kumar, P., & Sharma, K. K. (2001). Phe71 is essential for chaperone-like function in αA-crystallin. Journal of Biological Chemistry, 276(50), 47094-47099.

Sathish, H. A., Stein, R. A., Yang, G., & Mchaourab, H. S. (2003). Mechanism of chaperone Function in small heat-shock proteins fluorescence studies of the conformations of t4 lysozyme bound to αb-crystallin. Journal of Biological Chemistry, 278(45), 44214-44221.

Schäfer, K., Magnusson, U., Scheffel, F., Schiefner, A., Sandgren, M. O., Diederichs, K., & Mowbray, S. L. (2004). X-ray structures of the maltose–maltodextrin-binding protein of the thermoacidophilic bacterium Alicyclobacillus acidocaldarius provide insight into acid stability of proteins. Journal of Molecular Biology, 335(1), 261-274.

Schiraldi, C., Di Lernia, I., & De Rosa, M. (2002). Trehalose production: exploiting novel approaches. Trends in Biotechnology, 20(10), 420-425.

Sharma, A., & Satyanarayana, T. (2012). Cloning and expression of acidstable, high maltose-forming, Ca 2+-independent α-amylase from an acidophile Bacillus acidicola and its applicability in starch hydrolysis. Extremophiles, 16(3), 515-522.

She, Q., Singh, R. K., Confalonieri, F., Zivanovic, Y., Allard, G., Awayez, M. J., & Erauso, G. (2001). The complete genome of the crenarchaeon Sulfolobus solfataricus P2. Proceedings of the National Academy of Sciences, 98(14), 7835-7840.

Simon, S., Michiel, M., Skouri-Panet, F., Lechaire, J. P., Vicart, P., & Tardieu, A. (2007). Residue R120 is essential for the quaternary structure and functional integrity of human αB-crystallin. Biochemistry, 46(33), 9605-9614.

Sun, Y., & MacRae, T. H. (2005). The small heat shock proteins and their role in human disease. The Federation of European Biochemical Societies Journal, 272(11), 2613-2627.

Takagi, M., Tamaki, H., Miyamoto, Y., Leonardi, R., Hanada, S., Jackowski, S., & Chohnan, S. (2010). Pantothenate kinase from the thermoacidophilic archaeon Picrophilus torridus. Journal of Bacteriology, 192(1), 233-241.

Thürmer, A., Voigt, B., Angelov, A., Albrecht, D., Hecker, M., & Liebl, W. (2011). Proteomic analysis of the extremely thermoacidophilic archaeon Picrophilus torridus at pH and temperature values close to its growth limit. Proteomics, 11(23), 4559-4568.

Treweek, T. M., Meehan, S., Ecroyd, H., & Carver, J. A. (2015). Small heat-shock proteins: important players in regulating cellular proteostasis. Cellular and Molecular Life Sciences, 72(3), 429-451.

Treweek, T. M., Rekas, A., Lindner, R. A., Walker, M. J., Aquilina, J. A., Robinson, C. V., & Carver, J. A. (2005). R120G αB-crystallin promotes the unfolding of reduced α-lactalbumin and is inherently unstable. The Federation of European Biochemical Societies Journal, 272(3), 711-724.

Tyson, G. W., Chapman, J., Hugenholtz, P., Allen, E. E., Ram, R. J., Richardson, P. M., & Banfield, J. F. (2004). Community structure and metabolism through reconstruction of microbial genomes from the environment. Nature, 428(6978), 37.

Usui, K., Yoshida, T., Maruyama, T., & Yohda, M. (2001). Small heat shock protein of a hyperthermophilic archaeum, Thermococcus sp. strain KS-1, exists as a spherical 24 mer and its expression is highly induced under heat-stress conditions. Journal of Bioscience and Bioengineering, 92(2), 161-166.

Quinlan, R. A., Zhang, Y., Lansbury, A., Williamson, I., Pohl, E., & Sun, F. (2013). Changes in the quaternary structure and function of MjHSP16. 5 attributable to deletion of the IXI motif and introduction of the substitution, R107G, in the α-crystallin domain. Philosophical Transactions of the Royal Society Biological Sciencies, 368(1617), 20120327.

van de Vossenberg, J. L., Driessen, A. J., & Konings, W. N. (1998). The essence of being extremophilic: the role of the unique archaeal membrane lipids. Extremophiles, 2(3), 163-170.

van de Vossenberg, J. L., Driessen, A. J., Zillig, W., & Konings, W. N. (1998). Bioenergetics and cytoplasmic membrane stability of the extremely acidophilic, thermophilic archaeon Picrophilus oshimae. Extremophiles, 2(2), 67-74.

Vicart, P., Caron, A., Guicheney, P., Li, Z., Prévost, M. C., Faure, A., & Paulin, D. (1998). A missense mutation in the αB-crystallin chaperone gene causes a desmin-related myopathy. Nature Genetics, 20(1), 92.

Vos, M. J., Zijlstra, M. P., Kanon, B., van Waarde-Verhagen, M. A., Brunt, E. R., Oosterveld-Hut, H. M., Carra S, Sibon O. C. & Kampinga, H. H. (2010). HSPB7 is the most potent polyQ aggregation suppressor within the HSPB family of molecular chaperones. Human Molecular Genetics, 19(23), 4677-4693.

Waters, E. R. (2012). The evolution, function, structure, and expression of the plant sHSPs. Journal of Experimental Botany, 64(2), 391-403.

Weeks, S. D., Baranova, E. V., Heirbaut, M., Beelen, S., Shkumatov, A. V., Gusev, N. B., & Strelkov, S. V. (2014). Molecular structure and dynamics of the dimeric human small heat shock protein HSPB6. Journal of Structural Biology, 185(3), 342-354.

White, H. E., Orlova, E. V., Chen, S.,Wang, L., Ignatiou, A., Gowen, B. et al. (2006). Multiple distinct assemblies reveal conformational flexibility in the small heat shock protein Hsp26. Structure, 14, 1197–1204.

Woese, C. R., Kandler, O., & Wheelis, M. L. (1990). Towards a natural system of organisms: proposal for the domains Archaea, Bacteria, and Eucarya. Proceedings of the National Academy of Sciences, 87(12), 4576-4579.

Xi, D., Wei, P., Zhang, C., & Lai, L. (2014). The minimal α-crystallin domain of Mj Hsp16. 5 is functional at non-heat-shock conditions. Proteins: Structure, Function, and Bioinformatics, 82(7), 1156-1167.

Zhang, K., Ezemaduka, A. N., Wang, Z., Hu, H., Shi, X., Liu, C., & Yin, C. C. (2015). A novel mechanism for small heat shock proteins to function as molecular chaperones. Scientific Reports, 5, 8811.

APPENDICES

A. Buffer and Solutions

1. LB Medium (1L) pH:7.0

Tryptone	10 g
Yeast Extract	5 g
NaCl	10 g

Adjust pH to 7.0 and add 1.5% agar. Complete the volume to 1L with double distilled water. Autoclave at 121ºC for 20 min.

2. 50X TAE Buffer (1 L)

Tris-HCl	242 g
Glacial acetic acid	57.10 ml
0.5 M EDTA (pH:8.4)	100 ml
pH=8.4	

Complete the volume to 1L with distilled water, autoclave the solution at 121ºC for 20 min. Store at 4ºC.

3. Running Buffer For Agarose Gel Electrophoresis

50X TAE Buffer	6 ml
Distilled water	300 ml

4. Agarose Gel Preparation (1%)

Agarose	0.4 g
Running Buffer	40 ml
Ethidium Bromide	5 µl

B. Cloning Vector

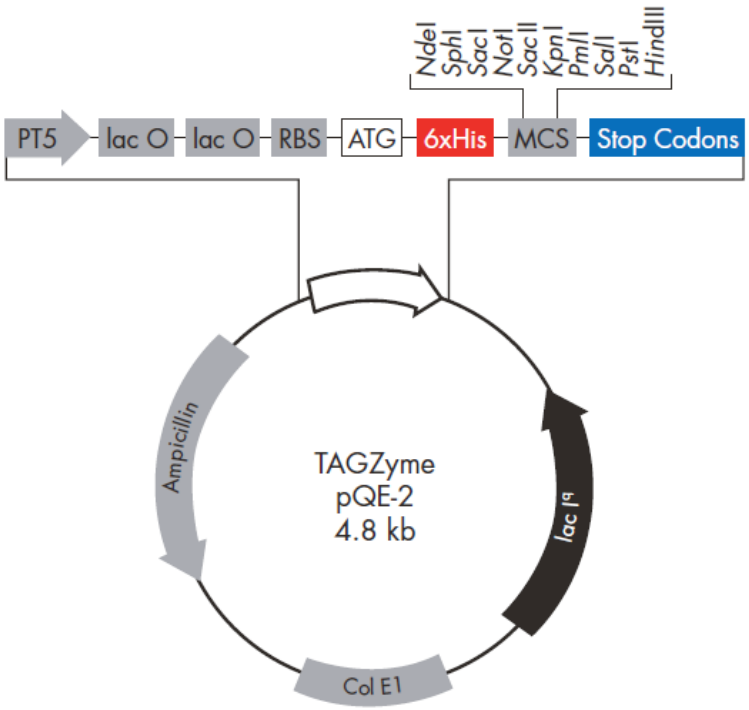

Figure B.1 pQE2 Vector (QIAGEN)

C. Molecular Size Markers

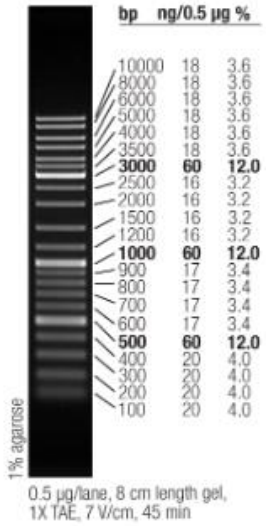

Figure C.1 O'Gene ruler DNA Ladder mix , Ready-to-use

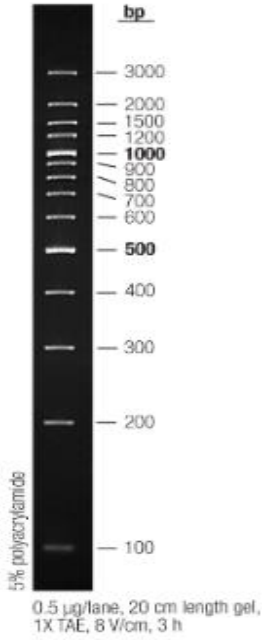

Figure C.2 Generuler 100 bp plus DNA Ladder

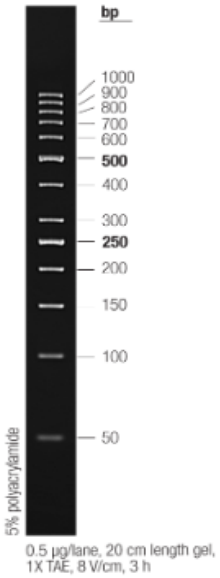

Figure C.3 Generuler 50 bp DNA Ladder

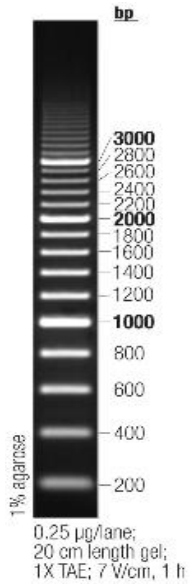

Figure C.4 O'RangeRuler 200 bp Ladder

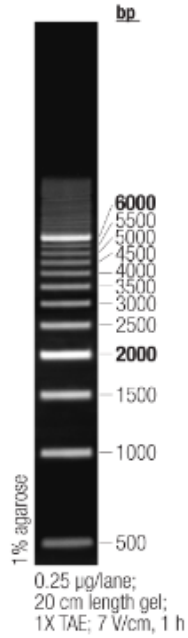

Figure C.5 O'Range Ruler 500 bp marker

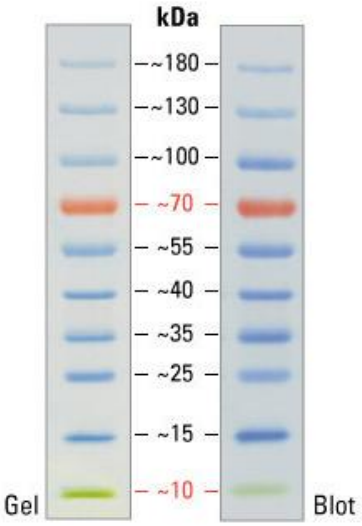

Figure C.6 PageRuler^{TM} Prestained Protein Ladder

MW, kDa	Protein	Source	Ref.
116.0	β–galactosidase	*E.coli*	2
66.2	Bovine serum albumin	bovine plasma	3
45.0	Ovalbumin	chicken egg white	4
35.0	Lactate dehydrogenase	porcine muscle	5
25.0	REase Bsp98I	*E.coli*	6
18.4	β–lactoglobulin	bovine milk	7
14.4	Lysozyme	chicken egg white	8

12% Tris-glycine SDS-PAGE

Figure C.7 Unstained Protein Molecular Weight Marker